國 立 交 通 大 學

電子工程學系電子研究所

博 士 論 文

直接序列分碼多重進接無線通訊系統之
分析及設計

Analysis and Design of Direct-Sequence Code-Division Multiple Access for Wireless Communications

研 究 生 ：林郁男

指導教授 ：林大衛

中華民國九十四年七月

直接序列分碼多重進接無線通訊系統之分析及設計

研究生：林 郁 男　　指導教授：林大衛 博士

國立交通大學

電子工程學系暨電子研究所

摘 要

直接序列分碼多重進接(DS-CDMA)技術已被廣泛的應用於第二代行動通訊系統並成為下一代通訊系統的主要技術之一。本論文的主要內容在深入地分析傳統技術之效能，並提出一個可增進其效能的片碼間插(chip-interleaving)技術。

首先，我們針對傳統系統在經迴旋碼(convolutional codes)之通道編碼後的檢測結果進行理論上的分析。基於隨機展頻碼(random-spreading codes)的假設，我們提出一個新穎且簡單的分析結果。我們也分析使用短展頻碼(short-spreading codes)和長展頻碼(long-spreading codes)的差別，分析結果顯示雖然在未經通道編解碼時，展頻碼的週期長度並未對檢測結果造成影響，但是由於長展頻碼有較佳的干擾隨機性(randomness)，其在經通道編碼的系統中效能明顯優於短展頻碼；而此差異在淡化通道下，相對較不明顯。此外，我們也發現直接序列分碼系統雖然能經耙狀接收器(rake receiver)及位元間插器(bit interleaver)分別得到路徑分集(path diversity)及時間分集(time diversity)，進而在淡化(fading)通道中有較好的表現，但是其效果仍較未經淡道化通道時來得差。因此，仍需進一步的分集技術。

多重用戶干擾(multiple access interference)是影響分碼多重進接系統容量的重要因素。因此，我們接著討論應用平行式干擾消除(parallel interference cancellation)檢測器以處理多重用戶干擾問題的系統。針對硬式(hard-limiting)干擾消除器，我們研究其在同步(synchronous)系統中的效能極限。經由分析我們發現，此檢測器在第兩級後的效能即未有明顯的差異，而當僅有兩用戶時，只要一級的干擾消除就夠；我們也驗證此效能的限制是來自於用戶間相互的干擾影響。

在接下來的部份，我們研究片碼技術。我們首先提出一個使用片碼間插技術的直接序列分碼系統(CIDS-CDMA)。此系統由於能額外提供內符碼分集(intra-bit diversity)，在淡化通道下有很穩健的效能。當合併使用位元間插技術時，此系統最大的分集度是展頻係數(spreading factor)和迴旋碼之自由距離(free distance)的乘積。我們從理論上分析此系統在未經和經過通道編碼的效能。分析顯示，檢測對象的移動速度及其片碼間插深度幾可完全決定其檢測效果的好壞，其他干擾用戶的情形並未對其有明顯的影響。我們也發現在此系統中，展頻碼的週期長度在完美片碼間插情形下，並未如同傳統系統一樣影響檢測結果。

在第四個部份，我們基於 3GPP 的寬頻分碼多重進接系統(WCDMA)設計了片碼間插寬頻分碼系統(CI-WCDMA)。片碼間插技術應用於實數分支(I-branch)以傳遞用戶資料。虛數分支(Q-branch)則用以傳送前導序列(pilot sequence)而在接收端利用傳統非片碼間插技術進行通道估測。在此系統中，我們亦應用了數種不同的非線性平行式干擾消除器。經由模擬驗證，此系統在淡化通道下的確有極為優異的效能表現。

最後，我們研究應用多展頻碼(multicode)的片碼間插分碼系統於慢速淡化(slow fading)通道中。經由適當的零填補(zero-padding)，此系統在非同步(asynchronous)及多重路徑(multipath)反射的情形下仍能維持展頻碼間的同步相關性(synchronous correlation)，進而減少干擾。我們提出一個基於高登序列(gold sequences)的設計範例，其能在檢測品質及系統容量中有較好的效能取捨。和最近所提出的片碼間插區塊展頻系統(chip-interleaved block-spread CDMA)相較，我們所提出的系統在通道編碼的系統中有較佳的效能。

Analysis and Design of Direct-Sequence Code-Division Multiple Access for Wireless Communications

Student: Yu-Nan Lin Advisor: Dr. David-W. Lin

Department of Electronic Engineering
& Institute of Electronics
National Chiao Tung University

Abstract

Direct-sequence code division multiple access (DS-CDMA) has been widely implemented in second generation cellular communications systems and become one of the most promising techniques in next generation system. In this thesis, we study the performance of conventional DS-CDMA systems and propose a chip-interleaved system which can greatly improve the performance.

First, we concentrate on the analysis of conventional DS-CDMA and begin the discussion with convolutional coded systems. Random-spreading codes are assumed. A novel and relatively simple theoretical result is presented. The performance difference between short- and long-code spreading is also studied and the results show that due to the randomness of interference over symbols, the system with long-code spreading performs much better than with short-code spreading although they have similar performance when channel coding is not applied. The results also show that although DS-CDMA can gain diversity from rake receiving (path diversity) and bit interleaver (time diversity), it still degrades a lot in fading channels and hence the need for other diversity sources.

Secondly, we consider the use of Parallel Interference Cancellation (PIC) in combating multiple access interference (MAI), which is the limiting factor to the capacity of DS-CDMA. The performance of hard-limiting PIC in synchronous systems is investigated. We show that hard-limiting PIC in such case has performance

limit at the second stage. In addition, for two-user, one stage is enough. And the performance limit comes from the mutual influence between desired and interfering users.

The use of chip-interleaving in DS-CDMA is studied. We present a chip-interleaved DS-CDMA (CIDS-CDMA) which is resistant to channel fading by leveraging intra-bit diversity. When combined with bit-interleaving, this system can, in the limit, provide a diversity order equal to the product of spreading factor and the convolutional code's free distance. Thus, CIDS-CDMA is much resistant to channel fading. Both channel coded and uncoded systems are theoretically analyzed. The analysis shows that the fading rate and chip-interleaving depth of the desired user itself almost single-handedly determines the resulting performance and the interfering users' fading speeds do not affect the performance significantly. It also reveals that in the case of perfect chip-interleaving, the spreading code period has no influence on the performance.

Fourthly, we proposed a chip-interleaved WCDMA (CI-WCDMA) based on several 3GPP WCDMA system features. In this system, data symbols are transmitted through I-branch while Q-branch is used for the transmission of pilot sequence. Channel estimation is done in Q-branch before chip de-interleaving as conventional systems. Several nonlinear PIC detectors are considered as the receiving structures. The result shows that the proposed system has a great improvement over conventional DS-CDMA system in fading channels.

Lastly, we demonstrate a multicode CIDS-CDMA which can improve the performance of DS-CDMA in asynchronous and multipath channels by effecting the synchronous correlations among the spreading codes in such conditions. Slow fading channels are considered. An example using gold sequences is presented and shows a better trade-off between performance and capacity. Compared to the recently proposed chip-interleaved block-spread CDMA (CIBS-CDMA), the presented scheme can attain better performance in channel-coded systems.

誌　　謝

這篇論文的完成，首先要感謝我的指導老師林大衛教授多年的教誨與指導。從老師身上，我學得許多從事研究所需具備的精神及態度，尤其是老師嚴謹的研究精神、對問題的堅持及執著更是深深地影響了我。在此，我要再次對林大衛老師表達我十二萬分的謝意與敬意。

同時，也要感謝實驗室的學長姐、同學、學弟妹們，不論是在學業上的討論、一起合作計劃時的配合，以及在生活上的相互幫忙，都使我這段求學過程格外不同。尤其要謝謝峰誠學長，在工作站的管理及撰寫程式上所給予莫大的幫助。此外，也要謝謝崑健和俊榮在許多方面所給予的幫助及討論。

最後，我要獻上最誠摯的感謝給予我的父母及家人，有你們在我背後的支持及鼓勵，我才能完成這篇論文。願與你們一同分享這份喜悅。

Contents

List of Figures

List of Tables

Chapter 1

Introduction

Nowadays, mobile communication has become part of our daily life. Direct-sequence code division multiple access (DS-CDMA) has been widely employed in the second-generation mobile communication systems. In CDMA, signal is spread with a spreading code, which is unique for each user, before transmission. Spreading process is operated in a chip rate much higher than the actual data rate and hence, results in noise-like transmitted signal. With spreading codes known in the receiver side, user signal can be extracted by despreading operation. Therefore, CDMA is more efficient in bandwidth usage compared to time-division multiple access (TDMA) and frequency-division multiple access (FDMA). In addition, wireless communications are normally subject to channel fading. For CDMA systems, multipath energy can be captured through rake-combining. Hence, there is path diversity in CDMA and makes it more robust in fading channels. Due to its success in the second-generation communication, a technique based on wideband CDMA (W-CDMA) has been accepted as one of the air interface technologies for next generation communication system [15],[22],[25],[30].

1.1 Motivation and Discussed Topics

Ideally, orthogonal sequences can be used as the spreading codes for CDMA systems. However, when the system is asynchronous or suffers frequency-selective fading, the orthogonality between users cannot be preserved at receiver side. Hence, in reality, multiple

access interference (MAI) has been a limiting factor to the capacity of DS-CDMA systems.

In the receiver side, various multiuser detection (MUD) technologies have been proposed to reduce MAI. In [18],[35],[48], decorrelating or zero-forcing detector is proposed to project desired user's signal into the space orthogonal to that spanned completely by the interfering users. Although decorrelating detector removes MAI perfectly, it suffers noise enhancement problem. MMSE linear detector is proposed to balance between MAI cancellation and noise enhancement [35],[45],[74]. When a receiver, for example the base station, knows all the users' spreading codes and channel state information (CSI), interference cancellation (IC) detector can be applied. The basic idea behind IC detector is simple: regenerate interference and then cancel them out. Interference regeneration is based on tentatively made decision and have more reliable regenerated interference, the IC detectors usually operates in multi-stage. There are different ways of canceling regenerated interference. Successive interference cancellation (SIC) [43],[51] cancels interference in an serial order such that the strongest interferer is the first canceled and the weakest one is the last canceled. On the other hand, parallel interference cancellation (PIC) [49],[71],[76] cancels all the reconstructed interference simultaneously. In this thesis, PIC is the main topic among various MUD techniques.

Recently, some have pay attention on the transmitter design for low MAI system. One research direction is to design new spreading sequences having low correlation values when the relative delay between sequences is within a range, which is named interference free window (IFW). Thus, there is reduced MAI as long as the maximum asynchronous delay plus multipath delay spread is less than IFW. LS-codes [10],[41],[62] used in LAS-CDMA is an example. Not designing new spreading code sets, another research direction is to effect spreading code properties in frequency-selective channels as in flat fading channels. Block precoding is the common technique to this problem as in [26],[80]. In this direction, we will study the use of chip-interleaving.

Wireless communications are usually subject to channel fading and diversity is the common strategy to remedy this impairment. In DS-CDMA systems, rake receiver is employed to lever path diversity and bit interleaver is applied for time diversity. However, later we will see that the performance of conventional DS-CDMA still degrades a lot due to channel fading. In regarding of this, chip-interleaving is considered as another way of levering diversity.

1.2 Organization of The Thesis

Basic operation of DS-CDMA is described in Chapter 2. We then study the performance of channel coded DS-CDMA over multiuser and multipath channels in Chapter 3. Random-spreading codes are assumed. Two channel conditions are considered. One is the Rayleigh fading channel and the other one is the modeling of perfect power control. By approximating the correlation among the spreading codes (rather than the ensuing interference) as Gaussian, we are able to inspect the influence of spreading code periods and obtain the analytical results with relatively simple expressions. The analysis shows that, due to the randomness in multiple access interference (MAI), long-code systems outperform short-code systems when channel coding is included.

In Chapter 4, we consider the systems with hard-limiting PIC. While PIC normally involved nonlinear functions, previous analyses mainly addressed linear PIC. We find that the performance of purely hard-limiting PIC may not improve after the second stage and for two-user case, one stage usually suffices. Approximate expressions for numerical evaluation of hard-limiting PIC are also proposed and shown to be accurate.

In the second part, we study the technique of chip-level interleaving both in slow and fast fading channels. The case in fast fading channels is discussed in Chapter 5. While practical channel coded systems use bit interleaving to effect inter-bit diversity, chip-level interleaving provides intra-bit diversity gain. We analyzes the performance of chip-interleaved DS-CDMA (CIDS-CDMA) without and with channel coding in Rayleigh

fading channels. It is concluded that, though there exists path diversity already, chip-interleaving still improves the performance greatly.

We design a chip-interleaving scheme based on several 3GPP WCDMA system features, such as the use of Q-branch to transmit control bits and I-branch to transmit data bit in a QPSK-like modulation scheme in Chapter 6. Different types of PIC detector is used in such system. The proposed chip-interleaved WCDMA (CI-WCDMA) is shown to have significant performance advantage compared to simple WCDMA in transmission over multipath fading channels.

Finally, the use of chip-interleaving in slow fading channels to alleviate MAI is addressed in Chapter 7. We show that while conventional DS-CDMA cannot preserve periodic correlation values of spreading codes over asynchronous and multipath channels, CIDS-CDMA can do this. A gluttonous code arrangement of Gold sequences is given as an example to show the superiority of this scheme.

1.3 Contributions of The Thesis

The main contributions of this thesis are:

1. We present the theoretical analysis for short- and long-code DS-CDMA systems over various channel conditions with random-spreading codes.

2. The performance of hard-limiting PIC is theoretically analyzed and we find that for two-user case, one stage PIC is enough while for more users case, the performance may not improved after second stage PIC.

3. We theoretically analyze the performance of chip-interleaved CDMA with convolutional coding in fading channels.

4. A practical design of chip-interleaving technology on the WCDMA system is proposed.

5. We demonstrate a multicode chip-interleaved DS-CDMA which can have reduced MAI and ISI over multipath channels.

Chapter 2

Overview of DS-CDMA Systems

In this chapter, we describe the basic operation of DS-CDMA systems. Signal model for uplink transmission is introduced, while it is of no difficulty to derive the downlink results. The detection results for some basic channels are also reviewed.

2.1 System Model

2.1.1 Transmitted Signal

Consider DS-CDMA systems employing BPSK modulation. The baseband signal transmitted for the kth user is given by

$$s_k(t) = \sum_{h=-\infty}^{\infty} b_k[h] a_k^{(h)}(t - hT_b) \tag{2.1}$$

with

$$a_k^{(h)}(t) = \sum_{n=0}^{N-1} a_k[hN + n] p(t - nT_c), \tag{2.2}$$

where T_b and T_c are the bit and the chip periods, respectively, $b_k[h] = \pm 1$ is the user datum, $a_k^{(h)}(t)$ is the spreading waveform of the kth user during the hth bit period, and $a_k[hN + n] = \pm 1$ is the corresponding spreading code, $N = T_b/T_c$ is the spreading factor, and $p(t)$ a square pulse of chip duration that is normalized so that $\int_0^{T_c} p^2(t)dt = 1$. A spreading code with (ideally) infinitely long period is termed a long code. On the other hand, a short code has its code period equal to the spreading factor and has $a_k[hN + n] = a_k[n]$.

2.1.2 Channel Model

Assume user k is subject to a multipath channel with the impulse response being

$$h_k(t) = \sum_{l=0}^{L_k-1} \alpha_k^{(l)}(t)\delta(t-\hat{\tau}_{k,l}) \tag{2.3}$$

where L_k is the maximum number of multipaths, $\delta(\cdot)$ is the Dirac delta function, $\hat{\tau}_{k,l}$ is the path delay, and $\alpha_k^{(l)}(t)$ is the time-varying path coefficient with its variance as $\sigma_{k,l}^2$. In Rayleigh fading channels, $\alpha_k^{(l)}(t)$ is complex Gaussian random process. In addition, the path coefficients from different paths are independent and we let $\sum_l^{L_k} \sigma_{k,l}^2 = 1$. When perfect power-controlled channels are considered, we let $|\alpha_k^{(l)}(t)| = \sigma_{k,l}$ for convenience.

Based on Clarke's 2-D scattering model [11], which assumes scattered waves travel horizontally and with uniformly distributed incident angles, the first-order and second-order correlation functions can be described as:

$$\begin{aligned}
R_c(\tau) &= E[\Re\{\alpha_k^{(l)}(t)\}\Re\{\alpha_k^{(l)}(t+\tau)\}] = \frac{1}{2}\sigma_{k,l}^2 \cdot J_0(2\pi f_d \tau) \\
R_s(\tau) &= E[\Im\{\alpha_k^{(l)}(t)\}\Im\{\alpha_k^{(l)}(t+\tau)\}] = \frac{1}{2}\sigma_{k,l}^2 \cdot J_0(2\pi f_d \tau) \\
R_{c,s}(\tau) &= R_{s,c}(\tau) = 0 \\
R(\tau) &= E\left[\alpha_k^{(l)}(t) \cdot (\alpha_k^{(l)}(t+\tau))^*\right] = \sigma_{k,l}^2 \cdot J_0(2\pi f_d \tau)
\end{aligned} \tag{2.4}$$

where $f_d = v/\lambda$ is the maximum Doppler frequency shift, v is the mobile velocity, λ is the radio wavelength, and $J_0(\cdot)$ is the zero-order Bessel function of the first kind.

Based on Clarke's model, Jakes derived the well-known Jakes' model for simulation of Rayleigh fading channels and generate each path coefficient, $\alpha_k^{(l)}(t) = \alpha_{k,I}^{(l)}(t) + j \cdot \alpha_{k,Q}^{(l)}(t)$ as

$$\begin{aligned}
\alpha_{k,I}^{(l)}(t) &= \frac{2}{\sqrt{(N)}}\left\{\sum_{n=1}^{M} 2\cos(\beta_n)\cos(w_n t) + \sqrt{2}\cos(\beta_0)\cos(w_d t)\right\} \\
\alpha_{k,Q}^{(l)}(t) &= \frac{2}{\sqrt{(N)}}\left\{\sum_{n=1}^{M} 2\sin(\beta_n)\cos(w_n t) + \sqrt{2}\sin(\beta_0)\cos(w_d t)\right\}
\end{aligned} \tag{2.5}$$

where $N = 4M+2$, $w_d = 2\pi f_d$, $w_n = w_d\cos(2\pi n/N)$, and

$$\beta_n = \begin{cases} \frac{\pi}{4}, & n = 0 \\ \frac{\pi n}{M}, & n > 0 \end{cases}. \tag{2.6}$$

With $M \geq 8$, this sum-of-sinusoids simulator can serve as a simple but accurate model and various modifications of Jakes' model have been proposed in the literatures [40],[52],[54],[79].

Recently, more characteristics of wireless channel have been studied. For example, 3-D channel model, which considers the vertical incident angles as well, is addressed in [12],[24],[78], the distribution of incident angles is discussed in [24], Zhao *et al.* studied the path number distribution in [77], and modeling of wideband channel is presented in [17],[32],[37]. More information about the channel model is addressed in Appendix B.

2.1.3 Received Signal

The received signal of DS-CDMA at the base station is the composition of all users' signals and is given as

$$r(t) = \sum_{k=0}^{K-1} \sqrt{2P_k} \sum_{l=0}^{L_k-1} \alpha_k^{(l)}(t) s_k(t - (\tau_k + \hat{\tau}_{k,l})) + \zeta(t) \tag{2.7}$$

where K is the total number of users, $\sqrt{2P_k}$ the normalized signal amplitude, τ_k the asynchronous delay uniformly distributed over $[0, T_b]$, and $\zeta(t)$ white Gaussian noise with power spectral density (PSD) equal to N_0. The signal-to-noise ratio (SNR) or average SNR is given by $\gamma_k = 2P_k N/N_0$.

2.2 Correlation Properties of Spreading Codes

Let $a_u[n]$ and $a_v[n]$ be two different binary sequences of period $= N$. The aperiodic, periodic (or even), and odd correlation functions of $a_u[n]$ and $a_v[n]$ are given by, respectively [58],

$$\theta_{u,v}(l) = \begin{cases} \sum_{n=0}^{N-1-l} a_u[n]a_v[n+l], & 0 \leq l < N-1, \\ \sum_{n=0}^{N-1+l} a_u[n-l]a_v[n], & 1-N \leq l < 0, \\ 0, & |l| \geq N, \end{cases} \tag{2.8}$$

$$R_{u,v}(l) = \theta_{u,v}(l) + \theta_{u,v}(l-N), \quad 0 \leq l \leq N-1, \tag{2.9}$$

and

$$\hat{R}_{u,v}(l) = \theta_{u,v}(l) - \theta_{u,v}(l-N), \quad 0 \leq l \leq N-1. \tag{2.10}$$

Most code designs are based on the periodic correlation. For example, Gold sequences have a 3-value periodic function given by

$$R_{u,v}(l) = \begin{cases} -1 & \text{for } 2^n - 2^{n-e} - 1 \text{ values of } l, \\ -1 + 2^{(n+e)/2} & \text{for } 2^{n-e-1} + 2^{(n-e-2)/2} \text{ values of } l, \\ -1 - 2^{(n+e)/2} & \text{for } 2^{n-e-1} - 2^{(n-e-2)/2} \text{ values of } l, \end{cases} \tag{2.11}$$

where n is the degree of primitive polynomials generating Gold sequences of period $N = 2^n - 1$, $e = 1$ when n is odd, and $e = 2$ when n is even; the periodic correlation functions when n is even for the small set of Kasami sequences take on the values in the set $\{-1, -2^{n/2}-1, 2^{n/2}-1\}$ and in the set $\{-1, -2^{\lfloor (n+2)/2 \rfloor}-1, 2^{\lfloor (n+2)/2 \rfloor}-1, -2^{n/2}-1, 2^{n/2}-1\}$ for the large set of Kasami sequences. More correlation properties of pseudo random sequences can be found in [60]. In simple synchronous channels, the zero-delay periodic correlation ($R_{u,v}(0)$) governs the performance of DS-CDMA systems. However, later we will see that the detection in asynchronous systems are actually controlled by the aperiodic correlation. In such a condition, most sets of codes, including the Gold, the Kasami, and the m-sequences, have performance close to that of random codes which are composed of independent binary random variable taking values $+1$ and -1 with equal probability [8],[33]. The investigation of the aperiodic correlation analytically is difficult and hence the need for numerical approaches.

2.3 Detection of DS-CDMA

In the following, we discuss the detection results of DS-CDMA under different channel conditions. To simplify the discussion, we discuss the system that uses short spreading codes. The systems with long-code spreading will be discussed in the Chapter 3. Assume perfect channel state information (CSI) is available.

2.3.1 Simple Synchronous Systems

When the transmission is synchronous ($\tau_k = 0$) with ideal channel condition ($h_k(t) = \delta(t)$), the received signal becomes

$$r(t) = \sum_{k=0}^{K-1} \sqrt{2P_k} s_k(t) + \zeta(t). \tag{2.12}$$

The decision signal for user k after despreading becomes

$$\begin{aligned} y_k[h] &= \Re\left\{ \int_{hT_b}^{(h+1)T_b} r(t) a_k^{(h)}(t - hT_b)\, dt \right\} \\ &= \sqrt{2P_k} N b_k[h] + \sum_{m \neq k}^{K-1} \sqrt{2P_m} R_{k,m}(0) \cdot b_m[h] + \Re\{\zeta_k[h]\} \end{aligned} \tag{2.13}$$

where

$$\zeta_k[h] = \int_{hT_b}^{(h+1)T_b} \zeta(t) \cdot a_k^{(h)}(t - hT_b)\, dt \tag{2.14}$$

denotes the noise term after despreading. From the result, it is clear that the decision signal heavily relies on the design of spreading codes. As orthogonal spreading codes ($R_{k,m}(0) = 0$), such as Walsh-Hardmard sequences, are used, the signals from other users are perfectly removed and in such case, DS-CDMA can serve as an ideal multiple access scheme.

2.3.2 Simple Asynchronous Systems

Next, we consider the asynchronous transmission over ideal channels. After despreading, the decision signal becomes

$$\begin{aligned} y_k[h] &= \Re\left\{ \int_{hT_b+\tau_k}^{(h+1)T_b+\tau_k} r(t) a_k^{(h)}(t - hT_b - \tau_k)\, dt \right\} \\ &= \sqrt{2P_k} N b_k[h] + \sum_{m \neq k}^{K-1} \sqrt{2P_m} \cdot \eta_{k,m}[h] + \Re\{\zeta_k[h]\} \end{aligned} \tag{2.15}$$

where

$$\eta_{k,m}[h] = \int_{hT_b+\tau_k}^{(h+1)T_b+\tau_k} s_m(t - \tau_m) a_k^{(h)}(t - hT_b - \tau_k)\, dt \tag{2.16}$$

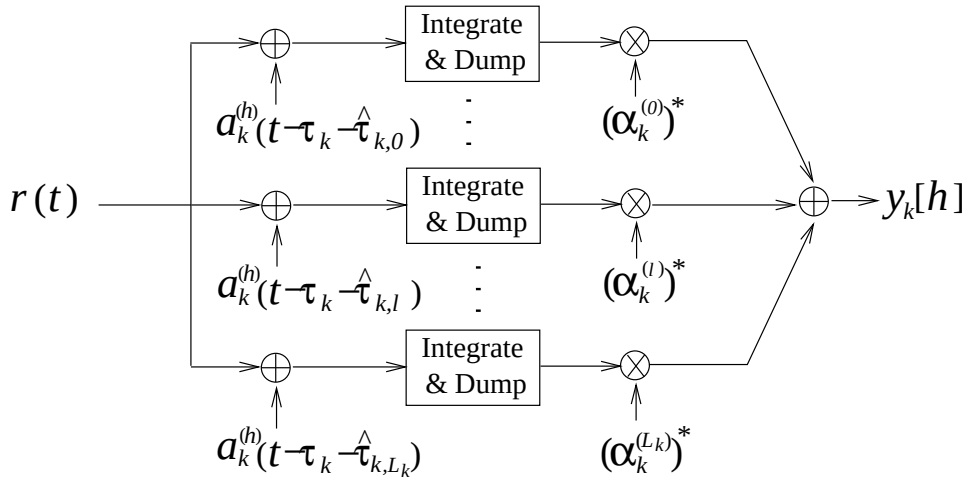

Fig. 2.1: A simple implementation of rake receiver.

denotes the MAI induced to user k by user m and $\zeta_k[h]$ is similarly defined as previous. Define $\Lambda_{k,m}(h,n,\delta)$ as

$$\begin{aligned}\Lambda_{k,m}(h,n,\delta) &= (1-\delta)\cdot\{b_m[h]\theta_{k,m}(n_{k,m}) + b_m[h+1]\theta_{k,m}(n-N)\} \\ &+ \delta\cdot\{b_m[h]\theta_{k,m}(n+1) + b_m[h+1]\theta_{k,m}(n+1-N)\}, \quad (2.17)\end{aligned}$$

when $n > 0$ and

$$\begin{aligned}\Lambda_{k,m}(h,n,\delta) &= (1-\delta)\cdot\{b_m[h]\theta_{m,k}(-n) + b_m[h-1]\theta_{m,k}(-n-N)\} \\ &+ \delta\cdot\{b_m[h]\theta_{m,k}(-(n+1)) + b_m[h-1]\theta_{m,k}(-(n+1)-N)\} \quad (2.18)\end{aligned}$$

when $n < 0$. Since $\Lambda_{k,m}(h,n,\delta)$ addresses the asynchronous correlation between users, we can compute $\eta_{k,m}[h] = \Lambda_{k,m}(h, n_{k,m}, \delta_{k,m})$ where $\tau_k - \tau_m = (n_{k,m} + \delta_{k,m})T_c$ with $n_{k,m} = \lfloor \frac{\tau_k - \tau_m}{T_c} \rfloor$. Knowing that $\theta_{k,m}(\cdot)$ is the aperiodic cross-correlation between $a_k[n]$ and $a_m[n]$, we can see that both the even correlation (when the consecutive bits have the same phase) and the odd correlation (when the consecutive bits have the opposite phases) affect the amount of MAI.

2.3.3 Rake Receiving for Multipath Transmission

Wideband signal normally undergoes frequency selective fading channels. One advantage of wideband transmission is the availability of frequency diversity although it also faces

intersymbol interference (ISI) problem. For DS-CDMA systems, with spreading and despreading process, a simple rake receiver [55] can both attain the diversity and remedy the ISI. Figure 2.1 shows a simple structure of rake receiver. Each finger of the rake receiver is synchronized to one desired path and acquires the signal form that path. Then, the despread signals form all the fingers are maximal-ratio-combined (MRC) to form the decision signal.

Consider a slow fading channel that the path coefficients remain unchanged during the detection and simply refer them to $\{\alpha_k^{(l)}\}$. With multiuser signals temporarily ignored, the despread signal at lth finger can be expressed as

$$\begin{aligned} y_k^{(l)}[h] &= \int_{hT_b+\tau_k+\hat{\tau}_{k,l}}^{(h+1)T_b+\tau_k+\hat{\tau}_{k,l}} r(t)\ a_k^{(h)}\ (t-hT_b-\tau_k-\hat{\tau}_{k,l})\ dt \\ &= \sqrt{2P_k}N\cdot\alpha_k^{(l)}\cdot b_k[h]+\sqrt{2P_k}\cdot\sum_{l'\neq l}^{L_0-1}\alpha_k^{(l')}\cdot\eta_k^{(l,l')}[h]+\zeta_k^{(l)}[h]. \quad (2.19) \end{aligned}$$

where $\eta_k^{(l,l')}$ denotes the interpath interference (IPI). With $\hat{\tau}_{k,l}-\hat{\tau}_{k,l'}=(n_k^{(l,l')}+\delta_k^{(l,l')})T_c$ and $n_k^{(l,l')}=\lfloor\frac{\hat{\tau}_k^{(l)}-\tau_k^{(\hat{l}')}}{T_c}\rfloor$, it is of no difficulty to obtain $\eta_k^{(l,l')}=\Lambda_{k,k}(h,n_k^{(l,l')},\delta_k^{(l,l')})$. Unlike MAI, the IPI comes from the non-ideal aperiodic autocorrelation of spreading codes. The decision signal after combining all the fingers' output becomes

$$y_k[h]=\Re\left\{\sum_{l=0}^{L_0}(\alpha_k^{(l)})^*\cdot y_k^{(l)}[h]\right\}. \quad (2.20)$$

In the case that the spreading factor is large or the autocorrelation of spreading codes is much lower, we can neglect the IPI and obtain

$$y_k[h]=\left(\sqrt{2P_k}N\sum_{l=0}^{L_k}|\alpha_k^{(l)}|^2\right)\cdot b_k[h]+\Re\left\{\sum_{l=0}^{L_k}(\alpha_k^{(l)})^*\cdot\zeta_k^{(l)}[h]\right\}. \quad (2.21)$$

Clearly, a simple rake receiver can fully capture the multipath energy and hence gain the path diversity. In practical application, IPI and MAI cannot be fully removed due to the non-ideal spreading codes properties and therefore, the rake receiver does not provide optimal decision result. However, its simplicity of implementation still draws great attention.

2.4 Random Spreading Codes

In general, long spreading codes are well modeled as random codes and can randomize the interference more efficiently. Short spreading codes, on the other hand, have deterministic correlation properties which can be utilized to effectively cancel interference. However, for asynchronous channels such as uplink transmission, the real correlation function regulating MAI is the aperiodic correlation. Since aperiodic correlations are hard to trace analytically, random codes also act as an appropriate model for short-code systems with asynchronous transmission.

To analyze the performance of DS-CDMA, MAI and IPI are usually modeled as Gaussian random variables and hence can be fully characterized by their variance. With this approximation, decision results can be evaluated by computing the variance of these Gaussian variables. Under assumption of random spreading codes, the variance of $\Lambda_{k,m}(h,n,\delta)$ can be computed as

$$\begin{aligned} E\{\Lambda^2_{k,m}(h,n,\delta)\} &= E\{(1-\delta)^2\}\cdot[(|n|)+(|n|-N)]\,. \\ &+ E\{\delta^2\}\cdot[(|n+1|)+(|n+1|-N)] \\ &= E\{1-2\delta+2\delta^2\}\cdot N. \end{aligned} \tag{2.22}$$

As δ is uniformly distributed over $[0,1]$, the result can be further computed as

$$E\{\Lambda^2_{k,m}(h,n,\delta)\} = \frac{2}{3}N. \tag{2.23}$$

Hence, when the asynchronous delays, $\{\tau_k\}$, are uniformly over $[0,T_b]$ and users' datum are independent, the variance of MAI term in (2.15) can be derived as

$$\sum_{m\neq k}^{K-1} 2P_m\cdot E\{\eta^2_{k,m}[h]\} = \frac{4N}{3}\cdot\sum_{m\neq k}^{K-1} P_m. \tag{2.24}$$

The signal-to-interference-plus-noise ratio (SINR) in simple asynchronous channels can be expressed as

$$\hat{\gamma}_k = \frac{1}{\frac{2}{3NP_k}\sum_{m\neq k}^{K-1} P_m + 1/\gamma_k}. \tag{2.25}$$

SINRs under other channel conditions can be computed in a similar way. As shown in (2.25), when a user increases the transmission power, other users' SINRs will be degraded. Therefore, DS-CDMA is a MAI-limited system.

2.5 Summary

In this chapter, we introduced the basic operation of DS-CDMA systems. Due to the non-ideal correlation functions, we have seen that the capacity of DS-CDMA is limited by MAI. Thus, the need for advanced interference techniques is self-evident. Though Gaussian approximation is quite accurate over a large operation range, we will later see that it loses some information for channel coded systems.

Chapter 3

Analysis of Bit-Interleaved DS-CDMA with Convolutional Coding

This chapter presents the performance analysis for the bit-interleaved DS-CDMA (BIDS-CDMA) with convolutional coding. Random spreading codes are assumed. By approximating the correlation among the spreading codes (rather than the ensuing interference) as Gaussian, we obtain novel and relatively simple results for the analysis. The performance difference between short- and long-code systems is also discussed and the results showed that with randomized interference over bits, long-code spreading has better channel decoding results.[1]

3.1 Introduction

Theoretical analyses of DS-CDMA system performance frequently assume use of random spreading codes. Besides the well-known Gaussian approximation to MAI, many have attempted more accurate analytical characterization of the performance of unchannel-coded conventional DS-CDMA under random-code spreading. In [38], the density function of the MAI is studied extensively, from which arbitrarily tight upper and lower bounds on bit error rates (BERs) can be obtained. Based on [38], some have proposed simplified methods for performance calculation [9],[29],[46],[47]. Comparatively, there are fewer

[1]Part of this chapter has been published in "Novel Analytical Results on Performance of Bit-Interleaved and Chip-Interleaved DS-CDMA with Convolutional Coding," *IEEE Trans. Vech. Technol.*, vol. 54, no. 3, pp. 996–1012, May 2005.

publications devoted to the performance analysis of channel-coded DS-CDMA. For long-code systems, an approximate analysis is simpler than for short-code systems due to the random correlations among spreading codes. For short-code systems, the analysis is more difficult. In [72], the authors employ computer simulation to obtain the histogram of signal-to-interference ratios (SIRs). However, from the simulation results it is somewhat difficult to derive simple intuitive insights concerning the SIR distribution. Similarly in [68], simulation results are used to determine the probability density function (pdf) of SIRs numerically. In [50], many observations of the difference between short-code and long-code systems with and without channel coding are made. But the analysis is through Monte Carlo simulation where the BERs can only be calculated as the spreading sequences are known and the distribution of SIRs can only be known through extensive computation. The analysis presented by Viterbi in [73] does not consider the interference statistics over symbols and hence, only holds for long-code systems.

In this chapter, we consider an analytical approach. By approximating the correlation among the spreading codes (rather than the ensuing interference) as Gaussian, we obtain novel, simple results concerning the transmission performance under various conditions. Unlike the conventional Gaussian approximation, the results are quite accurate for short-code systems under channel coding.

Another motivation of the present work comes from the following observation concerning the underlying mechanism that leads to the performance difference between long-code and short-code spreading in channel-coded DS-CDMA. With random spreading codes, the distribution of their correlations in a symbol interval is the same regardless of whether long-code or short-code spreading is used. In the absence of channel coding, this results in a similar average error performance for both kinds of spreading. In the presence of channel coding, however, we have a different picture. With long-code spreading, the correlations among different users' spreading codes change from symbol to symbol. In maximum-likelihood decoding, it is the total MAI in the Viterbi decoding delay (or the

total MAI in the span of a codeword in the case of block coding) that affects the error performance. Thus if the channel code's minimum Hamming distance is large, then by the law of large numbers, all users will be subject to a total MAI of substantially similar statistics and have similar error performance in equal noise. With short-code spreading, on the other hand, the correlations of the spreading codes remain the same over time. Hence the law of large numbers is not at work in the temporal direction as it is in a long-code system. Thus the MAI has a greater variance. Or, from another viewpoint, a proportion of the users will experience high MAI over an extended period of time. This results in poor decoding performance for these users as well as a poorer average error performance over all users when compared with a long-code system. Since this effect comes from the correlation among spreading codes, bit interleaving (the conventional way to deal with bursty errors) does not give a fully satisfactory solution.

3.2 Analysis of Synchronous Transmission

We start the discussion with synchronous transmission over flat fading channels. The received signal is, as previous, given by

$$r(t) = \sqrt{2P}\sum_{k=0}^{K-1} \alpha_k(t) s_k(t) + \zeta(t) \tag{3.1}$$

where $\sqrt{2P}$ is the normalized signal amplitude, $\{\alpha_k(t)\}$ the channel coefficients, $\zeta(t)$ white Gaussian noise, and $s_k(t)$ the transmitted DS-CDMA signal as described previously in Chapter 2. Two kinds of channel are considered: perfectly power-controlled and Rayleigh fading. In the former case, we let $|\alpha_k(t)|^2 = 1$ (for all k) for convenience. In the latter case, $\{\alpha_k(t)\}$ are time-varying, zero-mean, complex-valued Gaussian random variables, and we let $E\{|\alpha_k(t)|^2\} = 1$ for all k. In both cases, the value or the expected value of the received signal power for each user is simply P and no user is at a disadvantaged position. The SNR or average SNR is given by $\gamma = 2PN/N_0$. The Rayleigh fading case may be viewed as a system with perfect long-term power control. Although

in synchronous short-code systems, other kinds of spreading codes (such as the orthogonal codes) may yield lower interference, random codes have advantage in addressing the influence of asynchronism. Indeed, uplink transmission is usually asynchronous. Hence we assume random codes in the following discussion.

Assume the receiver employs conventional matched filtering and despreading. Without loss of generality, take user 0 as the desired user. To simplify the analysis, assume the path coefficients, $\alpha_k(t)$, remain unchanged during one bit and denote $\alpha_k[h]$ the coefficient within $[hT_b, (h+1)T_b]$. Assume CSI can be estimated without error. Then the decision signal for the hth bit is given by

$$y[h] = \Re\left\{\alpha_k[h] \cdot \int_{hT_b}^{(h+1)T_b} a_0^{(h)}(t - hT_b) r(t) dt\right\}. \tag{3.2}$$

We analyze the performance in the two channel conditions in two subsections.

3.2.1 Perfectly Power-Controlled Channels

Consider first the case of perfectly power-controlled channels, where the channel coefficients have a constant amplitude but random phases. Without loss of generality, let $\alpha_0[h] = 1$ and let $\alpha_k[h] = e^{j\theta_k[h]}$ for $k \neq 0$. Then the decision signal for bit h is given by

$$y[h] = \sqrt{2P} \cdot N \cdot b_0[h] + \eta[h] + \zeta[h] \tag{3.3}$$

where

$$\eta[h] \triangleq \sqrt{2P} \sum_{k=1}^{K-1} \rho_k[h] \cos\theta_k[h] b_k[h] \tag{3.4}$$

is the MAI, with $\rho_k[h]$ being the correlation between $a_0[hN+n]$ and $a_k[hN+n]$ defined as

$$\rho_k[h] \triangleq \sum_{n=0}^{N-1} a_0[hN+n] a_k[hN+n] \tag{3.5}$$

and $\theta_k[h]$ being the value of $\theta_k(t)$ (assumed constant during the bit period), and

$$\zeta[h] \triangleq \int_{hT_b}^{(h+1)T_b} a_0^{(h)}(t - hT_b) \Re\{\zeta(t)\} dt \tag{3.6}$$

is the noise in the despread signal. Since $\zeta(t)$ is white, we get $E\{\zeta^2[h]\} = N \cdot N_0$.

Short-Code Spreading

With short-code spreading, $\rho_k[h]$ becomes independent of h. Hence we drop the time index h. Conventional analysis takes ρ_k, $\cos\theta_k[h]$ and $b_k[h]$ all as random variables and models $\eta[h]$ as zero-mean Gaussian. Thus, with random spreading codes, the variance of $\eta[h]$ is given by

$$E\{\eta^2[h]\} = PN(K-1). \tag{3.7}$$

For analysis of average uncoded BER, this expression is applicable to both long- and short-code systems and leads to quite accurate results. For channel-coded systems, however, the decoding requires observing the received signal over a time interval spanning multiple bit periods. The corresponding performance analysis thus needs the statistics of interference (e.g., joint pdf) over such a multi-bit period, but the above variance only characterizes the interference statistics in individual bit periods. In a short-code system, suppose a user is assigned a spreading code that has high correlation values with other users' spreading codes. Then this user's signal will suffer from high interference. In a synchronous system, this condition will persist until the assigned spreading code are changed. (In an asynchronous system, the condition may change when the relative delays among the users are changed.) Bit interleaving does not help in this situation. Therefore, the transmission performance is worse than that predicted using (3.7) with the usual assumption of independent interference in different bit periods. The mathematics below provides more insights.

While our discussion concentrates on convolutional coding with soft-decision Viterbi decoding, the situation with block coding can be addressed in a related fashion. Assume the modulator maps channel coder output values 0 and 1 to -1 and $+1$, respectively. The following analysis is based on uniform error property (UEP), which means that the error probability is the same for all the transmitted codewords. When used with BPSK or QPSK over AWGN channels, binary linear codes satisfy UEP. Since convolutional codes belong to linear codes, it suffices to consider the all-zero code sequence only. The probability of

erroneously decoding it to a trellis path that remerges with the all-zero path and differs from it in d coded bits can be expressed as

$$P(d) = \text{Prob}\left(\sum_{l=1}^{d} y'[l] \geq 0\right) \tag{3.8}$$

where the index l runs over the set of d bits in which the two paths differ. The superscript $'$ has been used to simplify the notation because these d bits may not be consecutive in time. Term $P(d)$ a pairwise error probability for convenience. By (3.3),

$$\begin{aligned}\sum_{l=1}^{d} y'[l] &= -\sqrt{2P}\cdot dN + \sqrt{2P}\sum_{k=1}^{K-1}\rho_k\left(\sum_{l=1}^{d}\cos\theta'_k[l]b'_k[l]\right) + \sum_{l=1}^{d}\zeta'[l] \\ &\triangleq -\sqrt{2P}\cdot dN + \eta_p + \sum_{l=1}^{d}\zeta'[l]. \end{aligned} \tag{3.9}$$

Conditioned on a set of ρ_k, the quantity $\sum_{l=1}^{d}\cos\theta'_k[l]b'_k[l]$ can be modeled as a Gaussian random variable if d is large. And the conditional variance of η_p can be computed as

$$\begin{aligned} E\{\eta_p^2\} &= 2P\cdot\sum_{k=1}^{K-1}\rho_k^2\sum_{l=1}^{d}E\{\cos^2\theta'_k[l]\} \\ &= PdN\cdot\sum_{k=1}^{K-1}\left(\frac{\rho_k}{\sqrt{N}}\right)^2 \triangleq PdN\cdot\chi_{K-1}. \end{aligned} \tag{3.10}$$

Therefore, the resultant signal-to-interference-plus-noise ratio (SINR) conditioned on χ_{K-1} can be expressed as

$$\begin{aligned}\gamma_{Bs}^{p} &= \frac{2Pd^2N^2}{PdN\chi_{K-1} + d\cdot NN_0} \\ &= \frac{d}{\frac{\chi_{K-1}}{2N} + \frac{1}{\gamma}} \end{aligned} \tag{3.11}$$

and the conditional pairwise error probability given by

$$P_s(d|\chi_{K-1}) = Q\left(\sqrt{\gamma_{Bs}^{p}}\right) \tag{3.12}$$

where $Q(x)$ is the Gaussian Q function. The main difference in (3.10) from (3.7) is that no expectation over ρ_k is taken and hence the impact of constant correlations among the

spreading codes over the remerging distance is not overlooked. Notice that since the interference is modeled as Gaussian here, UEP still holds and the discussion of all-zero code sequence is enough for tracing the performance.

To find the unconditional error probability, we need the pdf of χ_{K-1}. With random spreading codes, the code correlations ρ_k observe the binomial distribution given by

$$P(\rho_k = a) = \frac{1}{2^N} \begin{pmatrix} N \\ \frac{N+a}{2} \end{pmatrix}, \; a = -N, -N+2, \ldots, N. \tag{3.13}$$

By the central limit theorem, ρ_k is approximately Gaussian when N is large. Then χ_{K-1} is the sum-square value of $K-1$ Gaussian random variables of zero mean and unit variance. Thus χ_{K-1} is a standard central χ^2 random variable with $K-1$ degrees of freedom, where the pdf of a standard central χ^2 random variable with n degrees of freedom is

$$f_{chi}(\chi) = \frac{1}{2^{n/2}\Gamma(\frac{n}{2})} \chi^{n/2-1} e^{-\chi/2}, \; \chi \geq 0, \tag{3.14}$$

with $\Gamma(p)$ being the gamma function defined as

$$\Gamma(p) = \int_0^\infty t^{p-1} e^{-t} dt, \; p > 0. \tag{3.15}$$

Though Gaussian approximation of ρ_k is not exact in the tail part of the pdf, it does not have major effect on the accuracy of the analysis, as later numerical results will demonstrate. Thus, the unconditional pairwise error probability can be obtained as

$$P_s(d) = \int_0^\infty P_s(d|\chi_{K-1}) \; f_{chi}(\chi_{K-1}) \; d\chi_{K-1}. \tag{3.16}$$

Often, BER is more useful than the pairwise error probability, but is less easy to obtain. Conditioned on χ_{K-1}, an upper bound on the BER is given by

$$P_b \leq \sum_{d=d_{free}}^{\infty} \beta_d \cdot P_s(d|\chi_{K-1}) \tag{3.17}$$

where β_d is the weight spectrum and d_{free} is the minimum free distance. Exact weight spectra of some low-rate convolutional codes can be found in [13]. Since (3.17) is a

union bound, it seriously overestimates the corresponding BER when the pairwise error probability is high. As a result, its average, i.e.,

$$E\left\{\sum_{d=d_{free}}^{\infty}\beta_d\cdot P_s(d|\chi_{K-1})\right\}=\sum_{d=d_{free}}^{\infty}\beta_d\cdot P_s(d), \tag{3.18}$$

merely gives a very loose bound on the average BER. Burr [7] presents approximate weight distributions of convolutional codes that are useful for BER below 10^{-2}. Since the pairwise error probabilities in our problem may spread over a greater range, the approximations in [7] are not tight enough. To get a tighter bound, we simulate transmission over additive white Gaussian noise (AWGN) channels under different SNRs and find the least number of weight spectrum terms required to bound the simulated BER. Let $d_{re}(\gamma)$ be the resulting maximum path distance that need be considered to bound the decoded BER at SNR $=\gamma$ at decoder input. Then the tighter bound on average BER can be evaluated as

$$P_e=\int_0^{\infty}\left[\sum_{d=d_{free}}^{d_{re}(\gamma_{Bs}^p/d)}\beta_d\cdot Q\left(\sqrt{\gamma_{Bs}^p}\right)\right]f_{chi}(\chi_{K-1})d\chi_{K-1} \tag{3.19}$$

where γ_{Bs}^p is as given in (3.11). Further, we find that, when the summation in (3.19) contains more than one term, a better approximation to the BER can be obtained if we replace β_d by $\beta_d/2$ for the maximum-distance term. This is used in our numerical results presented later.

Table 3.1 lists $d_{re}(\gamma)$ for the rate-1/2, constraint length-7 convolutional code with generator vectors $g_1=133_8$ and $g_2=171_8$. It has $d_{free}=10$. Since numerical results show that the influence of $d>16$ is hardly significant, we simply ignore them.

The techniques to obtain the unconditional pairwise error probability and the BER bound from the conditional pairwise error probability are mostly similar in all the other conditions discussed in subsequent sections. Hence we shall omit their discussion unless the difference warrants it.

Table 3.1: Maximum Path Distance in BER Estimation for the Example Code

γ (dB)	$[-\infty, -3)$	$[-3, -1)$	$[-1, 0.5)$	$[0.5, \infty)$
d_{re}	10	12	14	16

Long-Code Spreading

For long-code spreading, consider first a system where the period of spreading codes is an integer N_c times the spreading factor. Thus $a_k[hN+n] = a_k[(hN+n)\%(NN_c)]$ where $\%$ denotes the modulo operation. And there are a total of $(K-1)N_c$ different correlation values between any user's spreading code and the other interfering users' spreading codes. If these values occur the same number of times within the remerging distance of the channel code's trellis, the conditional variance of the interference in (3.9) is changed to

$$E\{\eta_p^2\} = \frac{Pd}{N_c} \sum_{k=1}^{K-1} \sum_{m=0}^{N_c-1} \rho_k^2(m) \triangleq \frac{PdN}{N_c} \chi_{N_c(K-1)}. \tag{3.20}$$

The case where the $(K-1)N_c$ correlation values do not repeat an equal number of times within the remerging distance of the channel code's trellis requires tedious mathematics to characterize precisely. Later simulation results will show that the performance is only slightly different from that calculated using the last equation.

Like χ_{K-1}, the quantity $\chi_{N_c(K-1)}$ is a χ^2 random variable, but with $N_c(K-1)$ degrees of freedom. Hence the conditional SINR is given by

$$\gamma_{BN_c}^p = \frac{d}{\frac{\chi_{N_c(K-1)}}{2NN_c} + \frac{1}{\gamma}}. \tag{3.21}$$

From this the corresponding pairwise error probabilities (conditional and unconditional) and BER can be obtained in a way similar to that for short-code spreading.

We note that the unconditional pairwise error probability is given by

$$P_l(d) = \int_0^\infty Q\left(\sqrt{\gamma_{BN_c}^p}\right) f_{chi}(\chi_{N_c(K-1)})\, d\chi_{N_c(K-1)}. \tag{3.22}$$

For large N_c (ideal long-code spreading has $N_c \to \infty$), $\chi_{N_c(K-1)}$ has very concentrated pdf (result of the law of large numbers) that decays faster than the Gaussian Q function

for values of $\chi_{N_c(K-1)}$ away from $E\{\chi_{N_c(K-1)}\}$. In this case,

$$P_l(d) \approx Q\left(\sqrt{\frac{d}{\frac{E\{\chi_{N_c(K-1)}\}}{2NN_c}+\frac{1}{\gamma}}}\right) = Q\left(\sqrt{\frac{d}{\frac{K-1}{2N}+\frac{1}{\gamma}}}\right) \triangleq Q\left(\sqrt{\gamma_{Bl}^{p}}\right). \tag{3.23}$$

Thus, in the limit, we obtain the same result as that obtained under conventional Gaussian approximation.

3.2.2 Rayleigh Fading Channels

Now consider Rayleigh fading channels. We assume a fully bit-interleaved, quasi-static condition where the fading coefficients for different users at different bit times are uncorrelated and stay unchanged during a bit period. Consequently, the maximal-ratio combined signal in the convolutional decoder can be expressed as

$$\sum_{l=1}^{d}\{y'[l]\} = -\sqrt{2P}\cdot N\cdot\sum_{l-1}^{d}|\alpha_0'[l]|^2+\eta_r+\zeta_r \tag{3.24}$$

where

$$\eta_r = \sqrt{2P}\sum_{k=1}^{K-1}\sum_{l=1}^{d}\rho_k'[l]\Re\left\{\alpha_k'[l]\left(\alpha_0'[l]\right)^*\right\}b_k'[l] \tag{3.25}$$

is the MAI and

$$\zeta_r = \sum_{l=1}^{d}\Re\{\alpha_0'[l]\zeta'[l]\} \tag{3.26}$$

is the additive noise. Since

$$\zeta[h] = \int_{hT_b}^{(h+1)T_b} a_0^{(h)}(t-hT_b)\zeta(t)dt, \tag{3.27}$$

the variance of ζ_r can be computed as

$$E\{\zeta_r^2\} = NN_0\sum_{l=1}^{d}|\alpha_0'[l]|^2. \tag{3.28}$$

The variance of η_r, however, depends on which type of spreading code is used.

Short-Code Spreading

Under short-code spreading, we have

$$\eta_r = \sqrt{2P} \sum_{k=1}^{K-1} \rho_k \left[\sum_{l=1}^{d} \Re \left\{ \alpha'_k[l] \left(\alpha'_0[l] \right)^* \right\} b'_k[l] \right]. \tag{3.29}$$

Rewrite

$$\begin{aligned} \Re \left\{ \alpha'_k[l] \left(\alpha'_0[l] \right)^* \right\} b'_k[l] &= \Re\{ |\alpha'_0[l]| \cdot |\alpha'_k[l]| e^{j(\theta'_k[l] - \theta'_0[l])} b'_k[l] \} \\ &\triangleq |\alpha'_0[l]| \cdot \hat{\alpha}'_k[l]. \end{aligned} \tag{3.30}$$

Then

$$\eta_r = \sqrt{2P} \sum_{k=1}^{K-1} \rho_k \left[\sum_{l=1}^{d} |\alpha'_0[l]| \cdot \hat{\alpha}'_k[l] \right]. \tag{3.31}$$

Since $\theta'_k[l]$ is uniformly distributed in $[0, 2\pi)$ under the Rayleigh fading assumption and $b'_k[l] = \pm 1$ with equal probability, $\hat{\alpha}'_k[l]$ is Gaussian. Given $\{\alpha'_0[l]\}$ and $\{\rho_k\}$, η_r is the combination of Gaussian random variables and is hence also Gaussian. Taking expectation over the "relative fading coefficients" $\hat{\alpha}'_k[l]$, we get

$$E\{\eta_r^2\} = P \sum_{k=1}^{K-1} \rho_k^2 \left[\sum_{l=1}^{d} |\alpha'_0[l]|^2 \right] \tag{3.32}$$

where we have used the fact that $E\{\hat{\alpha}'^2_k[l]\} = 1/2$ due to the earlier assumption that $E\{|\alpha_k(t)|^2\} = 1$. Consequently, we can express the SINR as

$$\begin{aligned} \gamma^r_{Bs} &= \frac{2N^2 \cdot \left(\sum_{l=1}^{d} |\alpha'_0[l]|^2 \right)^2}{\sum_{k=1}^{K-1} \rho_k^2 \left(\sum_{l=1}^{d} |\alpha'_0[l]|^2 \right) + 2N^2 \sum_{l=1}^{d} |\alpha'_0[l]|^2 / \gamma} \\ &= \frac{2dN}{K-1} \frac{\left[\sum_{l=1}^{d} |\sqrt{2}\alpha'_0[l]|^2 \right] / (2d)}{\left[\sum_{k=1}^{K-1} (\rho_k / \sqrt{N})^2 + 2N/\gamma \right] / (K-1)} \\ &\triangleq \frac{2dN}{K-1} F_{Bs}. \end{aligned} \tag{3.33}$$

Note that the numerator of F_{Bs} is a (normalized) χ^2 random variable of degree $2d$ and the denominator is a (normalized) χ^2 random variable of degree $K-1$ plus a constant.

In Appendix A, we show that when $X = (U/\nu_1)/[(V+c)/\nu_2]$ where U and V are independent χ^2 random variables of degrees ν_1 and ν_2, respectively, with ν_1 being an even number, and c is a constant, the pdf of X is given by

$$\begin{aligned} f_X(x) &= \frac{\nu_1/\nu_2}{\Gamma(\frac{\nu_1}{2})\Gamma(\frac{\nu_2}{2})} \left(\frac{\nu_1}{\nu_2}x\right)^{\frac{\nu_1}{2}-1} \left(\frac{\nu_2}{\nu_2+\nu_1 x}\right)^{\frac{\nu_1+\nu_2}{2}} e^{-\frac{c\nu_1}{2\nu_2}x} \\ &\quad \cdot \sum_{k=0}^{\nu_1/2} \left(\begin{array}{c} \nu_1/2 \\ k \end{array} \right) \left(\frac{c(\nu_2+\nu_1 x)}{2\nu_2}\right)^k \Gamma\left(\frac{\nu_1+\nu_2}{2}-k\right). \end{aligned} \tag{3.34}$$

When $c = 0$, X reduces to the well-known F distribution with (ν_1, ν_2) degrees of freedom [1, p. 946]. We thus term the distribution of X the $F(\nu_1, \nu_2, c)$ distribution for convenience. In this term, F_{Bs} observes the $F(2d, K-1, 2N/\gamma)$ distribution, which reduces to the F distribution with $(2d, K-1)$ degrees of freedom in interference-limited operation where the effect of noise can be neglected.

Long-Code Spreading

Under long-code spreading, the cross correlation between spreading codes change with bits. Thus we have

$$\begin{aligned} E\{\eta_r^2\} &= P \sum_{l=1}^{d} \sum_{k=1}^{K-1} |\alpha_0'[l]|^2 \rho_k'^2[l] \\ &\approx PN(K-1) \cdot \sum_{l=1}^{d} |\alpha_0'[l]|^2 \end{aligned} \tag{3.35}$$

where the last approximation comes from that for long-code spreading, $\rho_k'^2[l]$ approaches its mean due to the law of large numbers, as in perfectly power-controlled channels. And the SINR can be expressed as

$$\begin{aligned} \gamma_{Bl}^r &= \frac{N^2 \sum_{l=1}^{d} |\sqrt{2}\alpha_0'^2[l]|^2}{N(K-1)+2N^2/\gamma} \\ &\triangleq \frac{\chi_{2d}}{(K-1)/N+2/\gamma}, \end{aligned} \tag{3.36}$$

where χ_{2d} has the $2d$-degree χ^2 distribution.

3.3 Performance in Asynchronous and Multipath Channels

Let the received signal be given by

$$r(t) = \sqrt{2P}\sum_{k=0}^{K-1}\sum_{l_p=0}^{L_p-1}\alpha_k^{(l_p)}(t)s_k(t-(\tau_k+l_p)T_c)+\zeta(t) \tag{3.37}$$

where $\tau_k T_c$ is user k's asynchronous delay, L_p is the maximum number of multipaths for each user, and $\alpha_k^{(l_p)}(t)$ is the l_pth path coefficient of user k. Without loss of generality, let $\tau_0 = 0$, so that τ_k gives the relative delay of user k's signal with respect to user 0's signal in number of chips. And let τ_k, $k \neq 0$, be integers that are independent and uniformly distributed over $[0, N-1]$. For multipath channels we make the simplifying assumption that $\alpha_k^{(l_p)}(t)$ is normalized so that $E\{|\alpha_k^{(l_p)}(t)|^2\} = 1/L_p$. Further, we assume use of a rake receiver with L_p fingers.

As discussed in Chapter 2, for an asynchronous system with nonzero τ_k, each interfered bit of user 0 may be partially overlapping in time with two successive interfering bits of user k. The amount of interference thus depends on whether the interfering bits have equal or unequal signs. The above dependence of interference on bit patterns adds one degree of freedom per bit per interfering propagation path (in multipath channels) per interfering user signal. In multipath propagation, the output of each rake finger for user 0's signal contains interference from all L_p paths of each interfering user signal. It also contains the IPI from the $L_p - 1$ other paths of its own signal. The number of interference terms in the rake combiner output is therefore $[2L_p^2(K-1) + 2L_p(L_p-1)]N_c$, where NN_c gives the spreading code period in number of chips. (Thus $N_c = 1$ corresponds to short-code spreading whereas $N_c > 1$ long-code spreading.) However, some of the terms correspond to the same relative path delays and hence are not independent. In total, for each interfering user, there are only $2L_p - 1$ distinct relative delays, and for IPI there are only $2L_p - 2$ distinct relative delays. Hence the total degrees of freedom in interference are reduced to $2N_c[(K-1)(2L_p-1) + (2L_p-2)] = 2N_c[K(2L_p-1)-1]$.

3.3.1 Perfectly Power-Controlled Channels

Mathematically, the decision signal at rake receiver output for the hth bit of user 0 is given by

$$y[h] = \sqrt{2P}\left(Nb_0[h] + \sum_{k=1}^{K-1}\eta_k[h] + \eta_{IPI}[h]\right) + \sum_{l_p=0}^{L_p-1}\frac{\cos\theta_0^{(l_p)}[h]}{\sqrt{L_p}}\zeta[h] \tag{3.38}$$

where

$$\eta_k[h] = \frac{1}{L_p}\sum_{l_p=0}^{L_p-1}\sum_{l'_p=0}^{L_p-1}\cos\left(\theta_k^{(l'_p)}[h] - \theta_0^{(l_p)}[h]\right)\rho_k^{(l_p,l'_p)}[h] \tag{3.39}$$

is the interference from user k and

$$\eta_{IPI}[h] = \frac{1}{L_p}\sum_{l_p=0}^{L_p-1}\sum_{l'_p\neq l_p}^{L_p-1}\cos\left(\theta_0^{(l'_p)}[h] - \theta_0^{(l_p)}[h]\right)\rho_0^{(l_p,l'_p)}[h] \tag{3.40}$$

is the IPI, with $\rho_k^{(l_p,l'_p)}[h]$ being the correlation between user k's l'_pth path and user 0's l_pth path. Due to the independence among $\theta_k^{(l_p)}[h]$, the conditional variance of η_p (which is the interference in the channel decoder output) is given by

$$E\{\eta_p^2\} = \sum_{l=1}^{d}\left[\sum_{k=1}^{K-1}E\left\{\eta_k'^2[l]\right\} + E\left\{\eta_{IPI}'^2[l]\right\}\right]. \tag{3.41}$$

As stated previously, there are totally $2N_c(2L_p-1)$ different $\rho_k^{(l_p,l'_p)}[h]$ for each interfering user k. Although the different $\rho_k^{(l_p,l'_p)}[h]$ do not occur the same number of times in the above sum, we find that a simple and reasonable approximation can be obtained by assuming that they occur equal number of times. In this regard, let the different $\rho_k^{(l_p,l'_p)}[h]$ be denoted $\{\rho_k^{\dagger}[l_r], l_r = 0,\cdots,2N_c(2L_p-1)-1\}$. Then

$$\begin{aligned}\sum_{l=1}^{d}E\{\eta_k'^2[l]\} &= \frac{1}{2L_p^2}\sum_{l=1}^{d}\sum_{l_p=0}^{L_p-1}\sum_{l'_p=0}^{L_p-1}\left(\rho_k^{(l_p,l'_p)'}[l]\right)^2 \\ &\approx \frac{1}{2L_p^2}\left[\frac{dL_p^2}{2N_c(2L_p-1)}\sum_{l_r=0}^{2N_c(2L_p-1)-1}(\rho_k^{\dagger}[l_r])^2\right].\end{aligned} \tag{3.42}$$

For IPI there are $2L_p-2$ different relative path delays and they result in $2N_c(2L_p-2)$ distinct correlations $\rho_0^{(l_p,l'_p)}[h]$. Employing a similar notational designation as above, we

get

$$\sum_{l=1}^{d} E\{\eta_{IPI}'^2[l]\} \approx \frac{1}{2L_p^2}\left[\frac{dL_p(L_p-1)}{2N_c(2L_p-2)}\sum_{l_r=0}^{2N_c(2L_p-2)-1}(\rho_0^{\dagger}[l_r])^2\right]. \tag{3.43}$$

Thus

$$\begin{aligned} E\{\eta_p^2\} &\approx \frac{d}{4N_c(2L_p-1)}\left[\sum_{k=1}^{K-1}\sum_{l_r=0}^{2N_c(2L_p-1)-1}(\rho_k^{\dagger}[l_r])^2 + \sum_{l_r=0}^{2N_c(2L_p-2)-1}(\rho_0^{\dagger}[l_r])^2\right] \\ &\triangleq \frac{dN}{4(2L_p-1)}\chi_{2N_c[K(2L_p-1)-1]}. \end{aligned} \tag{3.44}$$

Accordingly, we can obtain an approximate SINR expression as

$$\gamma_{BN_c}^{p} = \frac{d}{\frac{\chi_{2N_c[K(2L_p-1)-1]}}{4NN_c(2L_p-1)} + \frac{1}{\gamma}} \tag{3.45}$$

where $\chi_{2N_c[K(2L_p-1)-1]}$ is a χ^2 variable of degree $2N_c[K(2L_p-1)-1]$.

The mean value of the SINR can be computed as

$$E\{\gamma_{BN_c}^{p}\} = \frac{d}{\frac{K(2L_p-1)-1}{2N(2L_p-1)} + \frac{1}{\gamma}}. \tag{3.46}$$

Figure 3.1 shows an numerical example for the case of $N = 32$, $\gamma = 13dB$, $K = 20$, and $d = 10$. It can observed that the SINR mean slightly decreased with the increase of path number but the influence becomes less significant when path number becomes larger. Therefore, we can have the conlusion that for short-code systems, the presence of multipath improves the performance since the interference is further randomized. For long-code systems, whose interference is already randomized even in single-path conditions, multipath channels degrade the performance slightly since the mean of the interference is marginally increased.

3.3.2 Rayleigh Fading Channels

In fading channels, the presence of multipaths also adds to the path diversity. We have

$$\eta_k[h] = \sum_{l_p=0}^{L_p-1}\sum_{l_p'=0}^{L_p-1}|\alpha_0^{(l_p)}[h]|\hat{\alpha}_k^{(l_p,l_p')}[h]\rho_k^{(l_p,l_p')}[h]. \tag{3.47}$$

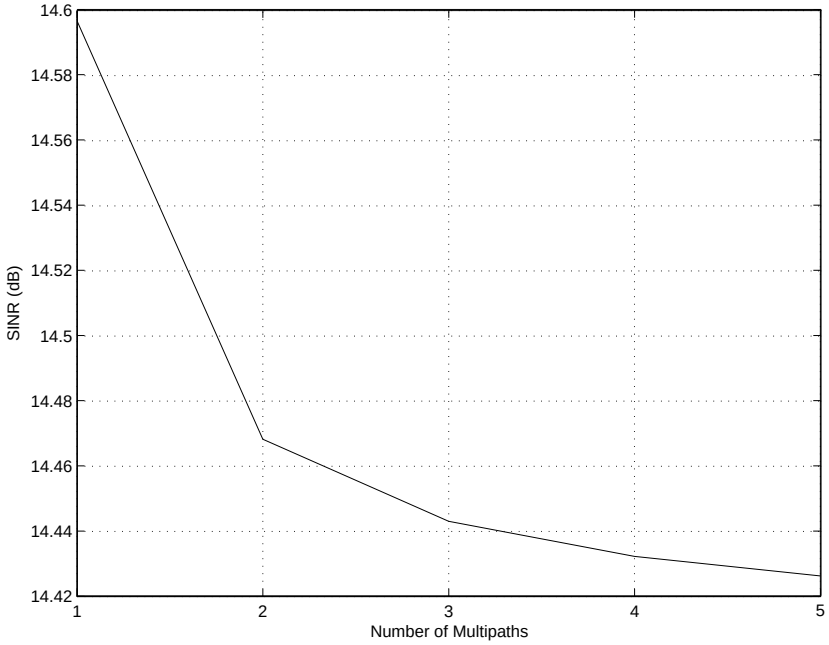

Fig. 3.1: The average SINR of perfectly power-controlled channels as function of multipath number, where $N = 32$, $\gamma = 13$ dB, $K = 20$, and $d = 10$.

where $\hat{\alpha}_k^{(l_p,l'_p)}[h] = \Re\{|\alpha_k^{(l'_p)}[h]|e^{j(\theta_k^{(l'_p)}[h]-\theta_0^{(l_p)}[h])}\}$ is Gaussian distributed and independent of both l_p and l'_p. Therefore, for a short-code system,

$$\begin{aligned}\sum_{l=1}^{d} E\{\eta_k'^2[l]\} &= \frac{1}{2L_p}\sum_{l=1}^{d}\sum_{l_p=0}^{L_p-1}|\alpha_0^{(l_p)'}[l]|^2\sum_{l'_p=0}^{L_p-1}\left(\rho_k^{(l_p,l'_p)'}[l]\right)^2 \\ &\approx \frac{1}{2dL_p^2}\left[\sum_{l=1}^{d}\sum_{l_p=0}^{L_p-1}|\alpha_0^{(l_p)'}[l]|^2\right]\cdot\left[\sum_{l=1}^{d}\sum_{l_p=0}^{L_p-1}\sum_{l'_p=0}^{L_p-1}\left(\rho_k^{(l_p,l'_p)'}[l]\right)^2\right] \\ &\approx \frac{1}{4(2L_p-1)}\left[\sum_{l=1}^{d}\sum_{l_p=0}^{L_p-1}|\alpha_0^{(l_p)'}[l]|^2\right]\cdot\left[\sum_{l_r=0}^{2(2L_p-1)-1}(\rho_k^{\dagger}[l_r])^2\right]. \quad (3.48)\end{aligned}$$

The variance of IPI can be found in a same way and hence the SINR can be computed as

$$\gamma_{Bs}^r = \frac{N^2\sum_{l=1}^{d}\sum_{l_p=0}^{L_p-1}|\alpha_0^{(l_p)'}[l]|^2}{\frac{1}{4(2L_p-1)}\left[\sum_{k=1}^{K-1}\sum_{l_r=0}^{2(2L_p-1)-1}(\rho_k^{\dagger}[l_r])^2+\sum_{l_r=0}^{2(2L_p-2)-1}(\rho_0^{\dagger}[l_r])^2\right]+\frac{N^2}{\gamma}}. \quad (3.49)$$

We thus arrive at

$$\gamma_{Bs}^r = \frac{2dN(2L_p-1)}{K(2L_p-1)-1}F_{Bs} \quad (3.50)$$

where F_{Bs} follows the $F(2dL_p, 2[K(2L_p-1)-1], 4N(2L_p-1)/\gamma)$ distribution.

When infinitely long spreading codes are used, due to the law of large numbers $(\rho_k^{(l_p,l'_p)}[l])^2$ approaches its mean given by $E\{(\rho_k^{(l_p,l'_p)}[l])^2\} = N$. Thus, the SINR for a long-code system is χ^2 distributed and has the expression

$$\gamma_{Bl}^r = \frac{\chi_{2dL_p}}{\frac{KL_p-1}{N} + \frac{2L_p}{\gamma}} \tag{3.51}$$

where χ_{2dL_p} obeys the $2dL_p$-degree χ^2 distribution.

3.4 Numerical Results and Discussion

In this section, we compare the performance of different systems by way of computer simulation. We also compare the simulation results with analysis. The rate-1/2 convolutional code of constraint length 7 with generators $g_1 = 133_8$ and $g_2 = 171_8$ is used in all simulations. And we employ soft-decision Viterbi decoding with traceback length $= 5 \cdot 7 = 35$. The simulation results are obtained through 10^3 simulation runs, where in each run the spreading codes of the users are generated randomly. Perfect channel estimation is assumed. To simulate perfect bit-interleaving, we let each bit be subject to different fading coefficients which are mutually independent. Practical channels are correlated in time. However, with propoer interleaver design, the condition of perfect bit-interleaver can be approached [73].

3.4.1 Synchronous Transmission

To start, consider BIDS-CDMA under perfectly power-controlled synchronous transmission. Figure 3.2 shows the BER performance versus number of users at spreading factor $N = 32$ and SNR $\gamma = 13$ dB. Clearly, long-code spreading has a much superior performance to short-code spreading and the difference in BER can exceed two orders of magnitude towards the lower end in number of users. The figure also shows that our analysis matches well with the simulation results. For comparison, we further simulate long-code BIDS-CDMA in random static channels, where not only the amplitudes but

also the phases of the channel coefficients remain unchanged over all time. The corresponding curve (marked "extremely static") in Fig. 3.2 shows that the performance is worse than in channels with time-varying phases. The reason is that the "channel coefficient correlations" $\cos\theta'_k$, $k = 1, \cdots, K-1$, in (3.9) are now constant over time and thus some large values in the set will result in high interference. The underlying mechanism is closely parallel to what has made the difference between short- and long-code systems. Therefore, for BIDS-CDMA systems, phase variations are beneficial to system performance, provided that the receiver can track them.

To see how the long-code period N_c (in number of bits) affects the performance of synchronous BIDS-CDMA, Fig. 3.3 shows the results for user number $K = 10$, $N = 16$, and $\gamma = 13$ dB. As predicted, BER decreases monotonically with N_c. The performance nearly flattens beyond $N_c = 32$. This is reasonable because 32 is already close to the rule-of-thumb decoding delay 35.

Next, consider BIDS-CDMA in Rayleigh fading, for which some results at $N = 32$ and $\gamma = 13$ dB are presented in Fig. 3.4. Again, long-code spreading outperforms short-code. Interestingly, the performance difference is much smaller than in perfectly power-controlled channels. While this can be appreciated from the analytical results, it can also be understood intuitively by noting that, due to fading, the correlation among received user signals is not solely determined by the spreading codes but also by the fading coefficients. The independent variation of fading coefficients due to perfect bit interleaving yields an averaging effect that improves the performance of short-code spreading relative to long-code.

3.4.2 Asynchronous and Multipath Channels

Now we turn to the asynchronous, multipath channel condition and present some results for illustration purpose.

Figure 3.5 shows the BER performance, as a function of path number, of asynchronous

systems with $N = 32$, $K = 20$, and $\gamma = 16$ dB. Not surprisingly, long-code systems still perform better. However, the performance difference between short- and long-code systems diminishes with the increase of multipath number. For long-code systems, since the interference has been randomized with long spreading codes, the increase of path number has trivial effect on perfectly power-controlled systems while the improves the performance in Rayleigh fading channels due to the additional path diversity. The marginally degradation on the performance with the increase of path number for long-code systems is due to the reduced average SINR as revealed by (3.46). Through these results, it also shows that the analysis agrees with the simulation data. Another observation is that although the appearance of multipath increases the diversity gain, the systems in Rayleigh faded channels still degraded a lot compared to that in unfaded channels. Hence, the systems need for other diversity sources.

The simulation results of using Gold sequences with $N = 63$, $L_p = 2$, and $\gamma = 13$ dB are shown in Fig. 3.6. For comparison, the analytical results for short-code systems are also presented. As can be seen from the figure, the simulated BER performance is quite close to the analytical results. Hence, random-spreading code is indeed a good approximation for Gold sequence under asynchronous transmission.

3.5 Summary

We presented a novel performance analysis for channel-coded, bit-interleaved DS-CDMA (BIDS-CDMA) under short- and long-code spreading in perfectly power-controlled and Rayleigh fading channels. Random-spreading codes are assumed since most spreading sequences have the similar correlation properties as random codes in asynchronous and multipath channels even when short-spreding codes are used. The theoretical results have relatively simple mathematical expressions. It was shown that long-code spreading had much superior performance to short-code, because the latter suffered from some persistent high interference induced by some highly correlated spreading codes whereas the former

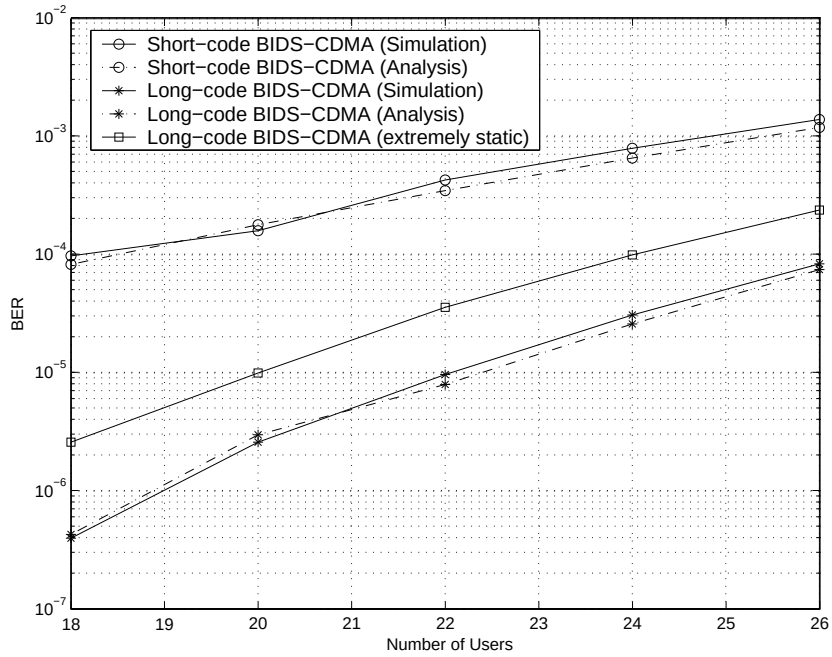

Fig. 3.2: Average BER of synchronous BIDS-CDMA under perfect power control as function of user number, where $N = 32$, $\gamma = 13$ dB, and long-code spreading employs an infinite code period.

was able to average down such interference. The difference between short- and long-code systems became smaller in Rayleigh fading because the different fading processes experienced by different users randomized the correlation among the received user signals. The results also showed that although DS-CDMA can gain diversity gain from rake receiving (path diversity) and bit interleaver (time diversity), it still suffers from noticeable performance degradation. In Chapter 5, we will show how the performance of conventional DS-CDMA in fast fading channels can be improved by way of chip-interleaving.

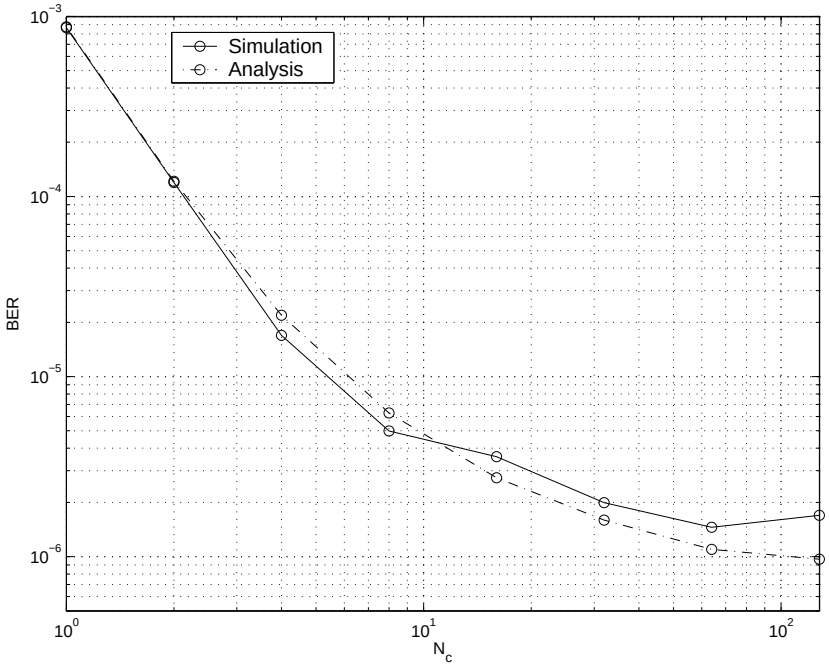

Fig. 3.3: Average BER of synchronous BIDS-CDMA under perfect power control as function of the spreading code period N_c in number of bits, where $N = 16$, $\gamma = 13$ dB, and $K = 10$.

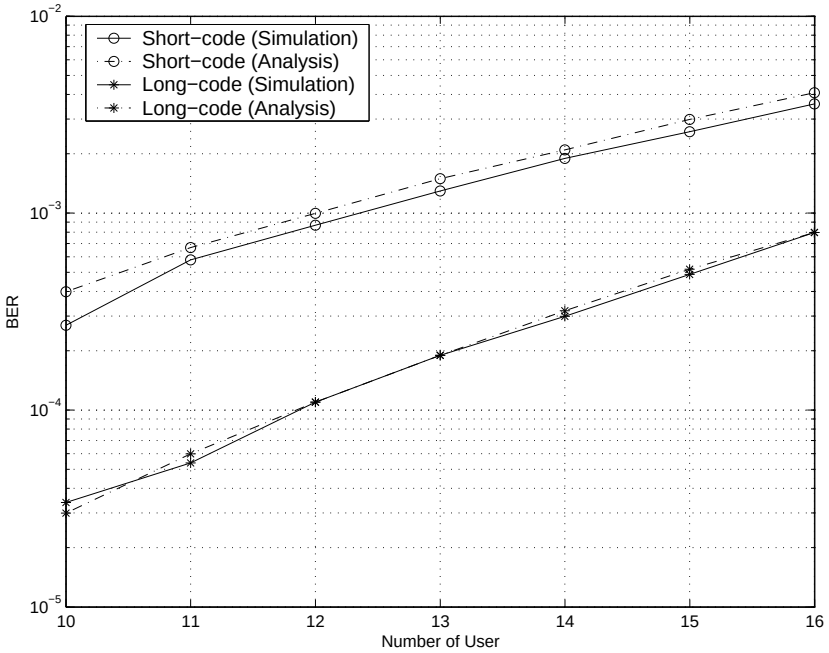

Fig. 3.4: Average BER of synchronous BIDS-CDMA in Rayleigh fading as function of user number, where $N = 32$, $\gamma = 13$ dB and long-code spreading employs an infinite code period.

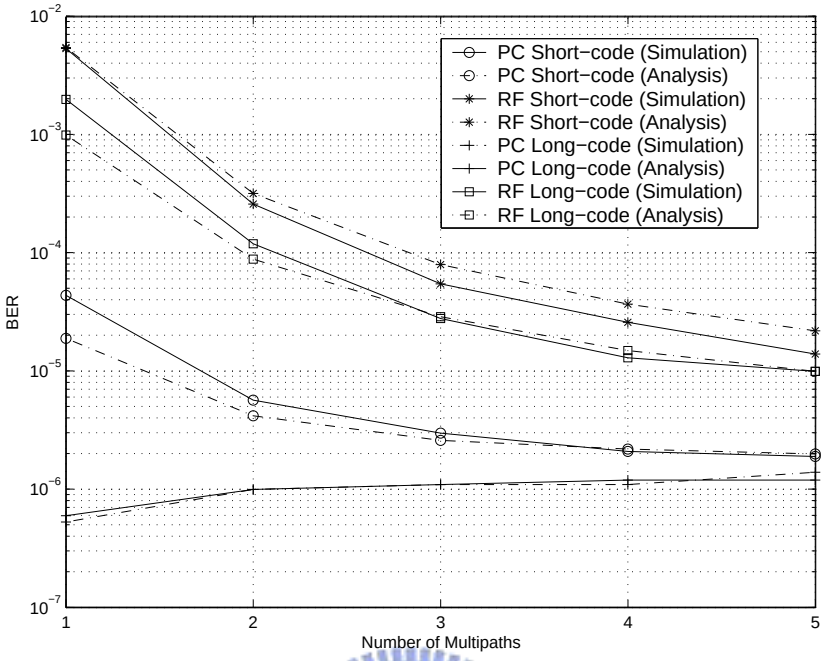

Fig. 3.5: Average BER of asynchronous systems as function of multipath number, where $N = 32$, $K = 20$ and $\gamma = 16$ dB. PC = perfect power control; RF = Rayleigh fading.

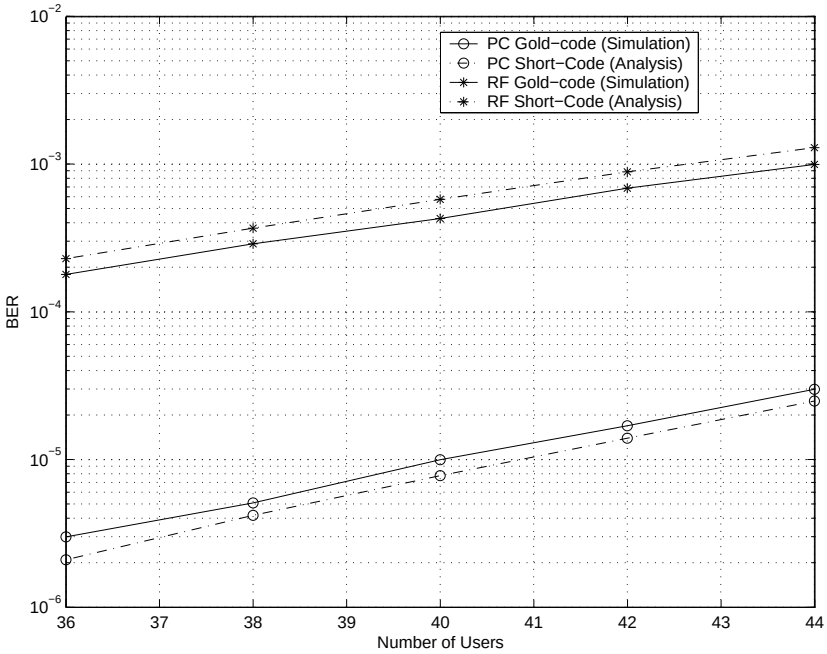

Fig. 3.6: Average BER of asynchronous systems as function of user number, where $N = 63$, $L = 2$ and $\gamma = 13$ dB. PC = perfect power control; RF = Rayleigh fading.

Chapter 4

Analysis of Hard-Limiting Parallel Interference Cancellation (PIC) for Synchronous CDMA Communication

As stated in Chapter 2, the capacity of DS-CDMA is limited by MAI. Among various interference techniques, Parallel Interference Cancellation (PIC) is one of the most efficient interference cancellation (IC) detector. In this chapter, we investigate the performance of hard-limiting PIC. The analysis starts with the two-user case. We find that the performance of purely hard-limiting PIC may not improve after the second stage. We also develop approximate expressions for numerical evaluation of the hard-limiting PIC performance. [1]

4.1 Introduction

Due to the inevitable non-orthogonality among codes, MAI is a major limiting factor to the capacity of CDMA communication systems. Many multiuser detection techniques have been proposed to reduce MAI effects [48],[49]. Among them, parallel interference cancellation (PIC) has received much attention. The main idea of PIC is to regenerate all other users' signals and cancel them from the desired signal at the same time. For better decision quality, multiple stages of PIC are usually considered. Fig. 4.1 shows the

[1] Part of this chapter bas been presented in "Analysis of hard-limiting parallel interference cancellation (PIC) for synchronous CDMA communication," in *Proc. IEEE Int. Symp. Circuits Syst.*, vol. V, pp. 13–16, May 2002.

basic structure of a multistage PIC receiver, where each reconstructor regenerates one user signal.

Several ways exist to regenerate a user's signal. Linear PIC employs linear operations in signal regeneration and MAI cancellation. Analyses of linear PIC are relatively plentiful in the literature. In [5] and [19], it is shown that linear PIC are asymptotically equivalent to the IIR decorrelator for asynchronous CDMA. [28] presents an expression for exact bit error rate (BER) using matrix algebra. An improved Gaussian approximation was developed in [6]. Hard-limiting nonlinear PIC, on the other hand, performs hard decisions to estimate the user data before regenerating the MAI. Though of lower complexity and hence being more practical, its performance is more difficult to analyze due to the nonlinear hard-limiting function.

Gaussian approximation (GA) is usually used in the analysis of BER performance. However, since residual interference after canceling regenerated signal is due to relative small number of users, it cannot be well approximated by Gaussian distributed random variable. This is also pointed out in [14]. Concerning numerical evaluation of the receiver performance, an exact BER (bit error rate) analysis is considered in [71] for asynchronous system. However, the evaluation of the BER requires tedious computation and only numerical tractable for two-user case. We note also that a combination of linear MMSE detector and nonlinear PIC is analyzed in [4]. Though simple and provided a tighter upper bound, the expression is not accurate enough for purely nonlinear PIC. A simpler alternative shedding a deeper insight is thus highly desirable. In this chapter, we analyze the performance of hard-limiting PIC by considering the cross-effect between users. We also provide an analysis for the best performance that hard-limiting PIC can reach.

4.2 System Model

We consider synchronous CDMA employing short-code spreading over ideal channel and assume perfect power control. For initial stage of PIC, interference cancellation is not per-

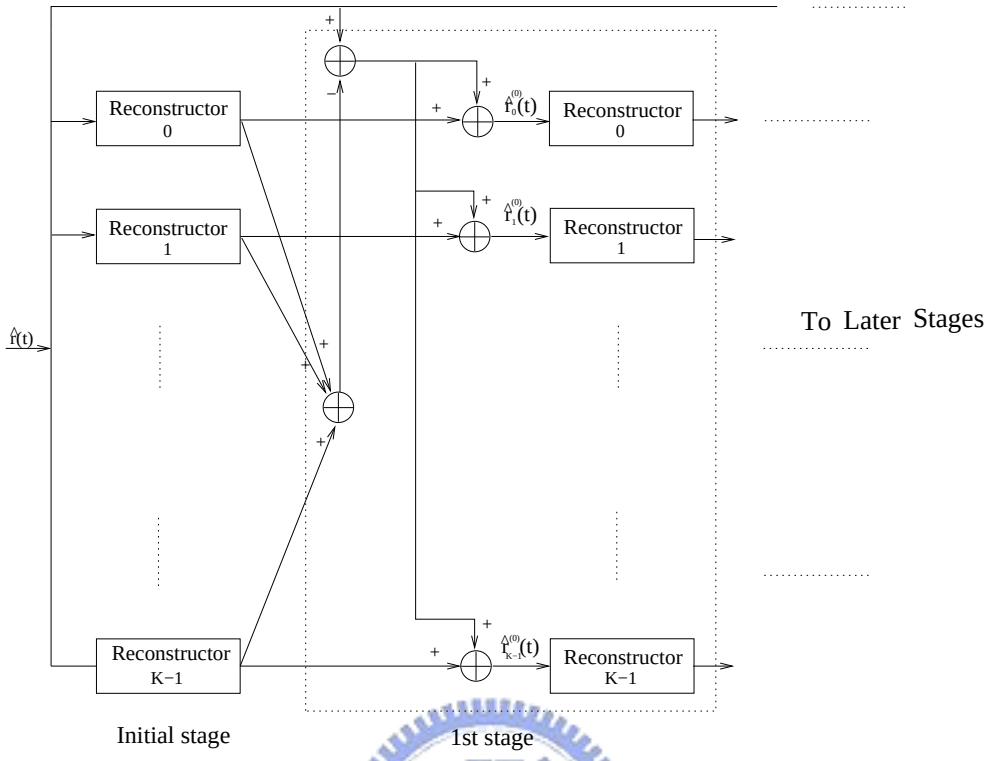

Fig. 4.1: Structure of PIC.

formed and the decision signal is directly obtained through despreading process. Hence, we rewrite the despreading result for user k in (2.13) as

$$y_k^{(0)}[h] = \sqrt{2P}Nb_k[h] + \sqrt{2P}N\sum_{m\neq k} b_m[h]\gamma_{m,k} + \zeta_k[h] \tag{4.1}$$

where $\gamma_{m,k}$ is the normalized zero-shift correlation between the spreading codes of user m and k (which is equal to $R_{k,m}(0)/N$ in (2.13)) and $\zeta_k[h]$ denotes the AWGN term with variance $N \cdot N_0$.

Fig. 4.2 shows the reconstructor used in hard-limiting PIC. The equivalent lowpass signal at reconstructor input for user k at stage v is

$$\hat{r}_k^{(v)}(t) = r(t) - \sqrt{2P}\sum_{m\neq k}\sum_{h=-\infty}^{\infty} \hat{b}_m^{(v-1)}[h]a_m^{(h)}(t - hT_b) \tag{4.2}$$

where $\hat{b}_m^{(v-1)}(n) = \text{sgn}\{y_m^{(v-1)}(n)\}$ is the decision at stage $v-1$. Thus the despread signal at the hard-limiter input for user k is

$$y_k^{(v)}[h] = \sqrt{2P}Nb_k[h]$$

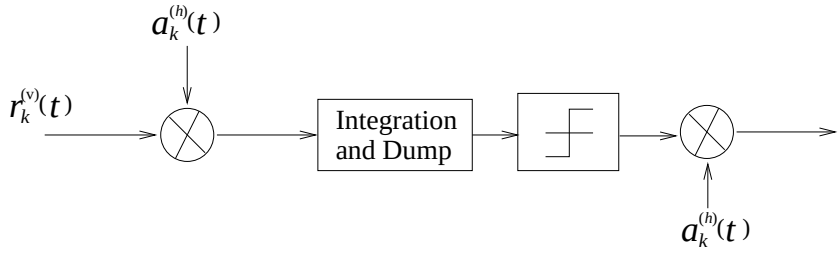

Fig. 4.2: Reconstructor for kth user in stage v.

$$+\sqrt{2P}N\sum_{m\neq k}\left(b_m[n]-\hat{b}_m^{(v-1)}[h]\right)\gamma_{m,k}+\zeta_k[h]. \tag{4.3}$$

For convenience, we drop the time index h in the following.

4.3 Performance Analysis

We present our analysis of the PIC performance in this section. To start, we also describe two analysis methods previously proposed.

4.3.1 Conventional GA Analysis

Conventional analysis like [14] takes the residual interference as Gaussian distributed random variable. Therefore, we only need to evaluate the variance of the residual interference to obtain the expression of BER. Let $P_k^{(v)}$ being the BER of user k at vth stage, the variance of residual interference plus noise term at stage v becomes

$$\sigma_{k,v}^2=2PN^2\sum_{m\neq k}[4P_m^{(v-1)}\cdot E\{\gamma_{m,k}^2\}]+NN_0 \tag{4.4}$$

Therefore, the BER can be easily computed by

$$P_k^{(v)}=Q\left(\frac{\sqrt{2PN^2}}{\sigma_{k,v}}\right). \tag{4.5}$$

Since IC is not performed at initial stage, $\sigma_{k,0}^2$ is a exception of (4.4) and

$$\sigma_{k,0}^2=2PN^2\sum_{m\neq k}E\{\gamma_{m,k}^2\}+NN_0. \tag{4.6}$$

4.3.2 Error Bit Based Analysis

At initial stage, MAI is contributed from many other users and can be well approximated by Gaussian random variable. However, from (4.3), we can find that if the bit error rate at previous stage is small enough, the residual interference is contributed by small number of other symbols. Therefore, Gaussian distributed random variable is not a good approximation for residual interference. Let the vector $\underline{b} = [b_0, \cdots, b_{K-1}]$, and define $\underline{\delta}^{(v)} = [\delta_0^{(v)}, \cdots, \delta_{K-1}^{(v)}] = \underline{b} - \underline{b}^{(v)}$. Though not exactly the same condition, we can modify the expression of BER in [4] for users at vth stage as

$$\begin{aligned} P_k^{(v)} &\cong Q\left(\sqrt{\frac{2PN}{N_0}}\right) \Pr\left(\delta_m^{(v-1)} = 0, m \neq k\right) \\ &+ \sum_{m \neq k} \frac{1}{2} \left[\sum_{b_m \in \{1,-1\}} Q\left(\frac{\sqrt{2PN}(1 + 2\gamma_{m,k} b_m)}{\sqrt{N_0}}\right) \right. \\ &\left. \cdot \Pr\left(\hat{b}_m^{(v-1)} \neq b_m, \delta_i^{(v-1)} = 0, i \neq m, k\right) \right] \\ &\cong Q\left(\sqrt{\frac{2PN}{N_0}}\right) \left(1 - \sum_{m \neq k} P_m^{(v-1)}\right) \\ &+ \sum_{m \neq k} \frac{1}{2} \left[\sum_{b_m \in \{1,-1\}} Q\left(\frac{\sqrt{2PN}(1 + 2\gamma_{m,k} b_m)}{\sqrt{N_0}}\right) \right] P_m^{(v-1)} \end{aligned} \tag{4.7}$$

The first term in the right-hand-side of (4.7) consider the probability of error when tentative decisions are all correct and the second term addresses the probability of error as one tentative decision occurs. Above expression ignores the outcomes when two or more bit decisions are wrong at one stage. This is reasonable since the probability of such condition is small.

4.3.3 Case of Two Users

We begin the analysis by considering the two-user case, and we first derive the BER in the first PIC stage. The initial stage yields, for user 0,

$$\hat{b}_0^{(0)} = \text{sgn}\{\sqrt{2P}Nb_0 + \sqrt{2P}Nb_1\gamma_{1,0} + \zeta_0\} \tag{4.8}$$

and the first stage yields, for user 1,

$$\hat{b}_1^{(1)} = \text{sgn}\{\sqrt{2P}Nb_1 + \sqrt{2P}N[b_0 - \hat{b}_0^{(0)}]\gamma_{0,1} + \zeta_1\}. \tag{4.9}$$

Since the spreading codes are not perfectly orthogonal, the noises ζ_0 and ζ_1 are correlated, with the normalized correlation given by

$$\rho_{0,1} = \rho_{1,0} = \frac{E\{\zeta_0 \cdot \zeta_1\}}{\sqrt{E\{\zeta_0^2\} \cdot E\{\zeta_1^2\}}} = \gamma_{0,1} = \gamma_{1,0} \stackrel{\triangle}{=} \gamma. \tag{4.10}$$

For convenience, let $f_{\zeta_0,\zeta_1}(\cdot,\cdot)$ denote the joint pdf of ζ_0 and ζ_1. Since $\hat{b}_1^{(1)}$ is dependent on the true symbols b_1 and b_0 and the initial decision $\hat{b}_0^{(0)}$, to find the BER for $\hat{b}_1^{(1)}$ we consider the following four conditions separately: (1) $b_1 = b_0 = \hat{b}_0^{(0)}$, (2) $b_1 = b_0 \neq \hat{b}_0^{(0)}$, (3) $b_1 \neq b_0 = \hat{b}_0^{(0)}$, and (4) $b_1 \neq b_0 \neq \hat{b}_0^{(0)}$.

For condition (1), consider only the case $b_0 = 1$, for the case $b_0 = -1$ is complementary. First, note that $\text{Prob}(b_1 = b_0) = \frac{1}{2}$. Next, the condition that $\hat{b}_0^{(0)} = b_0$ is, from (4.8), equivalent to

$$\zeta_0 > -\sqrt{2P}N(1+\gamma). \tag{4.11}$$

Thirdly, the condition that a decision error in $\hat{b}_1^{(1)}$ occurs is, from (4.9), equivalent to

$$\zeta_1 < -\sqrt{2P}N. \tag{4.12}$$

Combining (4.11) and (4.12), the joint probability that condition (1) holds and that a decision error occurs in $\hat{b}_1^{(1)}$ is

$$p_1^{(1)} = \frac{1}{2}\int_{-\infty}^{-\sqrt{2P}N}\int_{-\sqrt{2P}N(1+\gamma)}^{\infty} f_{\zeta_0,\zeta_1}(x_0,x_1)dx_0dx_1. \tag{4.13}$$

Similar analysis for conditions (2)–(4) results in the following joint probabilities:

$$p_2^{(1)} = \frac{1}{2}\int_{-\infty}^{-\sqrt{2P}N(1+2\gamma)}\int_{-\infty}^{-\sqrt{2P}N(1+\gamma)} f_{\zeta_0,\zeta_1}(x_0,x_1)dx_0dx_1, \tag{4.14}$$

$$p_3^{(1)} = \frac{1}{2}\int_{-\infty}^{-\sqrt{2P}N}\int_{-\infty}^{\sqrt{2P}N(1-\gamma)} f_{\zeta_0,\zeta_1}(x_0,x_1)dx_0dx_1, \tag{4.15}$$

$$p_4^{(1)} = \frac{1}{2}\int_{-\infty}^{-\sqrt{2P}N(1-2\gamma)}\int_{\sqrt{2P}N(1-\gamma)}^{\infty} f_{\zeta_0,\zeta_1}(x_0,x_1)dx_0dx_1. \tag{4.16}$$

Putting together, we obtain the unconditional BER of $\hat{b}_1^{(1)}$ as

$$\pi_1^{(1)} = \sum_{i=1}^{4} p_i^{(1)}. \tag{4.17}$$

Note that, by symmetry, $\pi_0^{(1)} = \pi_1^{(1)}$. Further, in MAI-dominant conditions, either $p_4^{(1)} \gg p_3^{(1)} \gg p_1^{(1)} \gg p_2^{(1)}$ or $p_2^{(1)} \gg p_1^{(1)} \gg p_3^{(1)} \gg p_4^{(1)}$, depending on whether $\gamma > 0$ or $\gamma < 0$.

The above analysis gives us a heuristic point that not only the desired user will been affected by other users but also it affects other users' tentative decision. The probabilities of making a wrong decision in different combination is not the same. In (4.7), they are taken as the same thus introduce approximation error.

To simplify the discussion of BER in the later stages, we only discuss the combination of $b_0 = b_1 = 1$ and $\gamma < 0$. Results for other combinations are similar. Figs. 4.3 and 4.4 show the error region for initial and first stage, respectively. Note that $\zeta_0' = \zeta_0/(\sqrt{2P}N)$ and $\zeta_1' = \zeta_1/(\sqrt{2P}N)$ there. Compare these two regions, we can find that the effect of initial stage tentative decision is just to split the original single limiting boundary for ζ_1' (since no tentative decision is involved at initial stage) into two boundaries that one is due to correct tentative decision and the other one is due to wrong tentative decision.

Now consider BER at second PIC stage, We have

$$\hat{b}_1^{(2)} = \text{sgn}\{\sqrt{2P}Nb_1 + \sqrt{2P}N[b_0 - \hat{b}_0^{(1)}]\gamma_{0,1} + \zeta_1\} \tag{4.18}$$

Consider each combination of $\hat{b}_0^{(1)}$ and $\hat{b}_1^{(0)}$, the subset in the (ζ_0', ζ_1')-plane for a erroneous decision of $\hat{b}_1^{(2)}$ is

$$\begin{aligned} &(\zeta_0' > -(1+2\gamma), \zeta_1' < -1) \\ \cup &(\zeta_0' < -(1+2\gamma), \zeta_1' < -(1+\gamma)) \\ \cup &(\zeta_0' < -1, -(1+\gamma) < \zeta_1' < -(1+2\gamma)). \end{aligned} \tag{4.19}$$

Continuing the trace for later stages, we can find that for each stage, the limiting boundaries are all the same as those in previous stages except the limiting boundary for

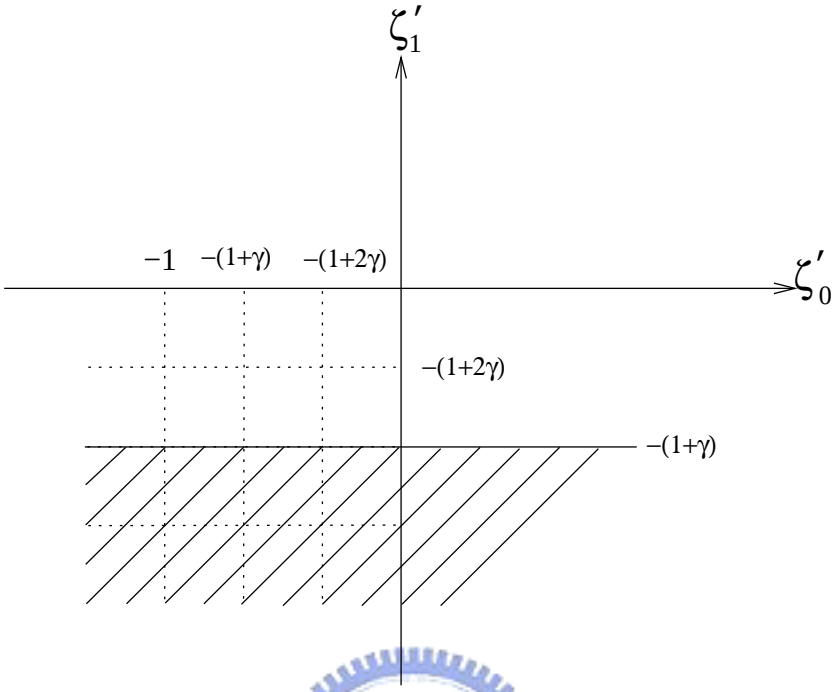

Fig. 4.3: Error region for initial stage PIC.

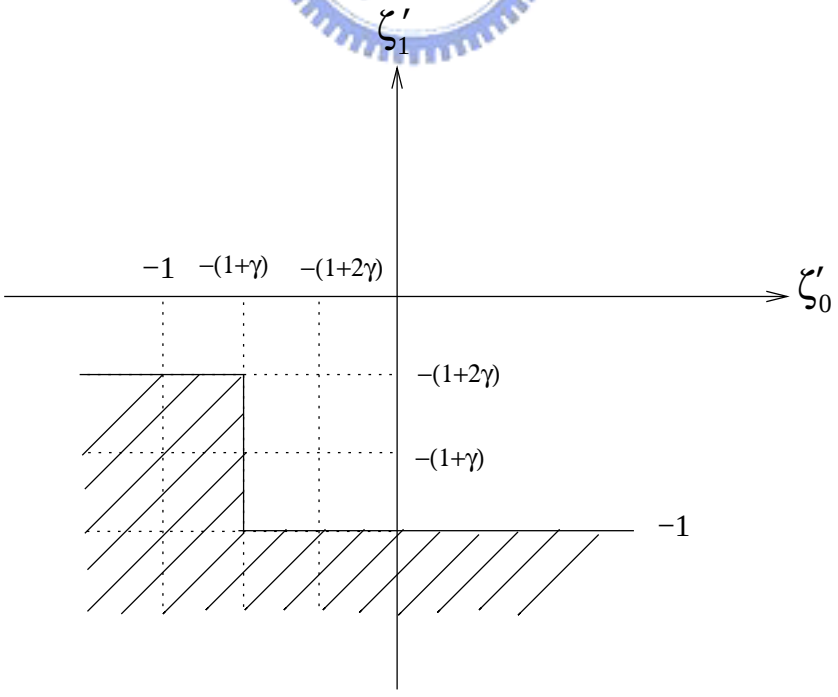

Fig. 4.4: Error region for first stage PIC.

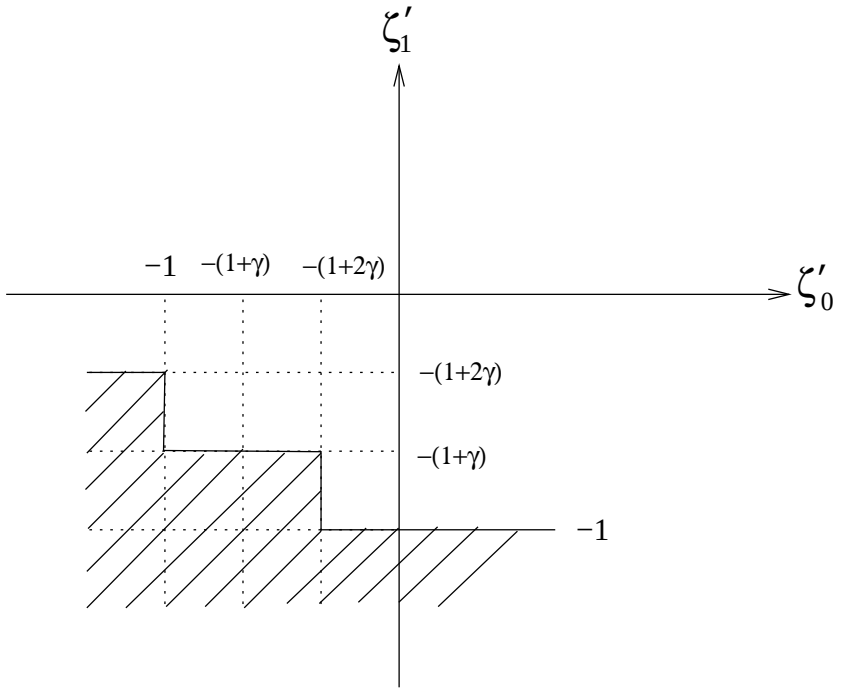

Fig. 4.5: Error region for second stage PIC.

the initial stage is split into two boundaries due to the fact that there is one more stage now. And in the second stage, all possible limiting boundaries have appeared. Thus, we can conclude that after the second stage, no more limiting region added in the (ζ'_0, ζ'_1)-plane. In fact, the error region fluctuates between two shapes but they result in the same BER. Figs. 4.4 and 4.5 show the error region for the first and the second stages, respectively. Compare these two regions, one can easily observe that although different in shape they have the same area. Following this observation, we can further conclude that for the two-user condition, one stage of PIC is enough and more stages provide no more capability of interference cancellation. Although no noise enhancement problem like that in decorrelating detector, hard decision PIC has "strong memory" about previous stages. Therefore, it is still an MAI-limited receiver.

4.3.4 Case of More Than Two Users

Consider the K-dimensional space formed by ζ_k, $k = 0, \cdots, K-1$ and any certain combination of the b_k (e.g., $b_k = 1\ \forall k$). For any k, the space is divided into two regions

such that $\hat{b}_k^{(0)} = b_k$ for ζ_k in one region and $\hat{b}_k^{(0)} \neq b_k$ for ζ_k in the other. For any k and a given combination of $\hat{b}_m^{(v-1)}$, the space is also divided into a region where $\hat{b}_k^{(v)} = b_k$ and a region where $\hat{b}_k^{(v)} \neq b_k$. In the latter condition, since there are 2^{K-1} different combinations of $\hat{b}_k^{(v-1)}$ where $m \neq k$, there are at most 2^{K-1} such "dividing values" for ζ_k. For any v, these values partition the K-dimensional space of ζ_k into a number of cells where each cell corresponds to a particular combination of $\hat{b}_k^{(v)}$. The operation of multistage PIC may be viewed as partitioning of the space into progressively more finely delineated cells and finding out to which partition the user signals should belong. As the number of dividing values in each dimension is finite, the partitioning will cease to change after finite stages of PIC. Like the discussion for two user condition, all limiting boundaries show up at second stage. And for each stage, the only difference in limiting boundaries of previous stage is the splitting of the boundaries due to initial stage into two boundaries. Thus, the partitioning process is fully grown after second stage. Therefore, the performance of hard-limiting PIC will not improve after the second stage. In addition, its performance does not approach the single-user limit.

For numerical evaluation of PIC's BER performance when $K > 2$, an exact analysis considering all possible combinations of data values, like that done in the two-user case, becomes cumbersome. Below we develop a way to evaluate it approximately.

Consider first the situation where BERs are low and the number of simultaneous users is not excessive. Hence the probability of simultaneous decision errors in two or more users' signals at any PIC stage is small. For simplicity, therefore, we may assume that only one user signal may be subject to decision error at any PIC stage and we derive the BER for a second user's signal. Without loss of generality, let them be users 0 and 1. Then in the initial and the first PIC stages, the decisions are again similar to that in (4.8) and (4.9), but now ζ_0 in (4.8) should be replaced by $\hat{\zeta}_0 = \xi_0 + \zeta_0$ where ξ_0 is the MAI given by

$$\xi_0 = \sqrt{2P}N \sum_{m=2}^{K-1} b_m \gamma_{m,0}. \tag{4.20}$$

Notice that the evaluation of (4.15) and (4.16) is computation intensive. We can translate the two-dimensional Gaussian probability integral into two separate integration as mention in [61] to simplify the evaluation. But here we have another simplification for our case as discussed below.

The normalized correlation between $\hat{\zeta}_0$ and $\hat{\zeta}_1$ becomes

$$\rho_{0,1} = \frac{\gamma_{0,1}}{\sqrt{1 + \frac{2PN}{N_0}\sum_{m=2}^{K-1}\gamma_{m,0}^2}}. \tag{4.21}$$

For large SNR, $\rho_{0,1} \approx 0$. In addition, model ξ_0 as Gaussian. Then we obtain the following approximations for $p_i^{(1)}$:

$$\begin{aligned}
p_1^{(1)} &= \frac{1}{2}Q\left(\frac{\sqrt{2P}N(1+\gamma_{0,1})}{\sqrt{NN_0 + E\{\xi_0^2\}}}\right) Q\left(\frac{\sqrt{2PN}}{\sqrt{N_0}}\right), \\
p_2^{(1)} &= \frac{1}{2}Q\left(\frac{\sqrt{2P}N(1+\gamma_{0,1})}{\sqrt{NN_0 + E\{\xi_0^2\}}}\right) Q\left(\frac{\sqrt{2PN}(1+2\gamma_{0,1})}{\sqrt{N_0}}\right), \\
p_3^{(1)} &= \frac{1}{2}Q\left(\frac{\sqrt{2P}N(1-\gamma_{0,1})}{\sqrt{NN_0 + E\{\xi_0^2\}}}\right) Q\left(\frac{\sqrt{2PN}}{\sqrt{N_0}}\right), \\
p_4^{(1)} &= \frac{1}{2}Q\left(\frac{\sqrt{2P}N(1-\gamma_{0,1})}{\sqrt{NN_0 + E\{\xi_0^2\}}}\right) Q\left(\frac{\sqrt{2PN}(1-2\gamma_{0,1})}{\sqrt{N_0}}\right).
\end{aligned} \tag{4.22}$$

The BER at the first stage under the condition that exactly one previous tentative decision error occurs therefore becomes

$$pb_{0,1}^{(1)} = p_2^{(1)} + p_4^{(1)}. \tag{4.23}$$

The above holds for any two users k and m. Therefore, for any user k, the average probability for one decision error in stage 1 can be expressed as

$$P_{one}^{(1,k)} = \sum_{m \neq k} pb_{k,m}^{(1)} \cdot \left[\prod_{i \neq m,k}(1 - P_i^{(0)})\right], \tag{4.24}$$

where $P_i^{(j)}$ denotes the BER of user i's signal in stage j, and the product term in the r.h.s. gives the probability of all other users having correct tentative decisions, And the resultant

BER in stage v accounting for up to one tentative decision error for user k user is

$$P_k^{(v)} = Q\left(\sqrt{\frac{2PN}{N_0}}\right) \cdot \left(1 - \sum_{m \neq k} P_m^{(v-1)}\right) + P_{one}^{(v,k)}. \tag{4.25}$$

Note that after first stage, all other users except the user considered as making wrong tentative decision make correct decisions, thus $\hat{\zeta}_i$ contains no MAI. Since $\hat{\eta}_i$ is different at initial stage and first stage, the integration regions of these two stages are not the same like the case of two users. Therefore, for case of more than two users, one stage cannot provide the same ability of IC as that in second stage like the case in two users condition. In conclusion, two-stage hard-limiting PIC is required for more than two users case.

Though the probability of more than one tentative decision having error is small, it is more likely when the number of users in the system becomes large. The complexity of analyzing the cross-effect between users grows exponentially with the number of users. It is not practical to do the same process like that for one error above. However, we have an observation that since each symbol are affected by more symbols from other users now, the cross-effect between users become small. Therefore, we can neglect the cross-effect and consider the impact of wrong decisions to desired user only. Here, we consider the condition that simultaneously two wrong tentative decisions occur. More simultaneous wrong tentative decisions can be easily extended. Without loss of generality, let user 0 and user 1 be the users with erroneous tentative decisions and user 2 being the desired user. The decision signal at vth stage will become

$$\begin{aligned} \hat{b}_2^{(v)} &= \text{sgn}\{\sqrt{2P}\,(b_2 + 2\gamma_{0,2}b_0 + 2\gamma_{1,2}b_1) + \zeta_2\} \\ &= \text{sgn}\{\sqrt{2P}\,(b_2 + 2\eta_2) + \zeta_2\}. \end{aligned} \tag{4.26}$$

We obtain the approximate average BER due to two decision errors as

$$\begin{aligned} P_{two}^{(v)} = &\sum_{m \neq k} \sum_{n \neq k,m} P_m^{(v-1)} P_n^{(v-1)} \prod_{i \neq m,n,k} (1 - P_i^{(v-1)}) \\ &\cdot \frac{1}{2} E\left\{ Q\left(\frac{\sqrt{2PN}(1 + 2\eta_2)}{N_0}\right) + Q\left(\frac{\sqrt{2PN}(-1 + 2\eta_2)}{N_0}\right)\right\}. \end{aligned} \tag{4.27}$$

4.4 Numerical Results

In this section, we present simulation results to verify the accuracy of our analysis. Synchronous CDMA with random spreading codes is simulated. As different correlation values of $\gamma_{m,k}$ may lead to different BERs, we present the average BERs in each case. It is cumbersome to average corresponding values of (4.25) under each possible combination of $\gamma_{m,k}$, $m \neq k = 0, \cdots, K-1$. In our comparison, we compute the pdf of the cross-correlation between codes and take each $\gamma_{m,k}$ as i.i.d. random variable. Average BERs are thus computed by taking expectation value for the expression over correlation variable. In (4.27), pdf of η_2 are also required, it can be evaluated by convolution of pdfs.

Consider first the two-user case. Fig. 4.6 shows some BER results, where "SF" stands for spreading factor, "GA" stands for Gaussian approximation of MAI, and "Error-bit" stands for error bit based analysis computed by (4.7). We see that (4.17) yields excellent match with the simulation results, while GA grossly underestimates the BERs. It is clear that GA highly underestimates the BERs. And for GA approximation, we only show BERs for SNR less than 10 dB, since BERs are too small for larger SNR.

Consider next the case with 10 users. Fig. 4.7 shows some BER results. Our method, which uses (4.25) and (4.27) to compute the BERs for up to two decision errors and uses (4.22) to compute the conditional error probabilities, provides quite precise predictions. Note that, all of the analyses have worse accuracy as SNR grows. But our analysis provide most modest precision loss among them.

In Fig. 4.8, we present BER over number of users under the condition that SNR = 10 dB and SF = 32. Our analysis has two different kinds of inaccuracy. As user number is small, the inaccuracy is due to the fact that we use (4.22). The other kind of accuracy is generated as user number becomes large. This is because in (4.27), we ignore the cross effect in simultaneous decision errors condition. When user number become large, the probability of simultaneous wrong tentative decisions becomes large. Thus, the inaccuracy reveals as user number becomes large. Though inaccuracy is generated, our analysis

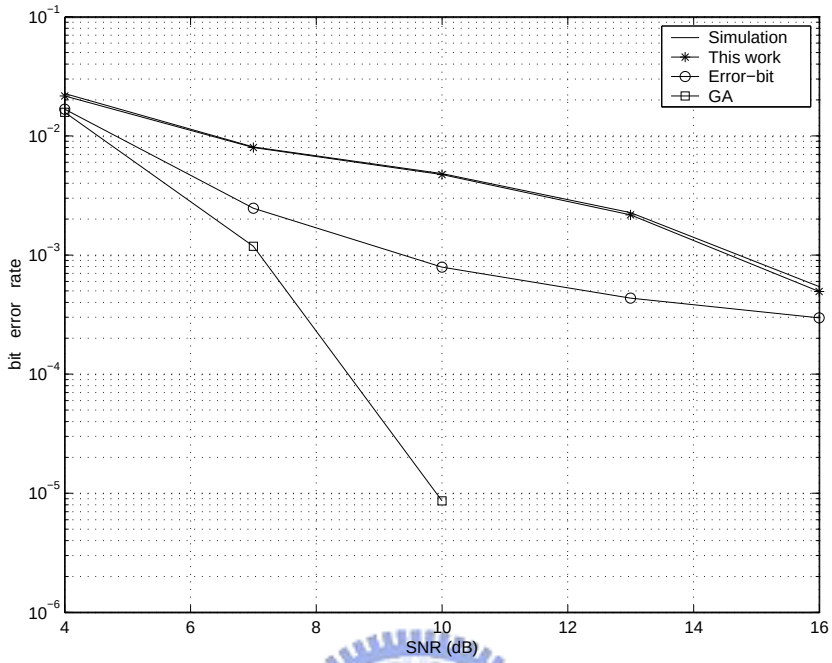

Fig. 4.6: One-stage PIC performance for $K = 2$ with SF = 8.

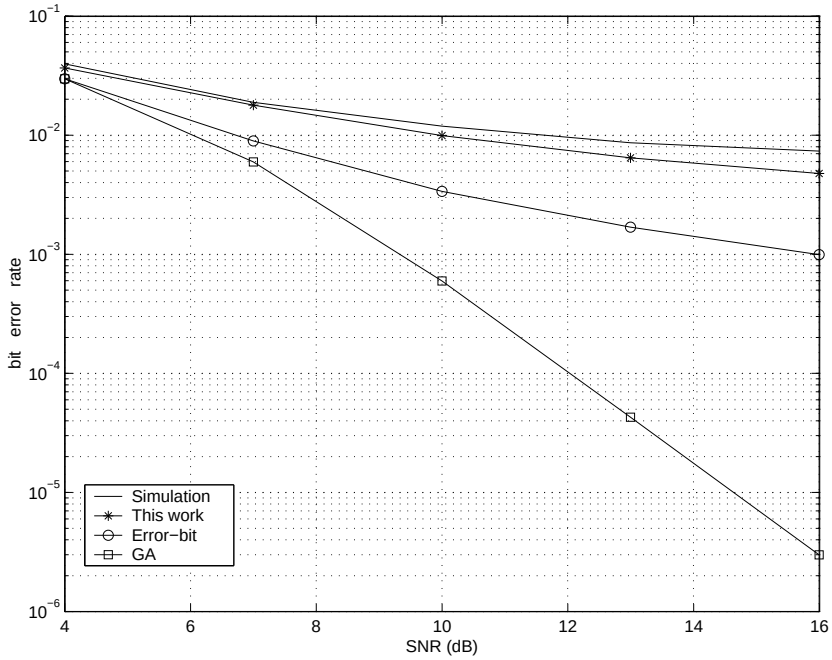

Fig. 4.7: One-stage PIC performance for $K = 10$ with SF = 32.

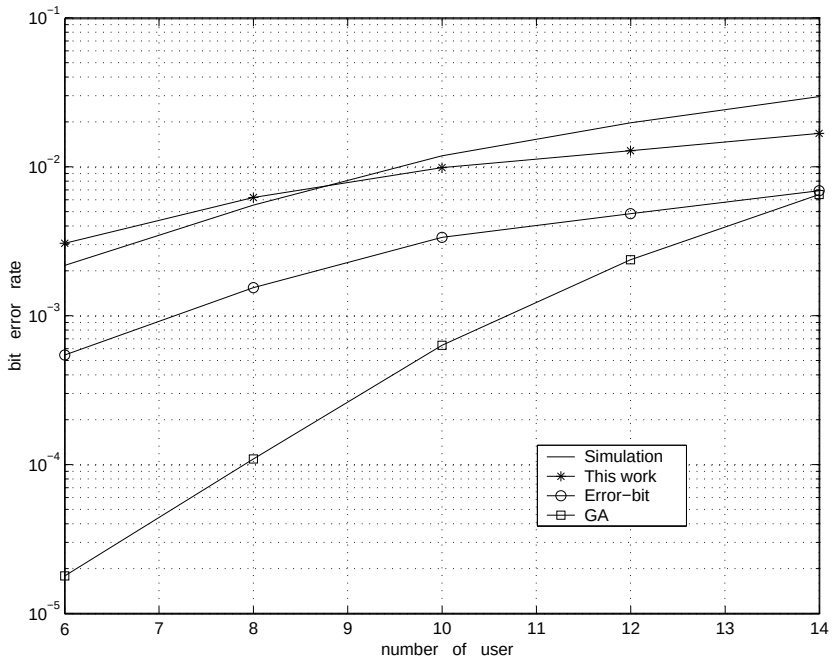

Fig. 4.8: Performance analyses for the first stage at SF = 32 and SNR = 10 dB.

provides relatively high accuracy for the average BER analysis. We also observe that GA is more precise when the user number becomes large, thus the MAI can be better modeled as Gaussian distributed random variable.

Results for second stage are shown in Fig. 4.9. It is shown that conventional analyses, especially GA, cannot provide any information for real performance. However, our analysis again yields relatively close predictions.

Simulations also show that the PIC performance does not improve after the first stage for the two-user case and neither for the more-user case after the second stage.

4.5 Summary

Though not optimal, hard-limiting PIC has modest complexity compared with other advanced PIC structures. In this chapter, we analyzed the performance of hard-limiting PIC in synchronous CDMA. Following our analysis, it can be shown that the performance of hard-limiting PIC may not improve after the second stage. And one stage is enough for the case of two users. By computer simulation, our analysis is shown to be accurate.

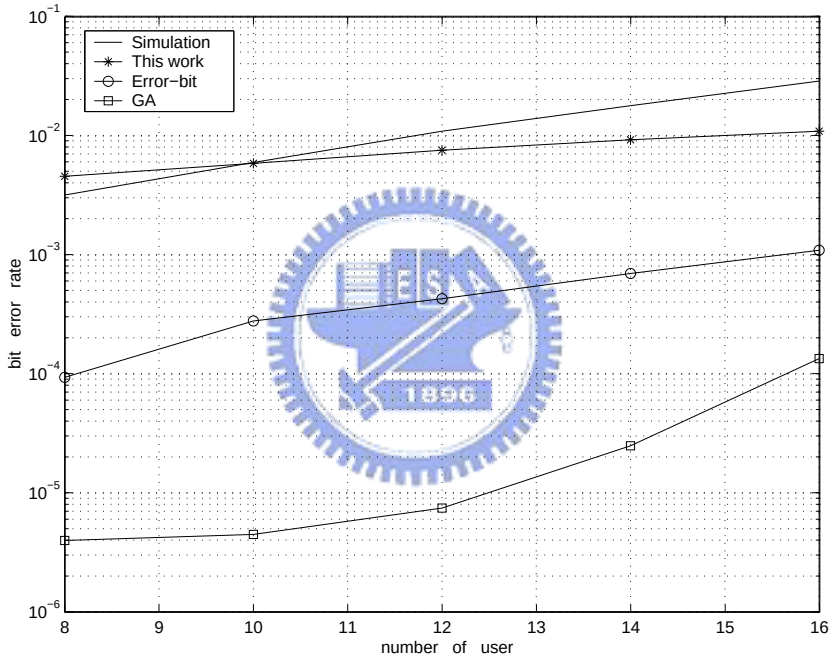

Fig. 4.9: Two-stage PIC performance at SF = 32 and SNR = 10 dB.

Chapter 5

A Chip-Interleaved DS-CDMA System Resistant to Channel Fading

In this chapter, a chip-interleaved DS-CDMA (CIDS-CDMA) system is addressed. By leveraging intra-bit diversity, we show that CIDS-CDMA is resistant to channel fading. Simple analytical results for both uncoded and channel-coded systems under Rayleigh fading channels are presented. The combination of bit- and chip-interleaving is also addressed and compared with conventional DS-CDMA.[1]

5.1 Introduction

In fading channel transmission, the average error performance is dominated by the performance at low SNR. Gain-combining diversity improves the average performance not only by enhancing the average SNR but also by reducing the normalized variance of the signal power. The latter will be termed the power-averaging effect for convenience. In multiple access communication over fading channels, the interference power also fluctuates in time. Proper diversity combining yields the power-averaging effect to both the signal and the interference to result in good diversity gain. Practical coded DS-CDMA systems, by

[1]Part of this chapter has been presented in "Multiple access over fading multipath channels employing chip-interleaving code-division direct-sequence spread spectrum," *IEICE Trans. Commun.*, pp. 114–121, Jan. 2003, "Chip-interleaving for performance improvement of coded DS-CDMA systems in Rayleigh fading channels," in *IEEE 58th Veh. Technol. Conf.*, Oct. 2003, pp. 1323–1327, and "Novel analytical results on performance of bit-Interleaved and chip-interleaved DS-CDMA with convolutional coding," *IEEE Trans. Vech. Technol.*, vol. 54, no. 3, pp. 996–1012, May 2005.

bit interleaving that spaces out the coded bits in a greater time span, effectively exploit the power-averaging effect through time diversity.

Chip-interleaved DS-CDMA (CIDS-CDMA) has been proposed by several research groups recently [25],[27],[63],[64], [69],[70],[80]. Unlike the interleaver used in concatenated coding, the interleaver in CIDS-CDMA is not for scrambling of information bits but for spreading of the chips of one modulated symbol out in time. Thus, it can disperse the effect of bursty noise to more bits and decrease the bit error probability [27],[63],[69], [70],[64]. When applied in multiuser environment, Giannakis *et al.* proposed the use of chip-interleaving and zero-padding to enable MAI-free transmission over multipath channels [80],[81]. Topics related to this direction will be elaborated in next chapter.

In this chapter, however, we consider chip-interleaving a way of leveraging intra-bit diversity in fading channels and theoretically analyze its performance over Rayleigh faded channels. The effect of MAI is also considered. As different interference characteristics may result from difference in the relative fading rates of user signals (which in turn may result from changes in user moving speeds), the transmission performance in this condition is an issue of interest to system design. The analysis of uncoded systems for a simplified channel environment will show that the relative fading rates between the interferes and the desired user signal have impact on the latter's transmission performance. However, the extent of the impact diminishes quickly with increase of the spreading factor or the user number. In the end, the chip-interleaving depth of the desired user signal itself almost single-handedly determines the diversity order and the resulting performance.

We also study the channel coded systems with short- and long-code spreading. [25] provided some numerical results of turbo coded systems in fading channels, but there are no analytical results. Frenger *et al.* [23] briefly touched the performance of coded chip-interleaved systems with long-code spreading. However, they did not address some important operational details of CIDS-CDMA that could have impact on system performance. Hence, it is of interest to examine the performance of coded systems analytically.

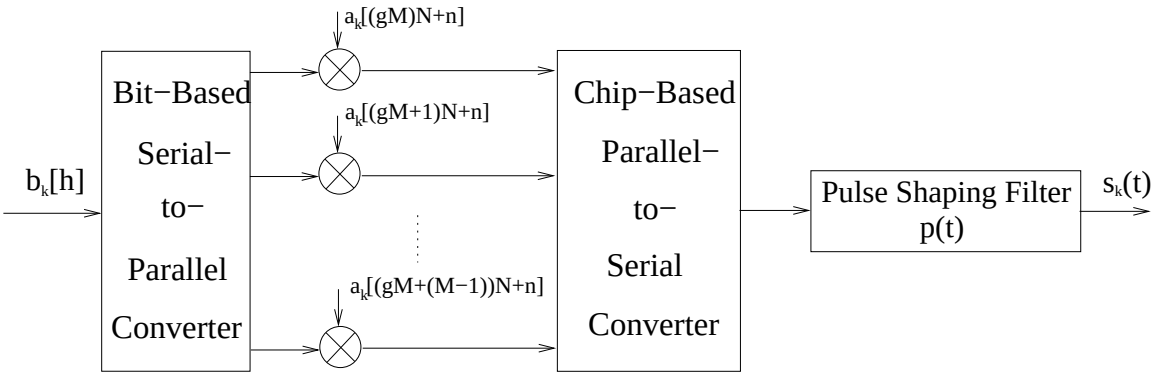

Fig. 5.1: A simple chip-interleaved system.

We consider two kinds of chip interleaving. First, simple CIDS-CDMA considers a set of bits at a time. Similarly indexed chips in the bits are grouped together for transmission. Secondly, combined bit-and-chip interleaving (BCIDS-CDMA) does bit interleaving in addition to chip interleaving. The influence on transmission performance of spreading code periods in both cases is addressed.

5.2 Signal Model

The modulated signal under CIDS-CDMA can be described as follows. For simplicity, assume use of BPSK after spreading. First, information bits are partitioned into blocks. After spreading as in conventional DS-CDMA, the bits in each block are transmitted with their chips interleaved. Figure 5.1 shows a simple CIDS-CDMA transmitter. Therefore, the lowpass-equivalent transmitted signal for the kth user is given by

$$s_k(t) = \sum_{g=-\infty}^{\infty} \sum_{m=0}^{M-1} b_k[gM+m] \sum_{n=0}^{N-1} a_k[gMN+mN+n] \cdot p(t-(gNM+nM+m)T_c), \tag{5.1}$$

where M is the block length or the interleaving depth (in number of bits) and g is the block index. Other parameters are defined as previous. Again, random spreading codes are assumed since they serve well to account for the effect of asynchronous transmission. Figure 5.2 shows an example of the CIDS-CDMA signal at $N = 4$ and $M = 2$ with each thin square denoting one output chip. The meanings of $\alpha_k^{\dagger}[i]$ and T_k will be explained

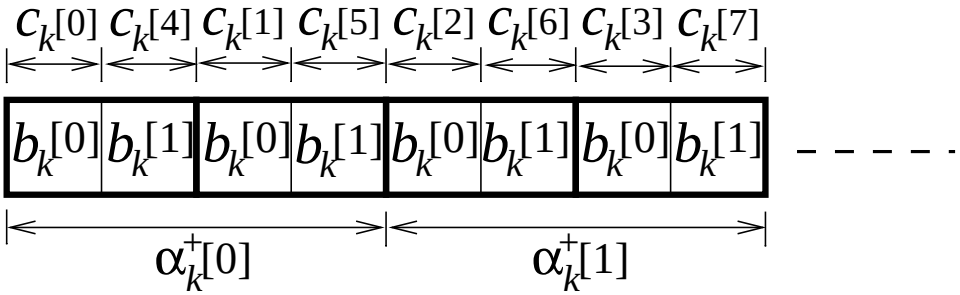

Fig. 5.2: A CIDS-CDMA signal example at $N = 4$, $M = 2$, and $T_k = 4$ chips.

later.

The received signal model used in Chapter 3 is also used here. However, in the following discussion, $\alpha_k[i]$ is used to denote the path coefficient within $[iT_c, (i+1)T_c]$ for the assumption that channel remain unchanged within one chip period.

5.3 Analysis of Synchronous Uncoded Systems

We inspect the performance of uncoded systems first. For ease of illustration, synchronous transmission over flat-fading channels is considered here and the transmission over more complicated channels is addressed in coded systems. Let T_k be the coherence time of the channel associated with user k. A simplified channel model where the fading coefficients are random variables that remain constant for T_k chips but are independent in two different T_k-chip periods is used in the following discussion. Accordingly, we let $\alpha_k[i] = \alpha_k^\dagger[m] = |\alpha_k^\dagger[m]|e^{j\theta_k^\dagger[m]}$ for $i = mT_k \cdots (m+1)T_k$. Figure 5.2 illustrates the situation where $T_k = 4$ chips. Later in some simulations, we will consider the more realistic multipath Rayleigh fading condition and compare the simulation results with analysis.

Without loss of generality, consider the detection of $b_0[0]$. Then the maximum-ratio-combined decision signal for $b_0[0]$ is

$$y_0[0] = \sqrt{2P}b_0[0]\sum_{n=0}^{N-1}\left|\alpha_0^\dagger[\lfloor\frac{nM}{T_0}\rfloor]\right|^2 + \sum_{k=1}^{K-1}\eta_k[0] + \zeta[0], \tag{5.2}$$

where

$$\zeta[0] = \Re\left\{\sum_{n=0}^{N-1}\left(\alpha_0^\dagger[\lfloor\frac{nM}{T_0}\rfloor]\right)^* \cdot a_0[n] \cdot \int_{(nM)T_c}^{(nM+1)T_c} \zeta(t)p(t-nMT_c)dt\right\} \tag{5.3}$$

and $\eta_k[0]$, $k = 1, \cdots, K-1$, is the interference from user k which is given by

$$\begin{aligned}\eta_k[0] &= \sqrt{2P}\cdot\Re\left\{\sum_{n=0}^{N-1} a_0[n]a_k[n]\left(\alpha_0^\dagger[\lfloor\frac{nM}{T_0}\rfloor]\right)^*\alpha_k^\dagger[\lfloor\frac{nM}{T_k}\rfloor]\right\}\cdot b_k[0] \\ &= \sqrt{2P}\cdot\left\{\sum_{n=0}^{N-1}\left|\alpha_0^\dagger[\lfloor\frac{nM}{T_0}\rfloor]\right|\cdot\hat{\alpha}_k^\dagger[\lfloor\frac{nM}{T_k}\rfloor]\right\}\cdot b_k[0] \end{aligned} \tag{5.4}$$

with

$$\hat{\alpha}_k^\dagger[\lfloor\frac{nM}{T_k}\rfloor] \triangleq a_0[n]a_k[n]\left|\alpha_k^\dagger[\lfloor\frac{nM}{T_k}\rfloor]\right|\cos\left(\theta_k^\dagger[\lfloor\frac{nM}{T_k}\rfloor] - \theta_0^\dagger[\lfloor\frac{nM}{T_0}\rfloor]\right). \tag{5.5}$$

Given $\theta_0^\dagger[\lfloor\frac{nM}{T_0}\rfloor]$, $\hat{\alpha}_k^\dagger[\lfloor\frac{nM}{T_k}\rfloor]$ is a Gaussian random variable since $|\alpha_k^\dagger[\lfloor\frac{nM}{T_k}\rfloor]|$ is Rayleigh distributed and $\theta_k^\dagger[n]$ is uniform under the Rayleigh fading assumption. Thus, conditioned on all other quantities in the RHS of (5.4) except $\{\hat{\alpha}_k^\dagger[\lfloor\frac{nM}{T_k}\rfloor]\}$, $\eta_k[0]$ is a combination of Gaussian random variables and hence is Gaussian distributed, too. Therefore, the BER is fully characterized by the Gaussian Q function in the form $Q(\sqrt{\gamma_{\mathrm{u}}})$ where γ_{u} is the SINR. The only remaining problem now is to find the SINR.

5.3.1 Implications of Chip Interleaving Depths of Interferers

Perfect Interleaving

If $M \geq T_k$ (i.e., perfect interleaving for interferer k), then $\lfloor\frac{nM}{T_k}\rfloor \geq n$. Due to the mutual independence among $\{\alpha_k^\dagger[n]\}$ at different n, the conditional variance of $\eta_k[0]$ from taking expectation over $\alpha_k^\dagger[\lfloor\frac{nM}{T_k}\rfloor]$ can be found to be

$$\begin{aligned} E\{\eta_k^2[0]\} &= 2P\left\{b_k^2[0]\sum_{n=0}^{N-1}\left|\alpha_0[\lfloor\frac{nM}{T_0}\rfloor]\right|^2\cdot E\{(\hat{\alpha}_k^\dagger[\lfloor\frac{nM}{T_k}\rfloor])^2\}\right\} \\ &= P\sum_{n=0}^{N-1}\left|\alpha_0^\dagger[\lfloor\frac{nM}{T_0}\rfloor]\right|^2, \end{aligned} \tag{5.6}$$

where the second equality holds since $E\{(\hat{\alpha}_k^\dagger[\lfloor\frac{nM}{T_k}\rfloor])^2\} = 1/2$ due to the assumption that $E\{|\alpha_k(t)|^2\} = 1$. It is interesting to note that, in this case, $E\{\eta_k^2[0]\}$ does not depend on the spreading sequences $a_0[n]$ and $a_k[n]$.

The variance of the noise term can be easily computed as

$$E\{\zeta^2[0]\} = N_0 \sum_{n=0}^{N-1} \left| \alpha_0^\dagger[\lfloor \frac{nM}{T_0} \rfloor] \right|^2 . \tag{5.7}$$

Therefore, if there is perfect interleaving for all the interferers, then the SINR is given by

$$\begin{aligned} \gamma_{\mathrm{u}} &= \frac{2P \left(\sum_{n=0}^{N-1} |\, \alpha_0^\dagger[\lfloor \frac{nM}{T_0} \rfloor]|^2 \right)^2}{(N_0 + (K-1)P) \cdot \left(\sum_{n=0}^{N-1} \left| \alpha_0^\dagger[\lfloor \frac{nM}{T_0} \rfloor] \right|^2 \right)} \\ &= \frac{\sum_{n=0}^{N-1} |\sqrt{2}\, \alpha_0^\dagger[\lfloor \frac{nM}{T_0} \rfloor]|^2}{2N/\gamma + K - 1}, \end{aligned} \tag{5.8}$$

Equation (5.8) can be simplified to different degrees depending on the channel coherence time of user 0 (see Sec. 5.3.2).

Imperfect Interleaving

If $M < T_k$ (i.e., imperfect interleaving for interferer k), then the interleaving depth is not large enough to break the autocorrelation among $\hat{\alpha}_k^\dagger[\lfloor \frac{nM}{T_k} \rfloor]$ at different n. Define $R_k = T_k/M$ and $D_k = N/R_k$, where both R_k and D_k are assumed to be integers for simplicity. Corresponding to (5.4), we have

$$\eta_k[0] = \sqrt{2P} b_k[0] \sum_{n'=0}^{D_k-1} \hat{\alpha}_k^\dagger[n'] \left\{ \sum_{r=0}^{R_k-1} a_0[n'R_k + r] \cdot a_k[n'R_k + r] \left| \alpha_0^\dagger[\lfloor \frac{(n'R_k + r)M}{T_0} \rfloor] \right| \right\}, \tag{5.9}$$

and its conditional variance becomes

$$\begin{aligned} E\{\eta_k^2[0]\} &= 2Pb_k^2[0] \sum_{n'=0}^{D_k-1} E\{\hat{\alpha}_k^{\dagger 2}[n']\} \left(\sum_{r=0}^{R_k-1} a_0[n'R_k + r] a_k[n'R_k + r] \cdot \left| \alpha_0^\dagger[\lfloor \frac{(n'R_k + r)M}{T_0} \rfloor] \right| \right)^2 \\ &= P \sum_{n'=0}^{D_k-1} \left(\sum_{r=0}^{R_k-1} a_0[n'R_k + r] a_k[n'R_k + r] \cdot \left| \alpha_0^\dagger[\lfloor \frac{(n'R_k + r)M}{T_0} \rfloor] \right| \right)^2 , \end{aligned} \tag{5.10}$$

where the first equality is due to the mutual independence among $\{\hat{\alpha}_k^\dagger[n']\}$. Unlike (5.6), the conditional variance is also dependent on $a_0[n]$ and $a_k[n]$. Since random-spreading codes are considered, by the law of large numbers we have

$$\lim_{D_k \to \infty} E\{\eta_k^2[0]\} = P \sum_{n=0}^{D_k-1} \sum_{r=0}^{R_k-1} \left| \alpha_0^\dagger[\lfloor \frac{(n'R_k + r)M}{T_0} \rfloor] \right|^2$$

$$= P \sum_{n=0}^{N-1} \left| \alpha_0^{\dagger}[\lfloor \frac{nM}{T_0} \rfloor] \right|^2 \tag{5.11}$$

with probability one. In other words, when the terms in the RHS of (5.10) are many, the distribution of their sum becomes highly concentrated around the same value as given in (5.6).

For smaller values of D_k, the conditional variance of the interference has a higher probability of deviating from (5.11). Since the BER increases sharply with decrease in SINR, smaller D_k will result in higher average BER than larger D_k. Several conclusions can be drawn from this observation. First, the BER computed using (5.11) gives a lower bound to the average BER. And secondly, note that for a given spreading factor N, a larger D_k implies a smaller $R_k = T_k/M$. Hence an interferer with longer coherence time (lower fading rate) than the interleaving depth will do harm to the desired signal. And the lower the fading rate, the more harm.

For non-integer R_k and D_k, $\eta_k[0]$ has a more complex expression than (5.9). However, (5.11) is still a good approximation to the conditional variance as long as $\lfloor \frac{N}{R_k} \rfloor$ is relatively large. In conclusion, the SINR is lower-bounded by (5.8).

5.3.2 Implications of Chip Interleaving Depth of Interfered User

If $M \geq T_0$ (i.e., perfect interleaving for user 0), then the SINR given in (5.8) can be simplified to

$$\gamma_{\mathrm{u}} = \frac{\chi_{2N}}{2N/\gamma + K - 1}, \tag{5.12}$$

where χ_{2N} is a chi-square random variable of $2N$ degrees (with mean equal to $2N$) due to the Rayleigh fading assumption.

If $M < T_0$, then assuming $R_0 \triangleq T_0/M$ and $D_0 \triangleq N/R_0$ are both integers, the SINR can be simplified to

$$\begin{aligned} \gamma_{\mathrm{u}} &= \frac{R_0}{2N/\gamma + K - 1} \sum_{n=0}^{D_0-1} |\sqrt{2}\, \alpha_0^{\dagger}[n]|^2 \\ &\triangleq \frac{R_0}{2N/\gamma + K - 1} \chi_{2D_0}, \end{aligned} \tag{5.13}$$

where χ_{2D_0} is chi-square of degree $2D_0$. For non-integral D_0, a good approximation is

$$\gamma_{\mathrm{u}} \approx \frac{N/\lfloor \frac{N}{R_0} \rfloor}{2N/\gamma + K - 1} \chi_{2\lfloor \frac{N}{R_0} \rfloor}. \tag{5.14}$$

Comparing (5.13) and (5.12), we see that the influence of an insufficient interleaving depth (lower than the coherence time) for the desired user is a reduction in the diversity order, whereas the mean of the SINR stays at $\frac{2N}{2N/\gamma+(K-1)}$. In fact, this mean SINR is exactly the SINR that one obtains with random spreading codes in static one-path channels.

5.4 Analysis of Synchronous Coded Systems

Next, we consider the performance of CIDS-CDMA with convolutional coding. Due to its simplicity, simple synchronous systems are considered first; the analysis for asynchronous and multipath channels is addressed later. Not to complicate the discussion, the analysis is focused on the case of perfect chip-interleaving.

5.4.1 Simple CIDS-CDMA

Short-Code Spreading

Consider short-code spreading first. The despread signal for bit h of user 0 is given by

$$\begin{aligned} y[h] &= \Re\left\{ \sum_{n=0}^{N-1} \alpha_0^*[i] \int_{iT_c}^{(i+1)T_c} r(t) a_0[n] p(t - iT_c) dt \right\} \\ &= \sqrt{2P} b_0[h] A_0[h] + \sqrt{2P} \sum_{k=1}^{K-1} b_k[h] \beta_k[h] + \zeta[h] \end{aligned} \tag{5.15}$$

where for convenience we let $i = (gMN + m) + Mn$ be the time index of the nth chip of $b_0[h]$ which is the mth bit in the $(g+1)$th data block, that is, $h = gM + m$. The noise term $\zeta[h]$ is given by

$$\zeta[h] = \sum_{n=0}^{N-1} |\alpha_0[i]| a_0[n] \cdot \int_{iT_c}^{(i+1)T_c} \Re\{ e^{-j\theta_0[i]} p(t - iT_c) \zeta(t) \} dt. \tag{5.16}$$

Besides, we have defined

$$A_0[h] = \sum_{n=0}^{N-1} |\alpha_0[i]|^2 \tag{5.17}$$

and

$$\begin{aligned}\beta_k[h] &= \sum_{n=0}^{N-1} |\alpha_0[i]|\{|\alpha_k[i]|\cos(\theta_k[i]-\theta_0[i])a_0[n]a_k[n]\} \\ &\triangleq \sum_{n=0}^{N-1} |\alpha_0[i]|\hat{\alpha}_k[i]. \end{aligned} \tag{5.18}$$

Again, we can show that $\hat{\alpha}_k[i]$ is Gaussian as previous section. Therefore, given the set $\{\alpha_0[i]\}$, $\beta_k[h]$ is also a Gaussian random variable. With perfect chip interleaving, both $A_0[h]$ and $\beta_k[h]$ are composed of N uncorrelated fading coefficients and, therefore, there is an Nth-order diversity for each bit.

With the despread signal given by (5.15), it remains to analyze the channel decoding results. Under convolutional coding, the path metric corresponding to a remerging path distance d is given by

$$\begin{aligned}\sum_{l=1}^{d} y'[l] &= -\sqrt{2P}\sum_{l=1}^{d} A_0'[l] + \sqrt{2P}\sum_{k=1}^{K-1}\sum_{l=1}^{d} b_k'[l]\beta_k'[l] + \sum_{l=1}^{d}\zeta'[l] \\ &\triangleq -\sqrt{2P}\sum_{l=1}^{d} A_0'[l] + \eta_{ci} + \zeta_{ci} \end{aligned} \tag{5.19}$$

where, again, the superscript $'$ has been used to simplify the notation because these d bits may not be consecutive in time. Assume that the d bits are contained in one chip-interleaving block. This will be the case most of the time when the chip-interleaving depth M is much larger than the time period spanned by the d bits. Then similarly indexed chips in these bits will experience similar fading because they are grouped together after chip interleaving. Let $\{\alpha_k^{\dagger}[n], n = 0, \cdots, N-1\}$ denote the N fading coefficients for user k associated, one each, with the N groups of interleaved chips of these bits. Then we can rewrite $A_0'[l] = \sum_{n=0}^{N-1} |\alpha_0^{\dagger}[n]|^2 = A_0'$ and $\beta_k'[l] = \sum_{n=0}^{N-1} |\alpha_0^{\dagger}[n]|\hat{\alpha}_k^{\dagger}[n] = \beta_k'$, which are independent of l. Thus

$$\eta_{ci} = \sqrt{2P}\sum_{k=1}^{K-1}\left\{\beta_k'\sum_{l=1}^{d} b_k'[l]\right\}. \tag{5.20}$$

Given $\{\alpha_0^{\dagger}[n]\}$ and $\{b_k'[l]\}$, by conditional Gaussianness of $\beta_k[h]$, η_{ci} is a combination of Gaussian random variables and is also Gaussian distributed. Accordingly, the pair-

wise error probability for the remerging path at distance d is given exactly by $P(d) = Q\left(\frac{\sqrt{2P}dA'_0}{\sqrt{E\{\eta_{ci}^2\}+E\{\zeta_{ci}^2\}}}\right) \triangleq Q(\sqrt{\gamma_{CIs}})$.

The variance of the additive noise can be found to be

$$E\{\zeta_{ci}^2\} = d \cdot \left(N_0 \sum_{n=0}^{N-1} |\alpha_0^\dagger[n]|^2\right). \tag{5.21}$$

Conditioned on a set of $b'_k[l]$ and $\alpha_0^\dagger[n]$, the variance of η_{ci} can be computed as

$$\begin{aligned} E\{\eta_{ci}^2\} &= 2P \sum_{k=1}^{K-1} \left\{ E\{\beta_k'^2\} \left[\sum_{l=1}^{d} b'_k[l]\right]^2 \right\} \\ &= P \sum_{k=1}^{K-1} \sum_{n=0}^{N-1} |\alpha_0^\dagger[n]|^2 \left[\sum_{l=1}^{d} b'_k[l]\right]^2 \\ &= P \cdot \left\{\sum_{n=0}^{N-1} |\alpha_0^\dagger[n]|^2\right\} \cdot \left\{\sum_{k=1}^{K-1} B_k'^2\right\}, \end{aligned} \tag{5.22}$$

where $B_k'^2 \triangleq (\sum_{l=1}^{d} b'_k[l])^2$ and the second equality holds since $E\{\hat{\alpha}_k^{\dagger 2}[n]\} = 1/2$ by the assumption that $E\{|\alpha_k(t)|^2\} = 1$. Consequently, the conditional SINR is given by

$$\begin{aligned} \gamma_{CIs} &= \frac{2dN}{K-1} \frac{\left[\sum_{n=0}^{N-1} |\sqrt{2}\alpha_0^\dagger[n]|\right]^2 / 2N}{\left[\sum_{k=1}^{K-1} (B'_k/\sqrt{d})^2 + 2N/\gamma\right] / (K-1)} \\ &\triangleq \frac{2dN}{K-1} F_{CIs}. \end{aligned} \tag{5.23}$$

Since γ_{CIs} depends on $\{\alpha_0^\dagger[n]\}$ and $\{b'_k[l]\}$, $P(d)$ is a conditional error probability. To get the unconditional pairwise error probability, we need the distribution of γ_{CIs}. When d is large, B'_k can be approximated as Gaussian. Then F_{CIs} is $F(2N, K-1, 2N/\gamma)$ distributed.

Long-Code Spreading

Now consider long-code spreading. Under it,

$$\beta_k[h] = \sum_{n=0}^{N-1} \Re\{\alpha_0^*[i]\alpha_k[i]a_0[hN+n]a_k[hN+n]\}. \tag{5.24}$$

Unlike short-code systems, even though the fading coefficients associated with each bit in the remerging path are the same, the corresponding $\beta'_k[l]$ is still a function of l because the spreading codes for different bits are different. The MAI is then given by

$$\eta_{ci} = \sqrt{2P} \sum_{k=1}^{K-1} \left\{ \sum_{l=1}^{d} \beta'_k[l] b'_k[l] \right\}. \tag{5.25}$$

By the assumed independence among $\beta'_k[l]$ for different k and l, its conditional variance is

$$E\{\eta_{ci}^2\} = 2P \sum_{k=1}^{K-1} \sum_{l=1}^{d} E\{\beta'^2_k[l]\} = P(K-1)d \cdot \sum_{n=0}^{N-1} |\alpha_0^\dagger[n]|^2. \tag{5.26}$$

The conditional SINR is thus

$$\gamma_{CIl} = \frac{d}{(K-1)+2N/\gamma} \cdot \sum_{n=0}^{N-1} |\sqrt{2}\alpha_0^\dagger[n]|^2 \triangleq \frac{d}{(K-1)+2N/\gamma} \chi_{2N} \tag{5.27}$$

where χ_{2N} is the sum-square value of $2N$ independent Gaussian random variables and therefore follows χ^2 distribution of degree $2N$. So the use of long code breaks the dependence of SINR on $\{b'_k[l]\}$.

In this case, we can obtain a closed-form expression for the unconditional pairwise error probability as [56, p. 781]

$$\begin{aligned} P_{CIl}(d) &= \int_0^\infty Q\left(\sqrt{\frac{d \cdot \chi_{2N}}{(K-1)+2N/\gamma}}\right) f_{chi}(\chi_{2N}) d\chi_{2N} \\ &= \left[\frac{1}{2}\left(1 - \sqrt{\frac{d}{d-1+K+2N/\gamma}}\right)\right]^N \\ &\quad \cdot \sum_{r=0}^{N-1} \binom{N-1+r}{r} \left[\frac{1}{2}\left(1 + \sqrt{\frac{d}{d-1+K+2N/\gamma}}\right)\right]^r. \end{aligned} \tag{5.28}$$

Moreover, when N is large, the PDF of χ_{2N} becomes concentrated about its mean. In this condition, $\sum_{d=d_{free}}^{\infty} \beta_d \cdot P_{CIl}(d)$ will be an accurate expression for the BER (cf. discussion about (3.18)).

5.4.2 Bit-and-Chip-Interleaved DS-CDMA

In simple CIDS-CDMA, since the fading coefficients remain unchanged within a section of M interleaved chips, the signal strength is the same for all the bits in one interleaved

block. Hence these bits fade together, albeit to a smaller extent thanks to the diversity gain from chip interleaving. For a coded system, this is undesirable because the bits are degraded in bursts to the detriment of the system's error-correcting capability. Consequently, bit interleaving is also beneficial in coded CIDS-CDMA systems for diversity over the bits in a decoding delay under convolutional coding (or over the bits in a codeword under block coding). We use the shorthand BCIDS-CDMA to denote a system with both bit and chip interleaving, keeping CIDS-CDMA for a system without bit interleaving.

Again, we first examine the case of short-code spreading. With perfect bit interleaving, the sets of N fading coefficients associated with successive coded bits are different. Under convolutional coding, therefore, there are dN uncorrelated fading coefficients for each user in computing the path metric. Re-define $\{\alpha_k^\dagger[n], n = 0, \cdots, dN-1\}$ as these dN independent fading coefficients for user k's signal and rewrite $A_0'[l] = \sum_{n=0}^{N-1} |\alpha_0^\dagger[lN+n]|^2$ while $\beta_k'[l] = \sum_{n=0}^{N-1} |\alpha_0^\dagger[lN+n]|\hat{\alpha}_k^\dagger[lN+n]$. Given $\{\alpha_0^\dagger[n]\}$ and $\{b_k'[l]\}$, η_{ci} is Gaussian distributed and its conditional variance is

$$E\{\eta_{ci}^2\} = 2P\sum_{k=1}^{K-1}\sum_{l=1}^{d} E\{\beta_k'^2[l]\} = P(K-1)\sum_{n=0}^{dN-1} |\alpha_k^\dagger[n]|^2. \tag{5.29}$$

The difference between (5.29) and (5.26) resides in the number of uncorrelated fading coefficients, which is equal to dN in the presence case. Similarly, the noise variance is obtained as

$$E\{\zeta_{ci}^2\} = N_0 \sum_{n=0}^{dN-1} |\alpha_k^\dagger[n]|^2. \tag{5.30}$$

Therefore, the conditional pairwise sequence error probability is determined by the SINR

$$\gamma_{BCI} = \frac{1}{(K-1)+2N/\gamma} \cdot \sum_{n=0}^{dN-1} |\sqrt{2}\alpha_0^\dagger[n]|^2 \triangleq \frac{\chi_{2dN}}{(K-1)+2N/\gamma}, \tag{5.31}$$

where χ_{2dN} is χ^2-distributed with $2dN$ degrees. In summary, the joint bit-and-chip interleaving effects a diversity order equal to the product of the spreading factor and the free distance of the convolutional code.

Usually, we expect $dN \gg 1$, which may cause some computational difficulty if we evaluate the unconditional pairwise error probability by a way similar to (5.28). An alternative in this case is given by [3, App. 7.1]

$$\int_0^\infty Q\left(\sqrt{\frac{\chi_{2dN}}{(K-1)+2N/\gamma}}\right) f_{chi}(\chi_{2dN})d\chi_{2dN}$$
$$= \frac{1}{2} - \frac{1}{2\sqrt{K+2N/\gamma}}\left[1 + \sum_{r=1}^{dN-1} \frac{(2r-1)!!}{(2r)!!}\frac{(K-1+2N/\gamma)^r}{(K+2N/\gamma)^r}\right]. \quad (5.32)$$

Note that our chip-interleaving scheme in Fig. 5.1 can be viewed as a row-input, column-output block interleaver of size $M \times N$. In [23], a single interleaver following the spreading function is used to interleave the output chips. For convenience, call it direct CIDS-CDMA. Let τ_c be the coherence time (in number of chips) of the fading channel. From earlier discussion, a good interleaver size to obtain sufficient intra-bit diversity in CIDS-CDMA is $\tau_c \times N$. To fully exploit the inter-bit diversity under convolutional coding, the block size of the bit interleaver in BCIDS-CDMA should be about $\tau_c \times D$ where D is the Viterbi decoding delay. A typical choice of D is $5L$ where L is the constraint length of the code. With BCIDS-CDMA, therefore, the combined interleaver size is $\tau_c \times (N + 5L)$. In contrast, direct CIDS-CDMA needs an interleaver of size $\tau_c \times 5LN$ to attain the same performance. BCIDS-CDMA is thus more efficient in terms of implementation.

Moreover, in [23], long codes are used. However, from the above analysis, we can see that long-code spreading has no advantage in perfectly interleaved BCIDS-CDMA. In conventional BIDS-CDMA, the role of long-code spreading is to vary the correlation among different user's bits over the decoding delay in convolutional coding (or over the length of a codeword in block coding). In perfectly interleaved BCIDS-CDMA, an equivalent effect is achieved by causing the interfering bits from different users to be associated with independent fading coefficients via bit interleaving.

5.4.3 Summary

Table 5.1 summarizes the conditional SINRs that govern the pairwise sequence error probabilities in Rayleigh fading channels for different systems, including the counterpart of BIDS-CDMA discussed in Chapter 3, in the interference-limited situation, where F_{ν_1,ν_2} denotes a random variable that observes the (ν_1, ν_2)-degree F distribution. In this situation, the corresponding average SINRs (or SIRs to be more exact) have simple mathematical expressions, which are also given in the table. Note that, when K is large (i.e., when there are many users), the average SIRs are nearly the same and are exactly or approximately equal to $\frac{2dN}{K-1}$, which is the SIR of long-code BIDS-CDMA in perfectly power-controlled channels. The difference among the systems consists in the difference in distribution of the conditional SIRs, which reflects the difference in the diversity orders that they exploit.

The above difference can be further appreciated by examining the outage probability in each case, which is the probability that the desired user cannot attain the target performance. Figure 5.3 shows the theoretical cumulative distribution functions (CDFs) of the pairwise error probabilities of different systems in Rayleigh fading at $N = 32$, $d = 10$, and $K = 20$, in interference-limited operation. The BCIDS-CDMA has very sharp slopes in the CDF curve, which means that it behaves much like transmission over an unfaded channel although the channel is actually subject to fading. Take 10^{-8} as the target pairwise error probability, for example. The outage probability is 0.12 for BCIDS-CDMA, whereas it is 0.36 for long-code CIDS-CDMA and 0.44 for long-code BIDS-CDMA. This further demonstrates that BCIDS-CDMA has the best performance.

Table 5.1: SINRs That Govern Pairwise Sequence Error Probabilities in Rayleigh Fading Channels for Different Systems Under Interference-Limited Operation

System	Conditional SIR	Average SIR
Short-code BIDS-CDMA	$\frac{2dN}{K-1}F_{2d,K-1}$	$\frac{2dN}{K-1}\frac{K-1}{K-3}$
Long-code BIDS-CDMA	$\frac{2dN}{K-1}F_{2d,d(K-1)}$	$\frac{2dN}{K-1}\frac{d(K-2)}{d(K-1)-2}$
Short-code CIDS-CDMA	$\frac{2dN}{K-1}F_{2N,K-1}$	$\frac{2dN}{K-1}\frac{K-1}{K-3}$
Long-code CIDS-CDMA	$\frac{d}{K-1}\chi_{2N}$	$\frac{2dN}{K-1}$
BCIDS-CDMA	$\frac{\chi_{2dN}}{K-1}$	$\frac{2dN}{K-1}$

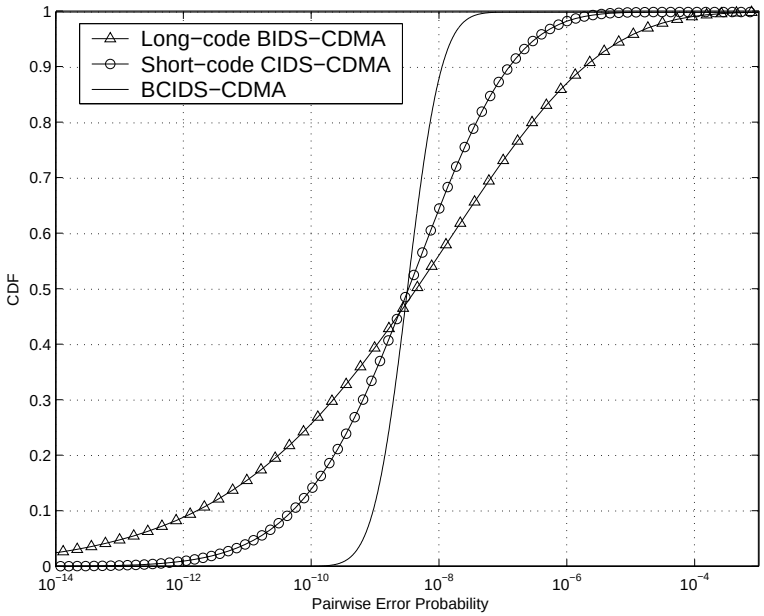

Fig. 5.3: CDFs of pairwise error probability of different DS-CDMA schemes in Rayleigh fading at $N = 32$, $d = 10$, and $K = 20$, under interference-limited operation.

5.5 Analysis of Coded Systems over Asynchronous and Multipath Channels

With the results for synchronous systems, it is easy to analyze the influence of asynchronism and multipath channels. As before, let the received signal be given by

$$r(t) = \sqrt{2P}\sum_{k=0}^{K-1}\sum_{l_p=0}^{L_p-1}\alpha_k^{(l_p)}(t)s_k(t-(\tau_k+l_p)T_c)+\zeta(t) \tag{5.33}$$

with $E\{|\alpha_k^{(l_p)}(t)|^2\} = 1/L_p$. And let τ_k, $k \neq 0$, be integers that are independent and uniformly distributed over $[0, NM-1]$. Further, we assume use of a rake receiver with

L_p fingers.

As disclosed by (5.20), the performance of short-code CIDS-CDMA is related to the combination of the interfering bits within the remerging path. Consequently, for asynchronous transmission over multipath channels, the number of bit combinations is altogether increased $2(2L_p-1)$ times similarly as discussed for short-code BIDS-CDMA in Sec. 3.3. Likewise, it has similar SINR expression to short-code BIDS-CDMA and can be written as

$$\gamma_{CIs}^{r} = \frac{2dN(2L_p-1)}{K(2L_p-1)-1} F_{CIs} \tag{5.34}$$

where F_{CIs} is $F(2NL_p, 2[K(2L_p-1)-1], 4N(2L_p-1)/\gamma)$ distributed.

For long-code CIDS-CDMA and BCIDS-CDMA, neither the code correlation properties nor the data bit combinations affect the performance. The only difference between these two systems is the diversity order. Mathematically, the interference from user k can be expressed as

$$\eta_k[h] = \sum_{l_p=0}^{L_p-1} \sum_{l_p'=0}^{L_p-1} \beta_k^{(l_p,l_p')}[h] \tag{5.35}$$

where

$$\begin{aligned} \beta_k^{(l_p,l_p')}[h] &= \sum_{n=0}^{N-1} b_k[h'] \Re\{(\alpha_0^{(l_p)}[i])^* \alpha_k^{(l_p')}[i] a_0[hN+n] a_k[h'N+n']\} \\ &\triangleq \sum_{n=0}^{N-1} |\alpha_0^{(l_p)}[i]| |\hat{\alpha}_k^{(l_p,l_p')}[i], \end{aligned} \tag{5.36}$$

with h' and n' denoting the bit and the chip indexes of the interfering signal at bit h and chip n of the interfered signal. The form of $\beta_k^{(l_p,l_p')}[h]$ is quite similar to (5.24) except that here we have kept the interfering bits $b_k[h']$ inside the summation rather than having it outside as in (5.25). This is because in asynchronous or multipath channels, we may have two bits interfering two different sections of the desired bit. Given $\{|\alpha_0^{(l_p)}[i]|\}$, $\hat{\alpha}_k^{(l_p,l_p')}[i]$ are Gaussian variables which are independent of l_p and l_p'. Without bit interleaving, we have, thanks to the use of long codes,

$$\sum_{l=1}^{d} E\{\eta_k'^2[l]\} = \sum_{l=1}^{d} \sum_{l_p=0}^{L_p-1} \sum_{l_p'=0}^{L_p-1} \sum_{n=0}^{N-1} |\alpha_0^{\dagger(l_p)}[n]|^2 \cdot E\{(\hat{\alpha}_k^{\dagger(l_p,l_p')}[n])^2\}$$

$$= \frac{d}{2}\sum_{l_p=0}^{L_p-1}\sum_{n=0}^{N-1}|\alpha_0^{\dagger(l_p)}[n]|^2 \tag{5.37}$$

where $\alpha_k^{\dagger(l_p)}[n]$, $n = 0, \cdots, N-1$, denote the N fading coefficients associated with the kth user's l_pth path within the remerging distance.

Employing similar arguments, we can derive the conditional variance of IPI as

$$\sum_{l=1}^{d} E\{\eta_{IPI}^{t2}[l]\} = \frac{d(L_p-1)}{2L_p}\sum_{l_p=0}^{L_p-1}\sum_{n=0}^{N-1}|\alpha_0^{\dagger(l_p)}[n]|^2. \tag{5.38}$$

The SINR is thus obtained as

$$\begin{aligned}\gamma_{CIl}^r &= \frac{2d^2\left(\sum_{l_p=0}^{L_p-1}\sum_{n=0}^{N-1}|\alpha_0^{\dagger(l_p)}[n]|^2\right)}{d(K-1)+d(L_p-1)/L_p+\frac{2dN}{\gamma}} \\ &\triangleq \frac{d}{KL_p-1+\frac{2NL_p}{\gamma}}\chi_{2NL_p}.\end{aligned} \tag{5.39}$$

With similar deviation, we easily come to

$$\gamma_{BCI}^r = \frac{\chi_{2NdL_p}}{KL_p-1+\frac{2NL_p}{\gamma}} \tag{5.40}$$

as the SINR for BCIDS-CDMA.

5.6 Numerical Results and Discussion

In this section, we compare the performance of different interleaving schemes by way of computer simulation. We also compare the simulation results with analysis. The simulation results are obtained through 10^3 simulation runs, where in each run the spreading codes of the users and channel coefficients are generated randomly.

5.6.1 Uncoded Systems

From the above analysis, what affects the BER performance is T_k/M, not the individual values of T_k and M. Thus, in the simulation, we set their individual values small for simplicity. Flat fading channel is assumed here. Below we first consider the simple

block-static fading channel model. Then we consider the more realistic case of Rayleigh fading channels.

Figure 5.4 examines the influence of the interferer's coherence time on the desired user's BER performance in the case of two users under block-static fading. We let each user's interleaving depth M be equal to the corresponding coherence time T_k and spreading factor M is 8. The coherence time of user 0 is $T_0 = 1$ whereas that of user 1, viz. T_1, varies from 1 to 8. The simulation results confirm the theoretical prediction that the faster-faded user 0 signal has a worse BER performance, and the performance difference increases with increasing T_1. On the other hand, also as theoretically predicted, the BER performance of the slower-faded user 1 signal remains constant irrespective of its fading rate. Note that with more users, the law of large numbers should have a more pronounced effect so that the performance disparity will diminish.

Now we consider a more realistic channel condition, where the sum-of-sinusoids statistical model for Rayleigh fading proposed in [79] is simulated. Let there be six users with maximum Doppler shifts $f_k = 222, 222, 111, 111, 55.56$, and 55.56 Hz, respectively. (At a carrier frequency of 2 GHz, for example, they correspond to three moving speeds of 120, 60, and 30 kmph, respectively.) Let the chip rate be 1.2288 Mcps, the spreading factor $N = 64$, and SNR $= 16$ dB. We first examine the simulation results. Then we compare them against the theory.

The solid lines in Fig. 5.5 depict the simulation results. Each line gives the average performance of the two users at the same speed. Note that the neighboring curves are offset from each other horizontally by a factor of 2 approximately. Therefore, the results evidently show that the performance only depends on the ratio of the desired user's own fading rate to its interleaving depth, which controls the diversity order the desired user can get. To compare the simulation results with the theory, we need to define coherence time in this context. While for some other applications a suitable definition is $0.423/f_k$ [59, p. 166], we find it yielding over-pessimistic estimates. A definition based on a time

correlation value $J_0(\pi f_k T_k) = 0.8$, or equivalently $T_k = 0.293/f_k$, yields better-matched estimates. At a chip rate of 1.2288 Mcps, this definition gives $T_k = 1622, 3244$, and 6480 for $f_k = 222$, 111, and 55.56 Hz, respectively. The theoretical estimates are shown in dashed lines in Fig. 5.5. They are quite accurate in the shapes of the curves compared to simulation, for larger interleaving depths and for higher maximum Doppler shifts. For smaller interleaving depths and lower maximum Doppler shifts, CIDS-CDMA can achieve greater diversity gains than theoretically predicted from the simplified channel model.

5.6.2 Coded Systems

The rate-1/2 convolutional code of constraint length 7 with generators $g_1 = 133_8$ and $g_2 = 171_8$ is used in all simulations. And we employ soft-decision Viterbi decoding with traceback length $= 5 \cdot 7 = 35$.

Perfectly Interleaved Transmission

To simulate perfect chip-interleaving condition, we let each chip-block be subject to independent channel gains. The chip-interleaving depth, M, is set as 256. Since we have the traceback length $35 \ll 256$, the symbols within the remerging path will be subject to the same set of channel coefficients as the assumption made for the analysis. For the simulation of BCIDS-CDMA, a bit-interleaver of size 256×64 is applied.

To start, figure 5.6 compares the performance of synchronous CIDS-CDMA systems in Rayleigh fading, at $N = 16$ and $\gamma = 16$ dB. Clearly, BCIDS-CDMA is by far the best. And long-code CIDS-CDMA is better than short-code. The theoretical analysis agrees well with the simulation results. The performance of asynchronous CIDS-CDMA over multipath channels is shown in fig. 5.7. It is seen form the figure that with increased multipath number, CIDS-CDMA has improved performance while BCIDS-CDMA is insensitive to the path number.

Figure 5.8 compares the results for several long-code systems in fading channels with

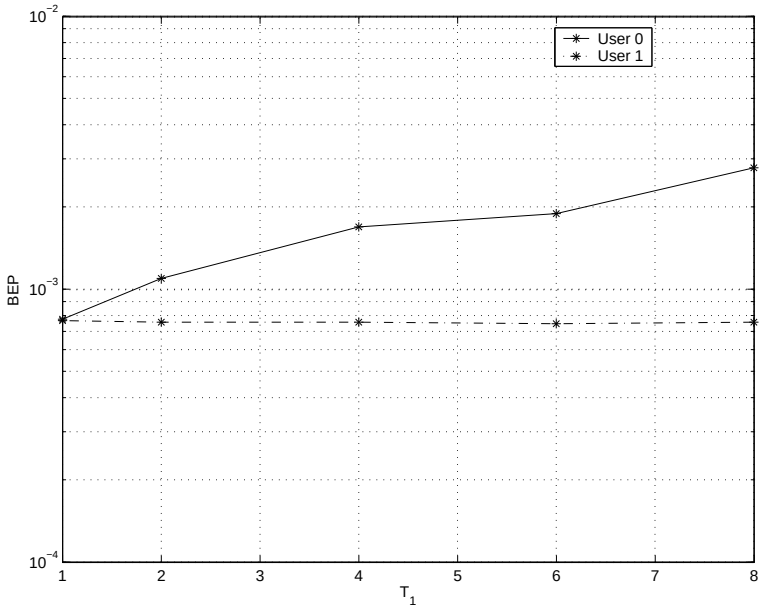

Fig. 5.4: BER performance of CIDS-CDMA in the case of two users, as a function of coherence time of user 1, at spreading factor $N = 8$.

$N = 32$, $L_p = 3$, and $\gamma = 16$ dB. BCIDS-CDMA obviously outperforms both BIDS-CDMA and simple CIDS-CDMA. Among the latter two, CIDS-CDMA has better performance. That CIDS-CDMA performs better than BIDS-CDMA is because the diversity in long-code BIDS-CDMA comes from bit interleaving and its order is equal to the free distance of the channel code. On the other hand, the diversity of long-code CIDS-CDMA comes from chip interleaving and its order is equal to the spreading factor. Since our spreading factor is larger than the free distance of the convolutional code, the long-code CIDS-CDMA has a higher diversity gain. The results also demonstrate that even with path diversity for all systems, BCIDS-CDMA still has evident advantage.

Correlated Rayleigh Fading Channels

Now we consider the correlated fading channels. Let the Doppler spread be $f_d = 222$ Hz. Then the coherent time is 1622 chips as computed in Sec. 5.6.1. Figure 5.9 shows the synchronous results at $\gamma = 13$ dB under different interleaver sizes, where the block sizes given for BCIDS-CDMA are the sum of that of the bit and the chip interleavers. It is clear

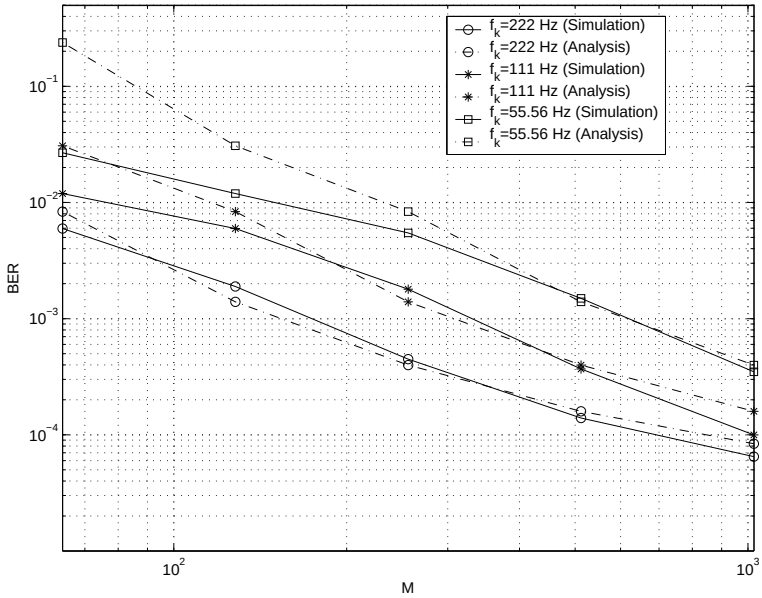

Fig. 5.5: BER performance of users with different maximum Doppler shifts versus the interleaving depth M, where $N = 64$ and SNR$= 16$ dB.

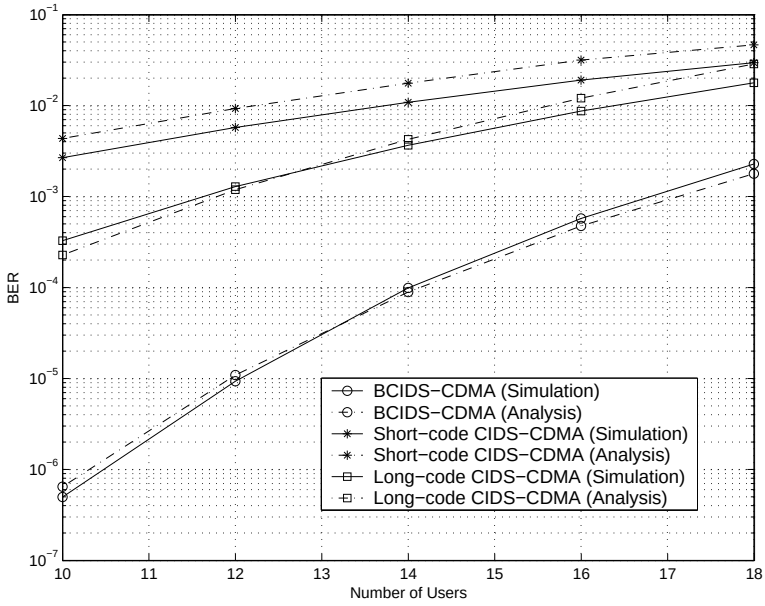

Fig. 5.6: Average BER of synchronous CIDS-CDMA systems, where $N = 16$ and $\gamma = 16$ dB.

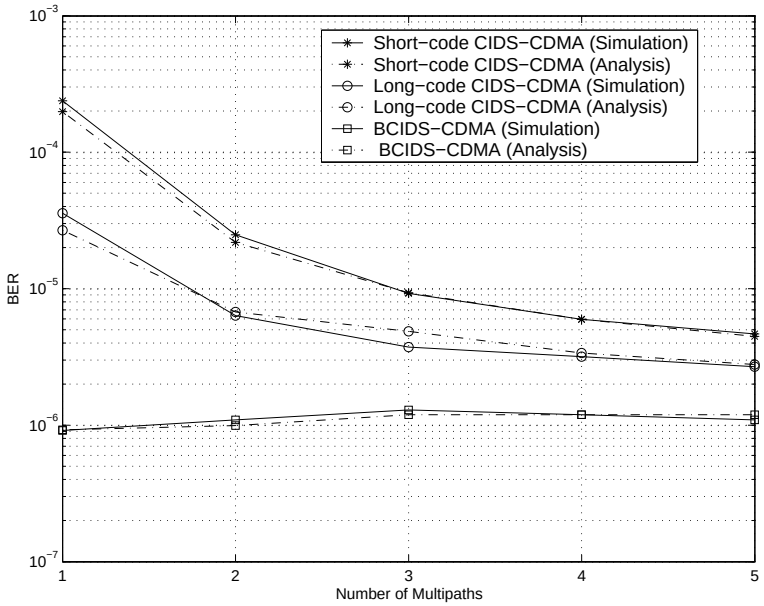

Fig. 5.7: Average BER of asynchronous CIDS-CDMA systems as function of multipath number, where $N = 32$, $K = 20$ and $\gamma = 16$ dB.

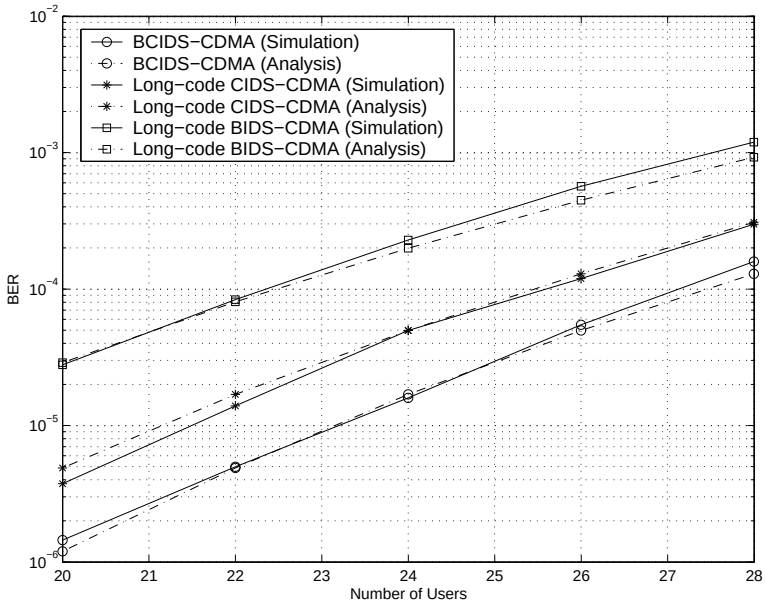

Fig. 5.8: Average BER of different asynchronous DS-CDMA systems in multipath Rayleigh fading at $N = 32$, $L_p = 3$ and $\gamma = 16$ dB.

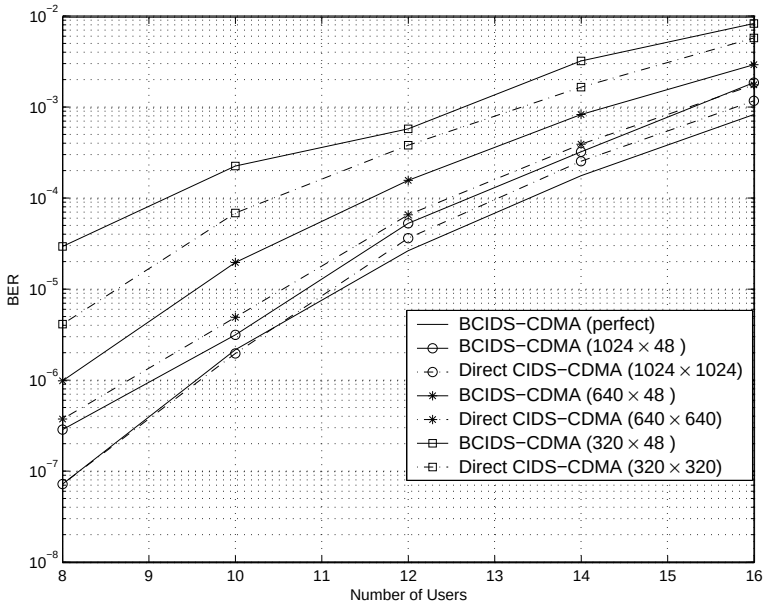

Fig. 5.9: Average BER of with different interleaver sizes in Rayleigh fading, where $N = 16$ and $\gamma = 13$ dB.

that, with proper design of the interleaver, the performance under perfect interleaving can be approached. An interleaving depth close to the coherence time does yield good performance as previously discussed. Also as discussed, at similar BER, BCIDS-CDMA needs a smaller interleaver size than direct CIDS-CDMA.

5.7 Summary

We addressed the performance of chip-interleaved DS-CDMA (CIDS-CDMA) with and without channel coding. Chip interleaving yields intra-bit diversity whereas bit interleaving, inter-bit diversity. Theoretical expressions for the performance under both short- and long-code spreading were derived and verified by simulation. It was shown that simple CIDS-CDMA could yield better performance than BIDS-CDMA, and joint bit-and-chip-interleaved DS-CDMA (BCIDS-CDMA) performed better than both. The large diversity gain provided by chip-interleaving can turn a fading channel into a nearly static one. In next chapter, we will show an design example based on 3GPP WCDMA [65].

Chapter 6

Chip-Interleaved WCDMA with Parallel Interference Cancellation

PIC is an effective means to mitigate MAI while its performance heavily relies on tentative decision. Chip-interleaving, a way of leveraging intra-bit diversity, can make symbol detection more reliable in fading channels. In this chapter, we therefore consider the combination of these two techniques. A chip-interleaving scheme based on some Third Generation Partnership Project (3GPP) Wideband code division multiple access (WCDMA) system features, such as the use of the Q-branch to transmit control bits and the I-branch to transmit data bits in a QPSK-like modulation scheme, is proposed. Simulation results show that the proposed chip-interleaved WCDMA (CI-WCDMA) transmission can have significant performance advantage compared to simple WCDMA in transmission over fading multipath channels with MAI.[1]

6.1 Introduction

In practice, wireless systems are usually subject to channel fading. Bit-interleaving is a common way to remedy channel fading in a channel coded system. However, most MUDs including PIC perform interference cancellation before channel decoding, for otherwise

[1]Part of this chapter has been presented in "Performance comparison of several parallel interference cancellation techniques under the 3GPP WCDMA specifications," in *Proc. Asia Pacific Conf. Commun.*, vol. 1, pp. 257-261, Oct. 2000 and "Chip-interleaved WCDMA with parallel-interference-cancellation receiver in multipath Rayleigh fading channels," in *Proc. IEEE Int. Conf. Acoustics Speech signal Processing*, May 2004, pp. 961–964.

the complexity becomes overwhelming. In this case, the inter-bit diversity provided by bit-interleaving provides no help to the MUDs. As illustrated in previous chapter, due to the resulting intra-bit diversity, chip-interleaving should provide great help to the performance of PIC.

The WCDMA wireless communication standard completed recently by 3GPP is now entering the stage of commercial operation. Based on some features of 3GPP WCDMA, we propose a chip-interleaved WCDMA (CI-WCDMA) technique here and examine its transmission performance in multipath Rayleigh fading channels. Different types of PIC detectors are addressed under the proposed system and show the superiority over hard-limiting PIC.

6.2 CI-WCDMA Signaling

In a chip-interleaved DS-CDMA system, bits are first spread as in conventional DS-CDMA and are then transmitted with interleaved chips. Consider the spreading and modulation method defined in the FDD mode of 3GPP WCDMA [65]. Figure 6.1 shows the proposed CI-WCDMA signaling scheme. As in WCDMA system, the data and control bits are first spread by channelization codes and carried in I- and Q-branches, respectively. A scrambling code is applied after block interleaving of the complex output chips. Let M be the interleaving depth in number of data bits and N the spreading factor of each data bit. Then we have NM chips in one interleaving block. The interleaving output forms N chip-blocks, with M chips per chip-block, for each interleaving block. With this chip-interleaver, we send the chips of each data bit in different chip-blocks and hence increase the intra-bit diversity. The control channel always uses 256 as the spreading factor and therefore $R = 256/N$ is the spreading factor ratio of data channel to control channel. And each interleaving block contains M/R control bits in addition to M data bits.

Consider one interleaving block. The transmitted signal by the kth user can be ex-

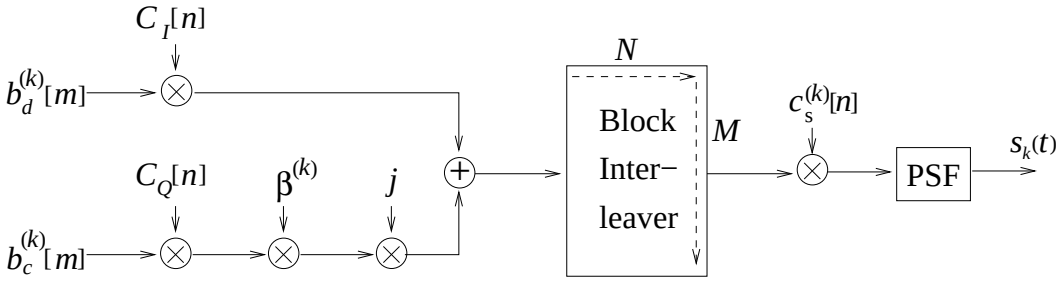

Fig. 6.1: The proposed CI-WCDMA signaling scheme.

pressed as

$$
\begin{aligned}
s_k(t) \;=\; & \sum_{n=0}^{N-1}\sum_{m=0}^{M-1}\Big[\Big(b_d^{(k)}[m]C_I[n] \\
& +j\beta^{(k)}\cdot b_c^{(k)}[\lfloor\frac{m}{R}\rfloor]C_Q[(mN+n)\%256]\Big) \\
& \cdot c_s^{(k)}[nM+m]p(t-(nM+m)T_c)\Big]\,, \qquad (6.1)
\end{aligned}
$$

where $b_d^{(k)}[m]$ and $b_c^{(k)}[m]$ denote the mth data and control bits for the user, respectively, $C_I[n]$ and $C_Q[n]$ are the orthogonal channelization codes for the data and the control channel, respectively, $c_s^{(k)}[n]$ is the scrambling code, T_c is the chip period, and $p(t)$ is a square pulse of chip duration that is normalized so that $\int_0^{T_c} p^2(t)dt = 1$. The quantity $\beta^{(k)}$ is a weighting factor which usually should be less than 1 for power efficiency. The channelization codes are Walsh-Hadamard sequences and the scrambling code is a pseudo-random sequence with much longer period than the spreading factor. Figure 6.2 gives an illustrative example of the CI-WCDMA signal with $M = 4$ and $N = 2$, where each thick rectangle marks a chip-block.

Asynchronous and multipath channels are considered and the expression (3.37) is still used in addressing the received signal.

6.3 Receiving of CI-WCDMA Signals

6.3.1 Rake-Like Receiver

A PIC receiver is usually built on a rake receiver. Like in conventional DS-CDMA, a rake-type receiver which can provide multipath diversity is also an efficient receiver structure

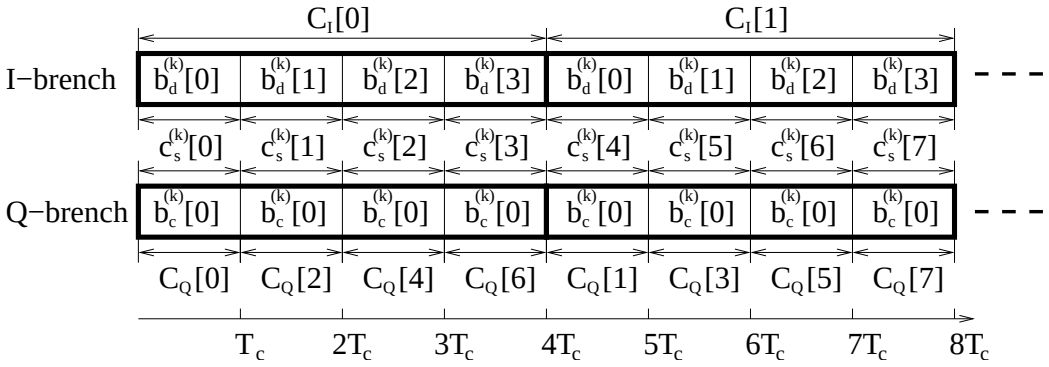

Fig. 6.2: An example of CI-WCDMA signal.

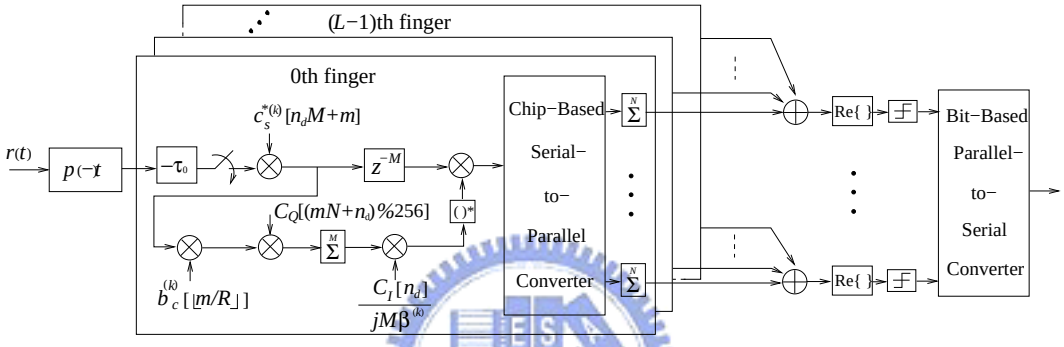

Fig. 6.3: A rake-like receiver for CI-WCDMA signals.

for CI-WCDMA signals. Figure 6.3 shows such a receiver, where z^{-M} denotes delay by M chips. Channel estimation is performed before chip De-interleaving using the control bits transmitted in the Q-branch. If the channel remains constant during each chip-block but varies independently randomly between chip-blocks, then with known control bits (pilot bits in 3GPP WCDMA language) and known channelization code, the maximum likelihood estimate of the channel coefficient in Gaussian noise and interference for each chip-block is the normalized correlation between the input signal samples and the product of the control bits and the channelization code in the chip-block. This is what shown in Fig. 6.3. Practical fading channels usually behave differently from the above and usually are not independent from chip-block to chip-block, and accordingly samples from several chip-blocks can be combined in a more complicated way to achieve better channel estimation. But such is not considered in this work.

After matched filtering and descrambling, the input signal to the lth finger of the rake-

like receiver for user k is given by

$$s_k^{(l)}[n] = c_s^{*(k)}[n] \cdot \int_{(n+\tau_k+l)T_c}^{(n+\tau_k+l+1)T_c} r(t) \cdot p(t-(n+\tau_k+l)T_c)dt. \tag{6.2}$$

The control bits $b_c^{(k)}[m]$ in 3GPP WCDMA may include pilot bits, power control bits and other control bits. In the following discussion, we treat them as only consisting of pilot bits (that is, all bits are known). The results can be easily extended to other situations. To estimate the channel coefficient of the lth path during the n_dth chip-block, we therefore calculate

$$\begin{aligned}
\hat{\alpha}_k^{(l)}[n_d] &= \frac{1}{j2M\beta^{(k)}} \sum_{m=0}^{M-1} \Big(s_k^{(l)}[n_d M + m] \\
&\quad \cdot b_c^{(k)}[\lfloor \frac{m}{R} \rfloor] C_Q[(mN+n_d)\%256] \Big) \\
&= \sqrt{2P} \cdot \alpha^{(k)}[n_d] + \sum_{l' \neq l}^{L-1} \eta_{l,l'}^{(k,0)}[n_d] \\
&\quad + \sum_{k' \neq k}^{K-1} \sum_{l'=0}^{L-1} \eta_{l,l'}^{(k,k')}[n_d] + \hat{\zeta}_l[n_d],
\end{aligned} \tag{6.3}$$

where $\hat{\zeta}_l[n_d]$ summarizes the effect of the AWGN, and $\eta_{l,l'}^{(k,k')}$ is the interference from the l'th path of user k' to the estimation of user k's lth path coefficient. Thus, the second and third terms in (6.3) are the interpath interference (IPI) and MAI, respectively. It can also be shown that for channel estimation, the "processing gain" provided by chip-interleaving in reducing the effect of IPI and MAI is M. Therefore, a larger interleaving depth increases the robustness of the channel estimate. But this is on the condition that the channel stays relatively constant over the chip-block. For fast fading channels a large M may not be beneficial.

Unlike channel estimation, data detection is performed after chip deinterleaving. Let $\hat{b}_d^{(k)}[m] = \text{sign}\{\Re\{y^{(k)}[m]\}\}$ be the decision for $b_d^{(k)}[m]$, we have the decision signal $y^{(k)}[m]$ as

$$y^{(k)}[m] = \sum_{l=0}^{L-1} \sum_{n_d=0}^{N-1} \left\{ s_l^{(k)}[n_d M + m] \left(\hat{\alpha}_k^{*(l)}[n_d] C_I[n_d] \right) \right\}$$

$$
\begin{aligned}
= \; & 2P \cdot b_d^{(k)}[m] \cdot \left(\sum_{l=0}^{L-1} \sum_{n_d=0}^{N-1} 2 \cdot \hat{\alpha}_k^{*(l)}[n_d] \alpha_k^{(l)}[n_d] \right) \\
& + \sum_{l=0}^{L-1} \sum_{l' \neq l}^{L-1} \xi_{l,l'}^{(k,0)}[m] + \sum_{l=0}^{L-1} \sum_{k' \neq k}^{K-1} \sum_{l'=0}^{L-1} \xi_{l,l'}^{(k,k')}[m] \\
& + \hat{\zeta}^{(k)}[m], \qquad (6.4)
\end{aligned}
$$

where $\xi_{l,l'}^{(k,k')}[m]$ has a similar interpretation as $\eta_{l,l'}^{(k)}[m]$ but the processing gain here is $2N$. By (6.4), it is clear that the decision signal is the combination of NL independently faded coefficients $\alpha_k^{(l)}[n_d]$. Thus, there is an intra-bit diversity of order NL in CI-WCDMA systems.

6.3.2 PIC Detector

The basic idea behind PIC is quite simple: regenerate the interference to all received user signals from all others and subtract such interference from the received signals simultaneously. For simplicity, only wideband PIC is described here. In the first stage of PIC, the regenerated received signal of user k can be written as

$$
\hat{r}_k(t) = \sum_{l=0}^{L-1} \hat{\alpha}_k^{(l)} \hat{s}_k(t - \tau_k T_c - l T_c), \qquad (6.5)
$$

where $\hat{s}_k(t)$ has the same expression as (6.1) except that $b_d^{(k)}[m]$ is replaced by $\tilde{b}_d^{(k)}[m]$, the tentative decision made in previous stages. Then for user k, we pass the following signal again to the rake-like receiver: $r(t) - \sum_{m \neq k}^{K-1} \hat{r}_m(t)$. Subsequent PIC stages regenerate $\hat{s}_k(t)$ and $\hat{r}_k(t)$ using the respectively previous stages' output in a similar fashion, in hope that better detection results can be obtained with more repetitions.

Several forms of tentative decision used to reconstruct interfers' signals have been proposed in the literature. We consider three forms here: simple hard decision, a soft decision approach, and a semi-hard decision approach. For hard decision PIC, we have

$$
\tilde{b}_d^{(k)}[m] = \text{sign}\{\Re[y^{(k)}[m]]\}. \qquad (6.6)
$$

The soft decision approach is from the so-called nonlinear minimum interference cancellation (NMIC) initially proposed in [16]. However, the computation presented there is

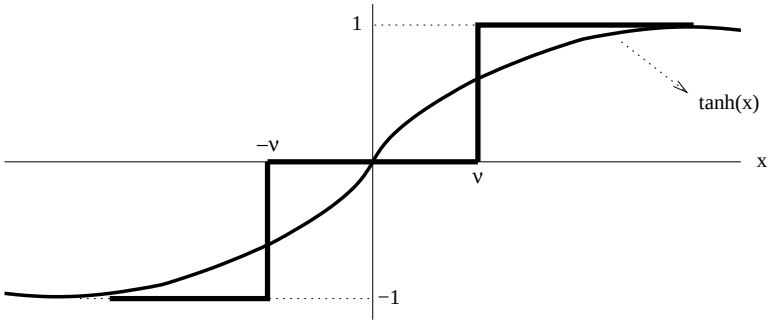

Fig. 6.4: Illustration of semi-hard detector.

complicated and only single-path channel is assumed. Here we obtain a simpler form of NMIC for multipath channel by assuming that the interference at different rake fingers are uncorrelated and the interference is Gaussian distributed. By applying MMSE estimator over white Gaussian noise channel, we obtain the soft decision for NMIC as

$$\tilde{b}_d^{(k)}[m] = \tanh\left(\Re\left[\frac{y^{(k)}[m]}{\sigma_k^2[m]}\right]\right) \tag{6.7}$$

where $\sigma_k^2[m]$ is the estimated variance of interference plus noise at rake output for mth bit. At each stage, $\sigma_k^2[m]$ is computed by decision-directed estimation and can be expressed as

$$\hat{\sigma}_k^2[m] = \left(\Re\{y^{(k)}[m]\} \cdot \text{sign}\{\Re[y^{(k)}[m]]\} - \sum_{l=0}^{L-1} |\alpha_k^{(l)}|^2\right)^2 \tag{6.8}$$

The semi-hard decision approach is relatively simple compared to NMIC and was initially proposed in [31, 21]. The key idea is to set a threshold. When the rake filter's output signal strength exceeds the threshold, a hard decision is made to detect the symbol. Otherwise the symbol is disregarded. However, an exact expression for the threshold is not given in [31, 21]. We choose to minimize the mean-square difference between the threshold decision curve and the NMIC soft-decision curve (6.7), that is, we choose ν, the threshold, to minimize $J(\nu)$, the mean-square difference defined as

$$J(\nu) = \int_0^{\nu} \tanh^2(x)dx + \int_{\nu}^{\infty} [1 - \tanh(x)]^2 dx. \tag{6.9}$$

This is illustrated in Figure 6.4 By numerical search we found that the minimum occurs at $\nu \approx 0.55$. Therefore, the operation of the threshold decision discipline can be described

as

$$\tilde{b}_d^{(k)}[m] = \begin{cases} 1, & \text{if } \Re\left(y^{(k)}[m]\right) > 0.55 \cdot \sigma_k^2[m], \\ 0, & \text{if } |\Re\left(y^{(k)}[m]\right)| < 0.55 \cdot \sigma_k^2[m], \\ -1, & \text{if } \Re\left(y^{(k)}[m]\right) < -0.55 \cdot \sigma_k^2[m]. \end{cases} \tag{6.10}$$

Evidently, the correctness of the tentative decisions $\hat{b}_d^{(k)}[m]$ will affect the PIC performance greatly. With chip-interleaving, the output of rake receiver is more resistant to channel fading effects and hence the regenerated signals are more correct. An alternative to wideband PIC is narrowband PIC, which does not regenerate the received signals but the resultant interference in the despread signals directly [49]. That is, $\xi_{l,l'}^{k,k'}[m]$ is regenerated and subtracted from $y^{(k)}[m]$. Narrowband PIC has exactly the same performance as wideband PIC but with lower complexity especially when the spreading factor is high. Variants of these basic PIC schemes also exist. No matter what the kind of PIC is performed, CI-WCDMA can always help the interference cancellation ability.

6.4 Simulation Results

In this section, we compare the performance of CI-WCDMA and non chip-interleaved WCDMA by computer simulation. Similar to the 3GPP WCDMA, we let the chip rate be 3.84 Mcps. Let the data spreading factor be $N = 32$ and $\beta = 8/15$ which results in 5.46 dB power difference between data and control channel. For the channel model, Rayleigh fading is considered and we let the number of multipaths be $L = 4$ with the path energies showing exponential decay and are equal to 0, -3, -6, and -9 dB, respectively; this is the same as case 3 and case 5 propagation condition specified in Annex B of [66] for velocity 120 km/hr and 250 km/hr mobile environment.

6.4.1 Uncoded Systems

Consider first quasi-static (or slow fading) channels, where the path coefficients remain constant during a chip-block and vary independently randomly from block to block. The interleaving depth M is set to 2560. Therefore, there are 10 control bits in each chip-block. Figures 6.5 shows the average BER of using hard limiting PIC in CI-WCDMA and

WCDMA with SNR=13 dB. Clearly, CI-WCDMA outperforms WCDMA and when the user number is large, one stage PIC in CI-WCDMA even has comparable performance as two stages PIC in WCDMA. The performance of different PIC detectors is given in Fig. 6.6 for CI-WCDMA and NMIC shows better detection results for its robustness in reconstructing interference.

6.4.2 Coded Systems

The rate-1/2 convolutional code of constraint length 7 with generators $g_1 = 133_8$ and $g_2 = 171_8$ is used in the following simulations. And we employ hard-decision Viterbi decoding with traceback length $= 5 \cdot 7 = 35$. The results for quasi-static channels with $M = 2560$, $K = 16$, and one stage PIC is shown in Fig. 6.7, where for both systems, a block bit-interleaver of size 640×32 is applied after convolutional encoding. Again, it can be observed that CI-WCDMA performs much better than WCDMA. Take 10^{-5} as the target BER, CI-WCDMA has about 4 dB SNR gain over WCDMA. The advantage of using nonlinear PIC is more pronounced in channel coded systems. NMIC provides about 2 dB and 1.5 dB gain over hard PIC for WCDMA and CI-WCDMA, respectively. Though not as effective as NMIC, semi-hard PIC provides remarkable gain and is attractive for its simplicity.

Next, we consider a more practical channel condition. We generate correlated Rayleigh fading channels by the baseband Doppler filtering method [59]. Channels of velocity $v = 120$ km/hr are simulated. Bit-interleaver size is set as 160×64 for both systems and $M = 1024$ is used for CI-WCDMA. Figure 6.8 illustrates the performance of two stages hard limiting PIC with SNR 13 dB. In such case, CI-WCDMA still shows its superiority over WCDMA. The number of users can be served in CI-WCDMA is 14 if target BER is 10^{-6}. And this effectively increases 27% capacity of W-CDMA, which can only serve 11 users.

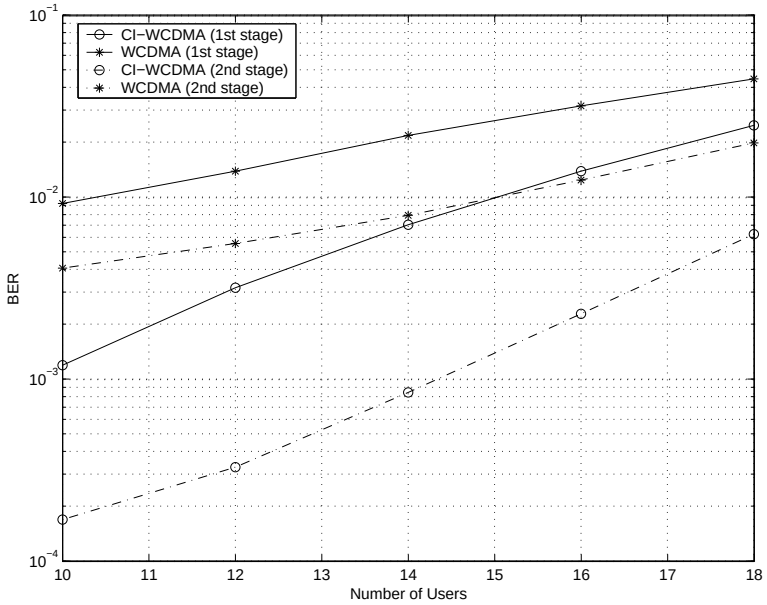

Fig. 6.5: Performance of Hard limiting PIC in CI-WCDMA and WCDMA as function of user number with SNR=13 dB.

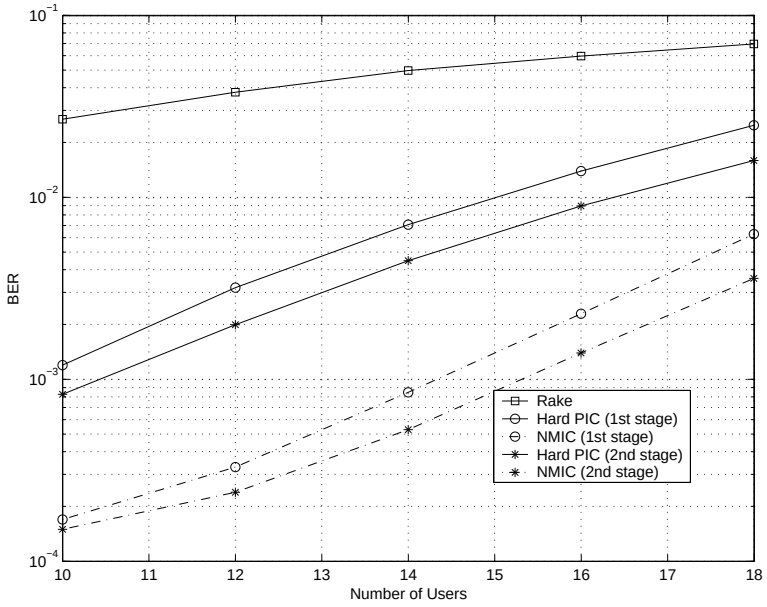

Fig. 6.6: Performance of different types of PIC in CI-WCDMA with SNR=13 dB.

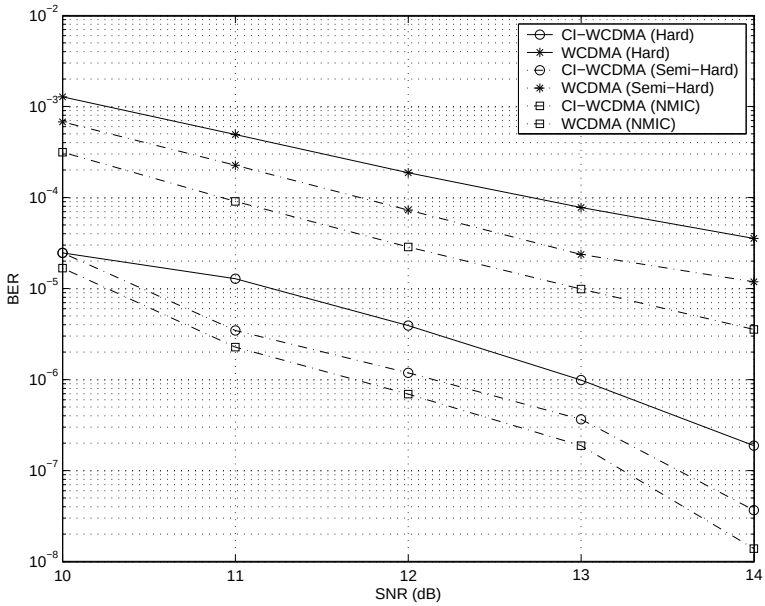

Fig. 6.7: Performance of different PIC detectors in channel coded WCDMA systems under quasi-static channels with $K = 16$.

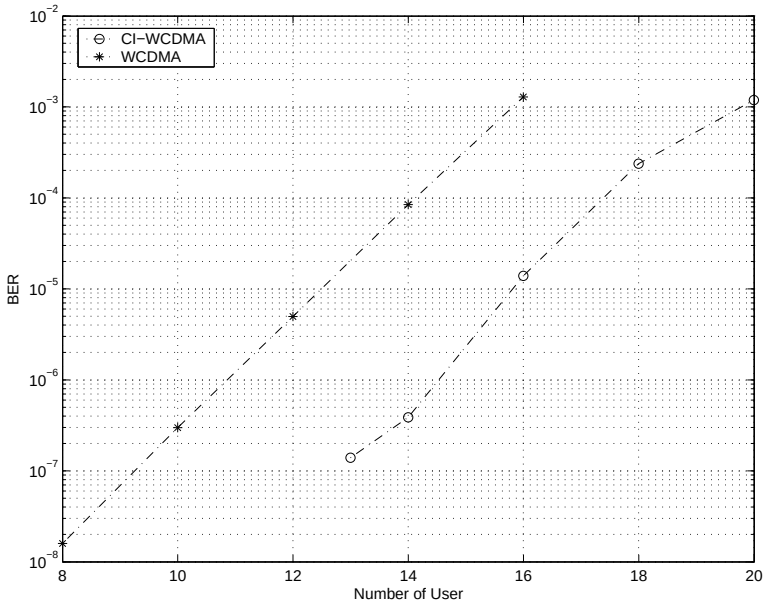

Fig. 6.8: Performance of Hard limiting PIC in channel coded WCDMA systems under correlated channels with SNR=13 dB.

6.5 Summary

In this chapter, we proposed a chip-interleaved WCDMA (CI-WCDMA) transmission scheme and considered two ways of signal reception, namely, rake-like receiver and PIC. Due to the intra-bit diversity provided by chip-interleaving, CI-WCDMA is shown to have better performance than simple WCDMA in various conditions. The performance gain is especially significant with PIC reception. In next chapter, we will show how the technique of chip-interleaving can be used to remove MAI under static channels.

Chapter 7

Multicode Chip-Interleaved DS-CDMA Concerning Interference

In previous chapters, we studied the provision of diversity in fast fading channels by chip-interleaving. In slowly fading channels, however, chip-interleaving can be used to reduce interference. We show that, with a certain way of multicode assignment, CIDS-CDMA can perform better than conventional DS-CDMA in asynchronous and multipath channels thanks to its ability to preserve the synchronous correlations among the spreading codes. Compared to the recently proposed chip-interleaved block-spread CDMA (CIBS-CDMA) that requires a single-user equalizer, the presented scheme can attain better performance in channel-coded transmission.[1]

7.1 Introduction

The capacity of a DS-CDMA system highly depends on the correlation properties of the spreading codes. Some well-known classes of spreading codes that have low inter-code correlations are the Gold, the Kasami, and the m-sequences. Their property of low inter-code correlations, however, may be lost in asynchronous transmission or multipath propagation, resulting in a performance close to that of random spreading [33].

[1]Part of this chapter has been presented in "A chip-interleaved synchronous DS-CDMA technique enabling MAI-free and reduced-ISI transmission with low complexity receiving," in *Proc. IEEE Workshop Signal Processing Advances Wireless Commun.*, pp. 487–491, July 2004, and submitted to *IEEE Trans. Wireless Commun* (revised version in review).

By chip-interleaved block spreading (abbreviated CIBS-CDMA) [80],[81], the orthogonality among spreading codes can be maintained in asynchronous or multipath propagation, and the multiaccess interference (MAI) is eliminated deterministically. Although intersymbol interference (ISI) will show up in multipath propagation, it can be dealt with using a single-user equalizer. However, an issue, heretofore unaddressed, arises when channel coding is employed. Briefly, if the residual ISI after equalization comes mainly from a small number of paths (in the equalized channel), then the performance of channel coding may suffer, because channel codes are normally designed for the white Gaussian noise condition whereas the residual ISI in this case is not white Gaussian. One remedy is to lengthen the equalizer for further ISI suppression. Another is to use turbo equalization that iterates between equalization and channel decoding [53],[36]. Both entail additional complexity, with the turbo equalizer also increasing the decoding delay.

Herein we present a multicode chip-interleaved DS-CDMA (CIDS-CDMA) scheme, which can be viewed as a modification of CIBS-CDMA, that not only maintains the spreading codes' synchronous correlations (to be defined later) in quasi-synchronous multipath channels but also facilitates low-complexity rake receiving for channel-coded transmission. With the employment of multiuser detector such as PIC, the proposed system can have better decoding results even in fully loaded systems.

7.2 CIDS-CDMA Signals

7.2.1 Transmitted Signal

In CIDS-CDMA, the modulated signals are formed as as follows. First, data symbols are partioned into blocks. After spreading, the symbols in each block are transmitted with their chips interleaved. Whereas CIBS-CDMA employs one spreading code for each data block of a user, we allow use of multiple spreading codes. Its implications will become clear later.

Let each block of interleaved data contain M_d symbols and, for the time being, assume

that each symbol in the block is spread with a different code. Assume that M_0 zero chips are padded after each M_d data chips as in [80], where M_0 may be null. Then the signal for block g of user k can be expressed as

$$\underline{s}_k(g) = \sqrt{2P}\mathbf{A}_k\underline{b}_k(g), \tag{7.1}$$

where $\sqrt{2P}$ is the normalized signal amplitude of each user, $\underline{b}_k(g) = [b_k(gM_d), \ldots, b_k((g+1)M_d - 1)]^T$ denotes the gth data block, and

$$\mathbf{A}_k = [\text{diag}(\underline{a}_k[0]), \mathbf{0}_{M_d \times M_0}, \ldots, \text{diag}(\underline{a}_k[N-1]), \mathbf{0}_{M_d \times M_0}]^T \tag{7.2}$$

is the "spreading matrix" with N being the spreading factor, $\underline{a}_k[n]$ $(n = 0, \ldots, N-1)$ the vector of the nth chips of the M_d codes, and $\mathbf{0}_{M_d \times M_0}$ the all-zero matrix of size $M_d \times M_0$. The dimension of $\mathbf{A}_k$ is $NM \times M_d$ where $M = M_d + M_0$. The number of output chips for each block after spreading is thus equal to NM.

Let $a_k^{(h)}[n]$ $(n = 0, \ldots, N-1)$ denote the spreading code for the hth data symbol of user k. Then, for block g,

$$\underline{a}_k[n] = [a_k^{(gM_d)}[n], \ldots, a_k^{((g+1)M_d-1)}[n]]^T, \tag{7.3}$$

where the absence of index g in the left-hand side reflects the fact that we use the same set of spreading codes for all blocks. (Change of spreading code assignment from block to block is not considered in this work. It may result in some performance gain whose amount depends on the operating condition, but the amount tends to be insignificant when users are many.) The *synchronous correlation* between the two codes for the h'th symbol of user m and the hth symbol of user k is defined as

$$\Lambda_{m,k}(h', h) = \sum_{n=0}^{N-1} a_m^{(h')}[n]a_k^{(h)}[n]. \tag{7.4}$$

7.2.2 Received Signal

Let the maximum possible delay spread for any user be $L-1$ chips and the channel response for user k be given by

$$h_k[n] = \sum_{l=0}^{L-1} \alpha_k^{(l)} \delta[n - \tau_k - l] \tag{7.5}$$

where τ_k is the initial delay of user k's signal. The model accommodates both synchronous and quasi-synchronous transmission. For convenience, define $\alpha_k^{(l)} = 0$ for $l < 0$ and $l \geq L$ and let $\tau_{\max} = \max_k\{\tau_k\}$. Let $M_0 \geq \tau_{\max} + L - 1$. After channel propagation, each block of user signal is spread over a time interval of no more than $NM + \tau_{\max} + L$ chips. In particular, the received signal in the interval $[gNM, (g+1)NM + \tau_{\max} + L - 1]$ (in unit of chips) due to user k's transmission can be expressed in vector form as

$$\underline{x}_k(g) = \mathbf{H}_{k,0}\underline{s}_k(g) + \mathbf{H}_{k,-1}\underline{s}_k(g-1) + \mathbf{H}_{k,1}\underline{s}_k(g+1), \tag{7.6}$$

where $\underline{x}_k(g)$ is an $(NM+\tau_{\max}+L-1)$-vector and $\mathbf{H}_{k,0}$, $\mathbf{H}_{k,-1}$, and $\mathbf{H}_{k,1}$ are $(NM+\tau_{\max}+L-1)\times NM$ Toeplitz matrices. Matrices $\mathbf{H}_{k,0}$ and $\mathbf{H}_{k,1}$ are lower triangular with their first columns given by $[\mathbf{0}_{1\times\tau_k}, \alpha_k^{(0)}, \ldots, \alpha_k^{(L-1)}, 0, \ldots, 0]^T$ and $[0, \ldots, 0, \alpha_k^{(0)}, \ldots, \alpha_k^{(L+\tau_{\max}-\tau_k-2)}]^T$, respectively, whereas $\mathbf{H}_{k,-1}$ is upper triangular with its first row given by $[0, \ldots, 0, \alpha_k^{(L-1)}, \ldots, \alpha_k^{(0)}, \mathbf{0}_{1\times(\tau_k-1)}]$.

In (7.6), the second and the third right-hand-side terms are the interference from the previous and the subsequent data blocks and have been named interblock-interference (IBI). Thanks to zero padding, these IBI terms can be made of no influence to data detection, as already noted in [80]. Hence we may ignore them in subsequent derivation. Then the total received signal in the above time interval is given by

$$\underline{x}(g) = \sum_{k=0}^{K-1} \underline{x}_k(g) + \underline{\zeta}(g), \tag{7.7}$$

where $\underline{\zeta}(g) = [\zeta[gNM], \ldots, \zeta[(g+1)NM + \tau_{\max} + L - 2]]^T$ is a vector of additive noise samples, assumed white Gaussian.

7.3 Effecting Synchronous Code Correlation After Multipath Propagation

The rake receiver, which is of lower complexity than many other receiver structures, can be used to receive the above CIDS-CDMA signal. To fully collect the energy in the lth path of user k's signal, the despreader input must contain the $(\tau_k + l)$th to the $(NM - M_0 - 1 + \tau_k + l)$th elements of $\underline{x}(g)$. Denote by $\mathbf{H}_{k,0}^{(l)}$ the matrix composed of the lth to the $(NM + l - 1)$th rows of $\mathbf{H}_{k,0}$ and by $\underline{\zeta}^{(l)}(g)$ the vector consisting of the lth to the $(NM + l - 1)$th elements of $\underline{\zeta}(g)$. Without loss of generality, consider detection of the 0th user signal. Despreading of the received signal for the lth path results in an M_d-vector given by

$$\underline{y}_0^{(l)}(g) = \sqrt{2P} \sum_{k=0}^{K-1} \mathbf{A}_0^T \mathbf{H}_{k,0}^{(\tau_0+l)} \mathbf{A}_k \underline{b}_k(g) + \mathbf{A}_0^T \underline{\zeta}^{(\tau_0+l)}(g). \tag{7.8}$$

Let $\mathbf{J}^{(h)}$ denote the $NM \times NM$ matrix whose elements are all zero except for the hth diagonal where the elements are all ones, where $h = 0$ refers to the main diagonal, $h > 0$ a sub-diagonal, and $h < 0$ a super-diagonal. ($\mathbf{J}^{(h)}$ is an h-unit delay operator.) Then

$$\begin{aligned} \mathbf{A}_0^T \mathbf{H}_{k,0}^{(\tau_0+l)} \mathbf{A}_k &= \mathbf{A}_0^T \cdot \sum_{d=0}^{L-1} \alpha_k[d] \mathbf{J}^{(\tau_k+d-\tau_0-l)} \mathbf{A}_k \\ &= \sum_{d=0}^{L-1} \alpha_k[d] \mathbf{A}_0^T \mathbf{J}^{(\tau_k+d-\tau_0-l)} \mathbf{A}_k. \end{aligned} \tag{7.9}$$

The matrix $\mathbf{A}_0^T \mathbf{J}^{(\tau_k+d-\tau_0-l)} \mathbf{A}_k$ is all zero except for the $(\tau_k + d - \tau_0 - l)$th diagonal. Let $(\mathbf{B})_{i,j}$ denote the (i, j)th element of matrix $\mathbf{B}$. Then for $j = i - (\tau_k + d - \tau_0 - l)$,

$$\left(\mathbf{A}_0^T \mathbf{J}^{(\tau_k+d-\tau_0-l)} \mathbf{A}_k\right)_{i,j} = \sum_{n=0}^{N-1} a_0^{(gM_d+i)}[n] a_k^{(gM_d+j)}[n] = \Lambda_{0,k}(gM_d + i, gM_d + j). \tag{7.10}$$

Hence

$$\mathbf{A}_0^T \mathbf{J}^{(\tau_k+d-\tau_0-l)} \mathbf{A}_k = \mathbf{J}^{(\tau_k+d-\tau_0-l)} \mathbf{D}^{(\tau_k+d-\tau_0-l)} \tag{7.11}$$

where $\mathbf{D}^{(l)}$ is a diagonal matrix whose i diagonal element is given by $\Lambda_{0,k}(gM_d + i, gM_d + i - l)$. In summary,

$$\underline{y}_0^{(l)}(g) = \sqrt{2P} \sum_{k=0}^{K-1} \mathbf{R}_{0,k}^{(l)} \underline{b}_k(g) + \underline{\zeta}_0^{(l)}(g) \tag{7.12}$$

where

$$\mathbf{R}_{0,k}^{(l)} = \sum_{d=0}^{L-1} \alpha_k[d]\mathbf{J}^{(\tau_k+d-\tau_0-l)}\mathbf{D}^{(\tau_k+d-\tau_0-l)}, \quad \underline{\zeta}_0^{(l)}(g) = \mathbf{A}_0\underline{\zeta}^{(\tau_0+l)}(g). \tag{7.13}$$

From the above, it is clear that the despreading result is entirely determined by the synchronous correlation of the spreading codes although the transmission is over a multipath channel. Thus, unlike conventional DS-CDMA whose performance depends on both the even and the odd code correlations [57], the multicode CIDS-CDMA has a more controllable performance.

The rake combiner output for $\underline{b}_0(g)$ is given by

$$\hat{\underline{b}}_0(g) = \sum_{l=0}^{L-1} (\alpha_0^{(l)})^* \underline{y}_0^{(l)}(g), \tag{7.14}$$

which contains ISI, MAI, and noise, in addition to the desired signal $\underline{b}_0(g)$.

Since the number of spreading codes having low synchronous correlation is limited, we should conserve code usage. From the above discussion, we can see that it suffices to have L spreading codes for each user, to be used periodically, when the multipath delay spread is not greater than $L-1$ chips.

7.3.1 An Example Using Gold Sequences

Any set of sequences with low (including zero) synchronous correlation can be used in the proposed system. However, all types of sequences are not equal considering system capacity. For example, only N/L users can be accommodated if Walsh-Hadamard sequences are used, but other sequences may permit more. A recent paper presents optimal binary sequence design for many combinations of processing gain and number of used spreading sequences [34]. However, to change the number of used sequences may require a redesign of all used sequences. In addition, Gold sequences are shown to be optimal in various conditions [34]. Hence we consider use of Gold sequences for reasons of flexibility and performance.

A set of Gold sequences of length N is constructed from a preferred pair of m-sequences of length N. The set contains $N+2$ sequences, including the preferred pair. Dropping one of the two m-sequences from the set results in a set where the correlation value between any two sequences is -1. This property is used in our code assignment strategy.

Unlike conventional spreading code assignment, we assign the spreading codes gluttonously as follows. We assign L of the $N+1$ Gold sequences to the first user, then another L to the second user, and so on, until we exhaust the $N+1$ sequences. Then we assign the $N+1$ sequences which are one cyclic shift of the original Gold sequences, and then those which are two cyclic shifts, and so on. This way, we can assure that in the despreading at each rake finger, there are always N among the $KL-1$ interfering signals that have a code correlation equal to -1. Numerical evaluation shows that the mean-square synchronous correlation of cyclically shifted Gold sequences is close to N, similar to random codes. Hence, by Gaussian approximation, the resultant bit error rate (BER) in random static channels when the multipaths are all of equal strength is given by

$$P_{\text{CI}} = \begin{cases} Q\left(\sqrt{\frac{1}{\frac{1}{SNR}+\frac{N}{2N^2L}+\frac{KL-N-1}{2NL}}}\right), & KL > N+1, \\ Q\left(\sqrt{\frac{1}{\frac{1}{SNR}+\frac{KL-1}{2N^2L}}}\right), & KL \le N+1. \end{cases} \tag{7.15}$$

In comparison, the performance of conventional DS-CDMA under random-code spreading is given by

$$P_{\text{conv}} = Q\left(\sqrt{\frac{1}{\frac{1}{SNR}+\frac{KL-1}{2NL}}}\right). \tag{7.16}$$

Comparing (7.15) with (7.16), it is clear that the performance of the proposed system is always better than the conventional one, especially when KL is not much larger than $N+1$.

7.4 Comparison with CIBS-CDMA

As discussed previously, CIBS-CDMA assigns one spreading code to each user, where the spreading codes are orthogonal. This deterministically eliminates MAI in multipath

propagation, but results in ISI which can be dealt with by single-user equalization. In comparison, the proposed scheme may employ orthogonal or nonorthogonal codes and it may assign one or more codes to a user, depending on the desired capacity and the channel condition. The proposed code assignment has several advantages.

First, for CIBS-CDMA, the residual ISI after single-user equalization may be far from being Gaussian when the equalized channel consists of only a small number of taps. Such ISI may highly degrade the performance of channel coding as can be seen in the numerical results of various studies [53], [36], [20], [75]. With multicode CIDS-CDMA, the total interference approaches Gaussian more closely due to the presence of a larger number of interferers (consisting of the different user signals, spread with multiple spreading codes and propagated over multipath channels). This is beneficial to the error correction capability of channel coding. And hence, when advanced multiuser detector, like PIC, is applied, multicode CIDS-CDMA can have better performance than CIBS-CDMA.

Second, the proposed multicode CIDS-CDMA provides a soft capacity as conventional DS-CDMA does, in the sense that the performance degrades gracefully as more users are accommodated. In contrast, the capacity of CIBS-CDMA is limited by the number of orthogonal sequences. (One could consider overloading the CIBS-CDMA system with additional users whose signals are spread with nonorthogonal spreading sequences. But then the added users may experience performance similar to that of conventional DS-CDMA due to MAI.)

7.5 Simulation Results

7.5.1 Comparison with Conventional DS-CDMA

Firstly, we present results for random static channels. We let each initial delay τ_k be uniformly distributed in $\{0, 1, \ldots, N-1\}$. Limiting $\tau_{\max}$ to $N-1$ is for easier comparison between conventional DS-CDMA and multicode CIDS-CDMA; it is not a fundamental limit to the proposed scheme. The multipaths have the same amplitude, with their phases

uniformly distributed in $[0, 2\pi)$. Gold sequences are used in both systems. Figure 7.1 shows the results for $N = 63$ and $L = 6$ at SNR $= 13$ dB. As pointed out in [33], the results for conventional DS-CDMA under asynchronous transmission match closely the theoretical result for random-code spreading (given in (7.16)). With the proposed code assignment, CIDS-CDMA clearly outperforms conventional DS-CDMA especially when the user number is small. The larger discrepancy between the simulation results and the theory at when K is about $(N+1)/L$ can be explained by noting that, because the number of spreading codes with different cyclic shifts is relatively small in this situation, the MAI has a greater variance about its mean than when K is larger.

The foregoing analysis and simulation have assumed that the channel responses remain unchanged during the whole chip-interleaving block so as to effect perfect synchronous correlation among the spreading codes. Therefore, question arises as to how multicode CIDS-CDMA performs in fading channels. Hence we consider transmission over multipath Rayleigh fading channels next. Let $N = 31$, $M_d = 152$, $M_0 = 12$, carrier frequency $= 2$ GHz, and chip rate $= 3.84$ Mcps (as in 3GPP [65]). Assume that $\tau_{\max} = 8$ chips, which corresponds to a maximum 625 m difference in initial path lengths, and assume that $L = 4$. For simplicity, let the total path energy be normalized per chip-block length, which is $31 \times 164 = 5084$ chips and about two slots in 3GPP. The results for different moving speeds are shown in Fig. 7.2. As can be expected, channel fading rate has minor impact on DS-CDMA since we have assumed quite accurate power control. Comparatively, faster fading does more harm to CIDS-CDMA because channel fading alters the correlation among users. Nevertheless, under the simulated parameters, CIDS-CDMA still outperforms DS-CDMA with slight capacity loss.

7.5.2 Comparison with CIBS-CDMA

Now we compare the proposed system with CIBS-CDMA. For spreading, we use Gold sequences of length 31 in multicode CIDS-CDMA and Walsh-Hadamard sequences of

length 32 in CIBS-CDMA. In both systems, we let $M_d = 144$, $M_0 = 12$ and $\tau_{\max} = 8$ chips and hence the transmission efficiency is 0.923 The 3GPP typical urban channel model (TUx) [67] is considered and to simplify the model, the time resolution is set to 1 chip duration by the way mentioned in Annex B of [67] and the resultant path delays are 0, 1, 2, 3, 5, 6, 7, and 8 chips, with the relative path energies being 0, -1.9, -0.3045, -3.6367, -5.183, -8.7855, -10.2, and -15.16 dB, respectively. Each simulation run involves one set of randomly generated phases, which are assumed to be uniformly distributed over $[0, 2\pi]$. The nonlinear minimum interference cancellation (NMIC) detector mentioned in Chapter 6 is applied here for CIDS-CDMA and a 4-path rake receiver is employed at each stage of interference cancellation. For CIBS-CDMA, decision feedback equalizer (DFE) with L_f feedforward and L_b feedback taps is applied and the equalization delay is set to $\lceil \frac{L_f+L}{2} \rceil$; we use "DFE($L_f$,$L_b$)" in the figures to denote different setting of DFE parameters.

Firstly, we compare the performance without FEC. Figure 7.3 shows the results in fully-loaded systems with $K = N$. As can be observed, CIBS-CDMA performs better in such case and already attain its best performance with DFE(16,8).

Next, we simulate channel-coded transmission where the channel code is the rate-1/2 binary convolutional code of constraint length 7 with generators $g_1 = 133_8$ and $g_2 = 171_8$. And we employ soft-decision Viterbi decoding with traceback length $= 35$. A 12×12 block bit-interleaver is inserted between the channel coder and the spectrum spreader to disperse the at times bursty errors for better decoding performance. The results of fully loaded systems are shown in Fig. 7.4. Apparently, CIDS-CDMA performs much better in such case; even one stage PIC can outperform CIBS-CDMA. This mainly results from the fact that the residual MAI is more Gaussian-like than residual ISI and hence conventional Viterbi decoder performs much better in CIDS-CDMA systems. The performance difference between long- and short-code DS-CDMA systems discussed in Chapter 5 is also an example of this effect. Also shown in the figure is the detection results of DS-CDMA. For

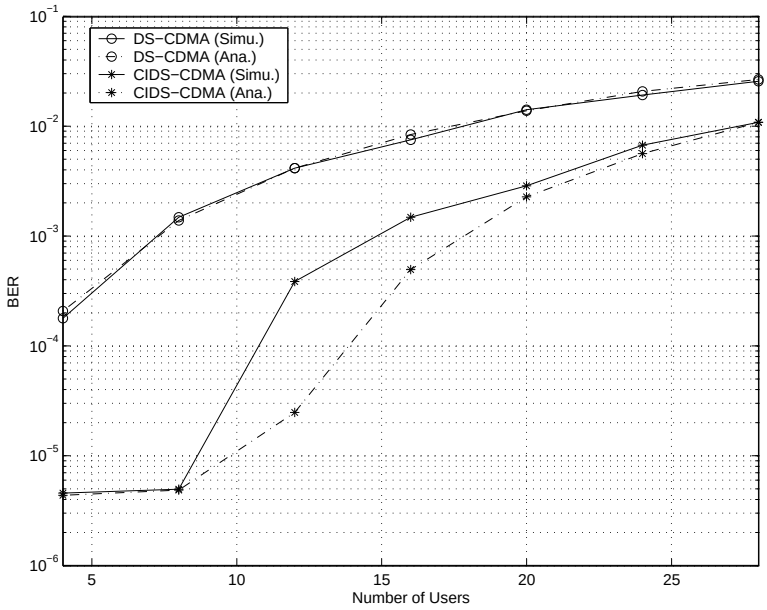

Fig. 7.1: BER performance of conventional DS-CDMA and CIDS-CDMA under Gold-sequence spreading, for different user numbers at $L = 6$, $N = 63$, and SNR $= 13$ dB.

fair comparison, only round$(31 * 0.923) = 29$ users are simulated since zero-padding is not required for DS-CDMA systems, where round(x) is a rounding function which rounds x to the nearest integer. It can be observed that DS-CDMA with NMIC does not present better decoding results than CIBS-CDMA in fully loaded systems. Hence, in addition to have much better performance in media-loaded systems, CIDS-CDMA also greatly improves the performance of DS-CDMA in heavily loaded situation.

7.6 Summary

In this chapter, we proposed a multicode chip-interleaved DS-CDMA scheme for transmission over slow-fading multipath channels. Through analysis and simulation, we showed that the proposed scheme had superior performance to conventional DS-CDMA in this condition, thanks to its ability to preserve the synchronous correlation among the spreading codes. As channel coding is employed, the proposed systems presents a superior performance than CIBS-CDMA even in fully loaded systems with the help of NMIC.

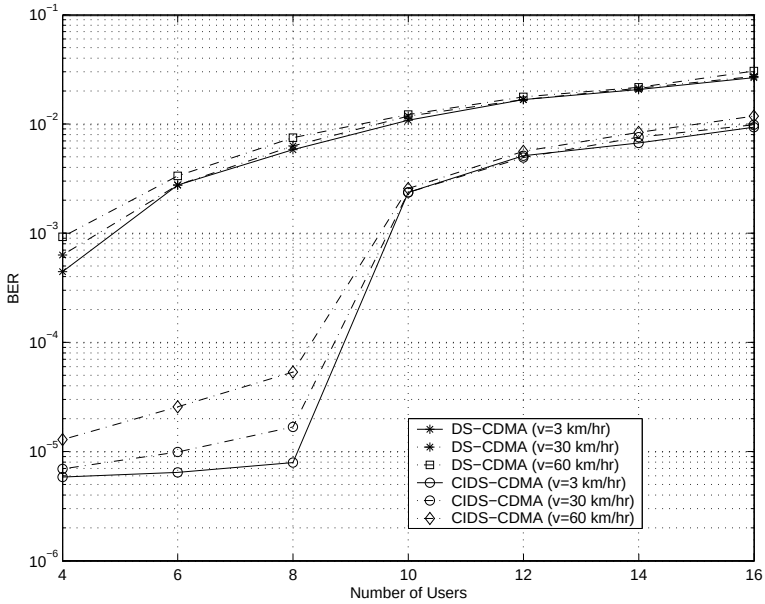

Fig. 7.2: BER performance of conventional DS-CDMA and CIDS-CDMA under Gold-sequence spreading, for different user numbers at $L = 4$, $N = 31$, and SNR $= 13$ dB under fading channels.

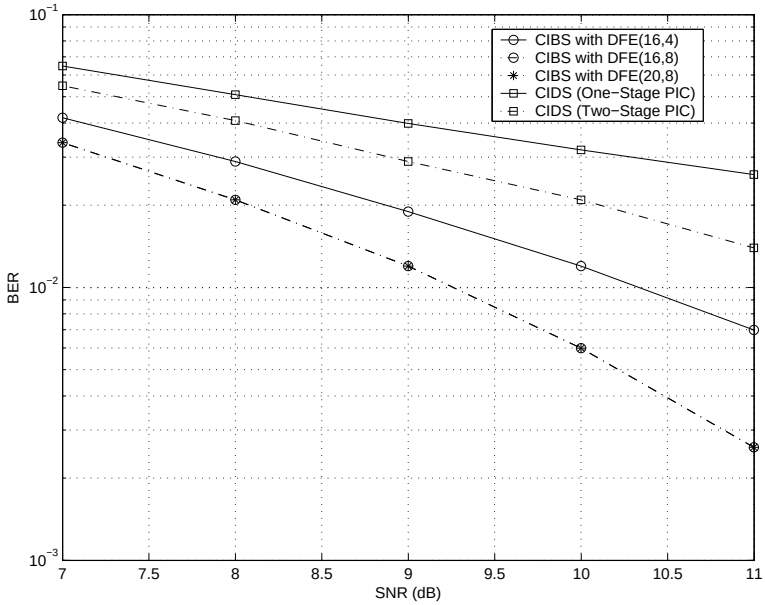

Fig. 7.3: BER performance of different CDMA systems before channel decoding at fully loaded case.

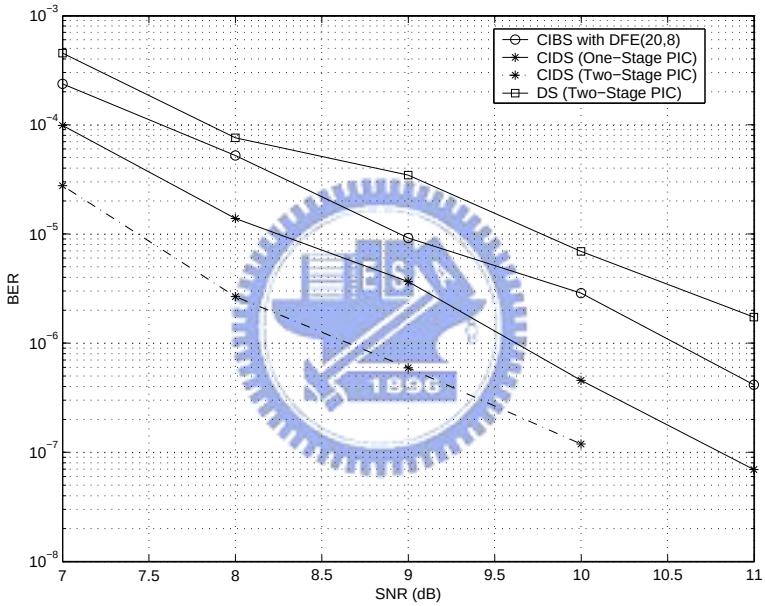

Fig. 7.4: BER performance of different CDMA systems after channel decoding at fully loaded case.

Chapter 8

Conclusions and Future Research Topics

In this thesis, we discussed the design and analysis of several transceiveing techniques based on DS-CDMA. The main results of the thesis are described in the following.

The analysis of conventional DS-CDMA with convolutional coding is discussed in Chapter 3. The analysis started with synchronous and flat-fading channels; the results was then extended to asynchronous and frequency-selective cases. By modeling the correlation among spreading codes as Gaussian, we obtain the simple BER expression which can be applied both to short- and long-code system. Due to the randomized interference over bits, the analysis showed that long-code spreading performs much better in channel coded systems especially when power control is perfect.

PIC is attractive for its simplicity and efficient in combating MAI. In Chapter 4, we discussed the performance of hard-limiting PIC. Two-user case was studied first and the result were then applied to the case of more users. Based on the analysis and numerical results, we found that purely hard-limiting PIC may not perform better after the second stage and for two-user case, one stage usually suffices.

While conventional DS-CDMA is discussed in Chapters 2 and 3, we addressed the chip-interleaved systems in the last chapters. Application of chip-interleaving in fast fading channels is first presented in Chapter 4. Both channel uncoded and coded CIDS-CDMA systems in Rayleigh fading channels are theoretically analyzed. It was shown

that while bit-interleaving already provides inter-bit diversity, the use of chip-interleaving still gains a lot for its provision of intra-bit diversity. The combination of bit- and chip-interleaving is also considered; the total diversity order in such case is the product of chip-interleaving depth and the free distance of convolutional codes used. The case when mobiles with different fading rates is also studied and it is revealed that the chip-interleaving depth of the desired user signal itself almost single-handedly determines the diversity order and the resulting performance.

In Chapter 5, we proposed a CI-WCDMA based on 3GPP WCDMA. The application of several nonlinear PIC detectors in such systems was investigated there. The estimation of path coefficients and parameters of PIC reconstructors was also presented. By way of computer simulation, it was observed that CI-WCDMA performs much better than WCDMA. Take 10^{-6} as the target BER, CI-WCDMA can increase 27% capacity of W-CDMA with the chosen system parameters. In addition, the introduce of nonlinear function in PIC can greatly improve the performance of PIC. Model the interference as Gaussian, we obtained a simpler expression for NMIC detector and with the result, a semi-hard PIC based on threshold setting can be derived. When NMIC is used in CI-WCDMA, there is about 1.5 dB SNR gain.

Finally, we research into the use of chip-interleaving in slow fading channels for reduced MAI and ISI. Thanks to its transmission structure, CIDS-CDMA can remain the code properties in frequency-selective channels at receiver side. A multicode assignment scheme was presented and the gluttonous code arrangement of Gold sequences was given as an example showing the superiority of such system over conventional DS-CDMA. The main advantage of such system is the better trade-off between performance and capacity. When the techniques of multiuser detection are applied in CIDS-CDMA, the detection quality is much better than that of CIBS-CDMA even in fully loaded condition.

We discussed the design and analysis of DS-CDMA systems in this thesis. Some potential research topics are as follows. Although the performance of hard-limiting PIC is

studied in Chapter 4, we did not get an exact proof for the performance limit and hence needs further researches. Secondly, synchronization for chip-interleaved systems is not discussed here. This may be done by a way similar to the design in Chapter 6 and worthwhile researches as well. Another potential topic is stemmed from Chapter 7; when the multipath delay spread is much large, the proposed multicode CIDS-CDMA may subject to performance loss due to insufficient multicode assignment. How to efficiently arrange the limited number of spreading codes is an important issue in such case. In addition, the application of other multiuser detection techniques in multicode CIDS-CDMA is also interesting.

Appendix A

The $F(\nu_1, \nu_2, c)$ Distribution

Let U and V be two independent χ^2 random variables with degrees ν_1 and ν_2, respectively, where ν_1 is an even number. We derive the pdf of the random variable

$$X = \frac{U/\nu_1}{(V+c)/\nu_2}. \tag{A.1}$$

To start, note that the joint PDF of U and V can be written as

$$f_{UV}(u,v) = \frac{1}{\Gamma(\frac{\nu_1}{2})\Gamma(\frac{\nu_2}{2})2^{\frac{\nu_1+\nu_2}{2}}} e^{-\frac{u+v}{2}} u^{\frac{\nu_1}{2}-1} v^{\frac{\nu_2}{2}-1}. \tag{A.2}$$

Let $Y = V$. Then the joint PDF of X and Y and that of U and V are related by

$$f_{XY}(x,y) = f_{UV}(u,v) \cdot |J| \tag{A.3}$$

where J is the Jacobian of the transformation given by

$$J = \det \begin{bmatrix} \frac{\partial u}{\partial x} & \frac{\partial u}{\partial y} \\ \frac{\partial v}{\partial x} & \frac{\partial v}{\partial y} \end{bmatrix} = (y+c)\frac{\nu_1}{\nu_2}. \tag{A.4}$$

Thus, the PDF of X can be found to be

$$\begin{aligned} f_X(x) &= \int_0^\infty \left[f_{UV}\left(\frac{x(y+c)\nu_1}{\nu_2}, y \right) \cdot (y+c)\frac{\nu_1}{\nu_2} \right] dy \\ &= \frac{\nu_1/\nu_2}{\Gamma(\frac{\nu_1}{2})\Gamma(\frac{\nu_2}{2})2^{\frac{\nu_1+\nu_2}{2}}} \left(\frac{\nu_1}{\nu_2} x \right)^{\frac{\nu_1}{2}-1} e^{-\frac{c\nu_1}{2\nu_2}x} \Gamma_m(\nu_1, \nu_2, c, x) \end{aligned} \tag{A.5}$$

where

$$\begin{aligned} \Gamma_m(\nu_1, \nu_2, c, x) &\triangleq \int_0^\infty (y+c)^{\frac{\nu_1}{2}} y^{\frac{\nu_2}{2}-1} e^{-\frac{(\nu_2+\nu_1 x)y}{2\nu_2}} dy \\ &= \sum_{k=0}^{\nu_1/2} \binom{\nu_1/2}{k} c^k \int_0^\infty y^{\frac{\nu_1+\nu_2}{2}-k-1} e^{-\frac{(\nu_2+\nu_1 x)y}{2\nu_2}} dy. \end{aligned} \tag{A.6}$$

Letting $z = \frac{\nu_2+\nu_1 x}{2\nu_2} y$, we can manipulate the last integration into

$$\left(\frac{2\nu_2}{\nu_2+\nu_1 x}\right)^{\frac{\nu_1+\nu_2}{2}-k} \int_0^\infty z^{\frac{\nu_1+\nu_2}{2}-k-1} e^{-z} dz = \left(\frac{2\nu_2}{\nu_2+\nu_1 x}\right)^{\frac{\nu_1+\nu_2}{2}-k} \Gamma\left(\frac{\nu_1+\nu_2}{2}-k\right) \tag{A.7}$$

where the last equality is by definition of the gamma function. Therefore, the PDF of X is given by

$$\begin{aligned} f_X(x) &= \frac{\nu_1/\nu_2}{\Gamma(\frac{\nu_1}{2})\Gamma(\frac{\nu_2}{2})} \left(\frac{\nu_1}{\nu_2}x\right)^{\frac{\nu_1}{2}-1} \left(\frac{\nu_2}{\nu_2+\nu_1 x}\right)^{\frac{\nu_1+\nu_2}{2}} e^{-\frac{c\nu_1}{2\nu_2}x} \\ &\quad \cdot \sum_{k=0}^{\nu_1/2} \binom{\nu_1/2}{k} \left(\frac{c(\nu_2+\nu_1 x)}{2\nu_2}\right)^k \Gamma\left(\frac{\nu_1+\nu_2}{2}-k\right). \end{aligned} \tag{A.8}$$

Appendix B

Three-Dimensional Channel Modeling

We have used relatively standard wireless channel models in the study reported in the main body of this dissertation. There has been continued activity in obtaining more precise channel models in the research community. We provide a brief survey of some relevant recent studies in this appendix. They may be useful in future research.

B.1 Introduction

Two-dimensional scattering model proposed by R. H. Clarke assumed the scattered waves travel horizontally. However, in urban and indoor environments, this may not be true. Hence, a 3-D model, which considers both the azimuth and elevation plane, would be helpful in modeling more general wireless communication environments.

B.2 3-D Modeling

Assume a mobile is moving along a straight line in the xy plane as shown in Fig. B.1. Mathematically, the field of lth multipath ray can be expressed as [78]

$$E_l(t) = E_l^0 \cdot \exp[-j \cdot (2\pi \cdot \frac{v \cdot t}{\lambda} \cdot \cos(\alpha_l - \gamma) \cdot \cos\beta_l + \varphi_l^0)] \tag{B.1}$$

where $E_l^0 = E_0 a(\alpha_l) b(\beta_l)$, E_0 is the common amplitude of the multipath plane waves incident on the mobile receiving antenna, $a(\alpha_l)$ and $b(\beta_l)$ are the antenna responses for the plane wave arriving at the azimuth angle α_l and the elevation angle β_l in 3-D space. φ_0

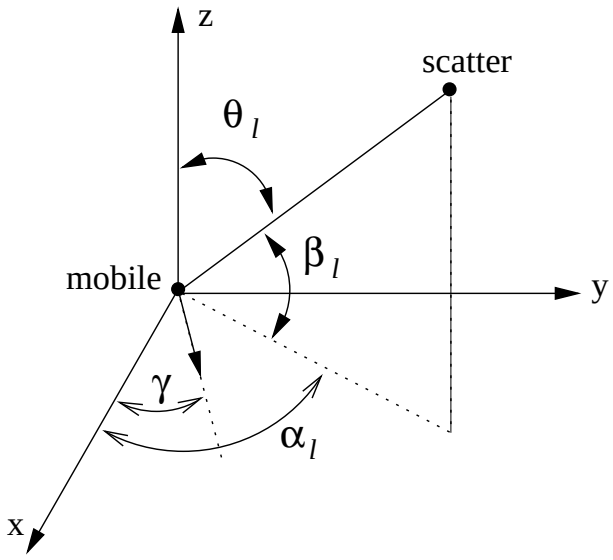

Fig. B.1: Geometry for 3-D scattered environment.

denotes the initial phase, v the mobile speed, λ the wave length, and γ the angle between the x axis and the direction along which the mobile is moving. The total field is

$$E(t) = \sum_l E_l(t) \tag{B.2}$$

and, without loss of generality, the autocorrelation function for the times t and $t+\tau$ can be calculated as

$$R(\tau) = \int_\alpha \int_\beta g_\alpha(\alpha) g_\beta(\beta) \cdot P_\alpha(\alpha) P_\beta(\beta) \cdot \exp[-j2\pi f_D \tau \cos\alpha \cdot \cos\beta] \cdot d\alpha d\beta \tag{B.3}$$

where $f_D = v/\lambda$, $g_\alpha(\alpha) = |a(\alpha)|^2$, $g_\beta(\beta) = |b(\beta)|^2$, $P_\alpha(\alpha)$ and $P_\beta(\beta)$ are the pdf's of the AoAs in both the azimuth and elevation planes, respectively. In the 2-D case, if α is uniformly distributed in $[0, 2\pi]$ and omidirection antennas are used, then

$$R(\tau) = \frac{1}{2\pi} \int_0^{2\pi} e^{j2\pi \frac{v\tau}{\lambda} \cdot \cos\alpha} d\alpha = J_0(2\pi f_D \tau). \tag{B.4}$$

The corresponding power spectral density can be obtained by applying Fourier transformation.

The pdf's of the angle-of-arrival (AoA) in azimuth and elevation planes affect the resultant Doppler spectra. The AoAs in the azimuth plane are usually assumed to be

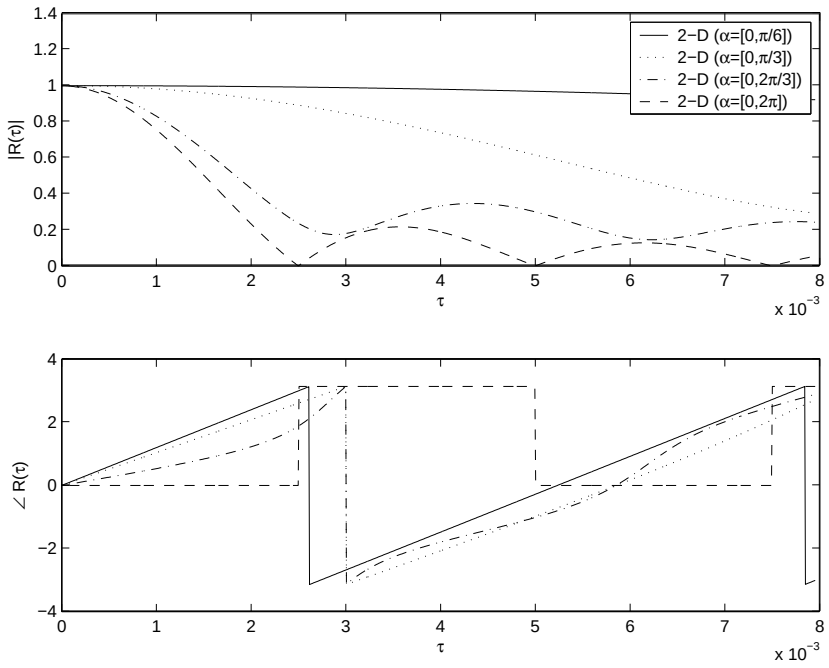

Fig. B.2: Autocorrelation functions under different angle spreads.

uniformly distributed over a range. On the other hand, there are different types of pdf's are presented. For example,

$$P_\beta(\beta) = \begin{cases} \frac{\pi}{4|\beta_m|}\cos\left(\frac{\pi}{2}\cdot\frac{\beta}{\beta_m}\right), & |\beta| \le |\beta_m| \le \frac{\pi}{2} \\ 0, & o.w., \end{cases} \tag{B.5}$$

$$P_\beta(\beta) = \begin{cases} \frac{1}{2\sin\beta_m}\cos\beta, & |\beta| \le |\beta_m| \le \frac{\pi}{2} \\ 0, & o.w. \end{cases} \tag{B.6}$$

Furthermore, Gaussian, Laplacian, and double-sided exponential function are also used in some other papers. It is observed in [24] that paths with elevations between 0^o and 40^o contain about 90% of the received power for Urban mobile radio.

B.3 Measured Doppler Spectra

Zhao *et al.* performed the outdoor and indoor channel measurement at 5.3 GHz in Helsinki, Finland [77],[78]. Several types of Doppler spectra are found at the different taps of the tapped-delay-line (TDL) models.

As shown in Fig. 4 of [78], there are three different types of Doppler spectra called as

"horned", "narrow", and "flat". Applying 3-D model, the characteristics of these types of Doppler spectra can be concluded as follows.

- The "horned" spectra are due to large AoA ranges of waves from the azimuth plane and the AoAs of waves in the elevation plane just change the relative amplitude values across the center part of spectrum.
- The "narrow" spectra are due to narrow angular ranges both in the azimuth and elevation planes.
- The "flat" spectra are due to large AoA ranges in both azimuth and vertical planes.

B.4 Examples

We consider 2-D model and assume the azimuth angles are uniformly distributed over $[\alpha_1, \alpha_2]$. To begin, we observe the influence of angle spread and Fig. B.2 shows the autocorrelation functions under different angle spreads. It can be observed smaller angle spread induce larger correlation. In addition, due to limited angel spread, the autocorrelation is not a real number, that is, the real and imaginary part of received signal is correlated. Next, the influence of angle position is addressed. Figure B.3 shows the autocorrelation when the incident angles have same spread range but different positions. Clearly, the correlation becomes larger when the incident angle is about the moving direction of the mobile.

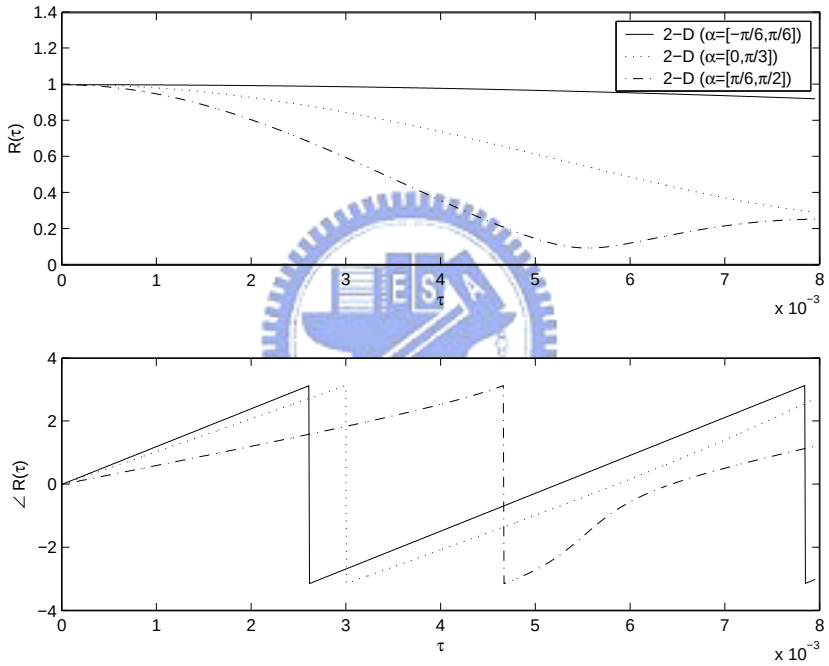

Fig. B.3: Autocorrelation functions under different angle positions.

Bibliography

[1] H. Abramowitz and I. A. Stegun, *Handbook of Mathematical Functions.* New York: Dover, 1964.

[2] F. Adachi, "Coherent multi-code DS-CDMA mobile radio access," *IEICE Trans. Commun.*, vol. E79-B, pp. 1316–1325, Step. 1996.

[3] Y. Akaiwa, *Introduction to Digital Mobile Communication.* New York: Wiley, 1997.

[4] H.-M. Anders and K.-S. Cho, "MMSE/PIC multiuser detection for DS/CDMA systems with inter- and intra-cell interferecne," *IEEE Trans. Commun.*, vol. 47, Feb. 1999.

[5] R. Buehrer and B. Woerner, "The asymptotic multiuser efficiency of m-stage interference cancellation receivers," in *Proc. IEEE Int. Symp. Pers. Indoor Mobile Commun.*, pp. 570–574, 1997.

[6] R. M. Buehrer and B. D. Woerner, "Analysis of adaptive multistage interference cancellation for CDMA using an improved Gaussian approximation," *IEEE Trans. Commun.*, vol. 44, pp. 1308–1321, Oct. 1996.

[7] A. G. Burr, " Bounds and approximations for the bit error probability of conventional codes," *Electron. Lett.*, vol. 29, no. 14, pp. 1287–1288, July 1993.

[8] C.-K. Chan and W.-H. Lam, "A simplified aperiodic cross-correlation model for direct-sequence spread-spectrum multiple-access communication systems," in *Proc. IEEE Int. Conf. Commun. (ICC'94)*, pp. 1516–1520, May 1993.

[9] J. Cheng and N. C. Beaulieu, “Accurate DS-CDMA bit-error probability calculation in Rayleigh fading,” *IEEE Trans. Commun.*, vol. 50, no. 1, pp. 3–15, Jan. 2002.

[10] B.-J. Choi and L. Hanzo, “On the design of LAS spreading codes,” in *Proc. IEEE Veh. Technol. Conf.* pp.2172–2176, 2002.

[11] R. H. Clarke, “A statistical theory of mobile-radio reception,” *Bell Syst. Tech. J.*, pp. 957–1000, July. – Aug. 1968.

[12] R. H. Clarke ans W. Lin Khoo, “3-D mobile radio channel statistics,” *IEEE Trans. Veh. Technol.*, pp. 798–799, 1997.

[13] J. Conan, “The weight spectra of some short low-rate convolutional codes,” *IEEE Trans. Commun.*, vol. 32, no. 9, pp. 1050–1053, Sep. 1984.

[14] D. G. M. Cruickshank, “Suppression of multiple access interference in a DS-CDMA system using Wiener filtering and parallel cancellation,” in *Proc. IEE–Commun.*, vol. 143, pp. 226–230, Aug. 1996.

[15] E. Dahlman, P. Beming, J. Knutsson, F. Ovesjö, M. Persson, and C. Roobol, “WCDMA–the radio interface for future mobile multimedia communications,” *IEEE Trans. Veh. Technol.*, vol. 47, no. 4, pp. 1105–1118, Nov. 1998.

[16] D. Divsalar, M. K. Simon, and D. Raphaeli, “Improved parallel interference cancellation for CDMA,” *IEEE Trans. Commun.*, vol. 46, no. 2, Feb. 1998.

[17] M. Döuling, D. Didascalou and W. Wiesbeck, “Wideband channel modeling and diversity techniques for satellite-UMTS,” in *Proc. IEEE Veh. Technol. Conf.*, vol. 5, pp. 2770–2774, Step. 1999.

[18] A. Duel-Hallen, “Decorrelationg decision-feedback multiuser detector for synchronous code-division multiple-access channels,” *IEEE Trans. Commun.*, vol. 41, no. 2, pp. 285–290, Feb. 1993.

[19] H. Elders-Boll, A. Busboom, and H. Schotten, “Spreading sequences for zero-forcing DS-CDMA multiuser detectors,” in *Proc. IEEE Int. Symp. Pers. Indoor Mobile Commun.*, pp. 53–57, 1997.

[20] M. V. Eyuboğlu and S. U. H. Qureshi, “Reduced-state sequence estimation for coded modulation on intersymbol interference channels,” *IEEE J. Select. Areas Commun.*, vol. 7, no. 6, pp. 989–995, Aug. 1989.

[21] R. Fantacci, “Proposal of an interference cancellation receiver with low complexity for DS/CDMA mobile communication systems,” *IEEE Trans. Veh. Technol.*, vol. 48, no. 4, pp. 1039–1046, July 1999.

[22] U.-C. Fiebig *et al.*, “Design study for a CDMA-based third generationmobile radio system,” *IEEE J. Select. Areas Commun.*, vol. SAC-12, pp. 733–743, May 1994.

[23] P. Frenger, P. Orten, and T. Ottosson, “Coded-spread CDMA using maximum free distance low-rate convolutional codes”, *IEEE Trans. Commun.*, vol. 48, no. 1, pp. 135–144, Jan. 2000.

[24] J. Fuhl, J.-P. Rossi, and E. Bonek, “High-resolution 3-D direction-of-arrival determination for urban mobile radio,” *IEEE Trans. Antenna and Propagation*, vol. 45, no. 4, pp. 672–682, Apr. 1997.

[25] D. Garg and F. Adachi, “Chip interleaved Trubo codes for DS-CDMA mobile radio in a fading channel”, *Electron. Lett.*, vol. 38, no. 13, pp. 642–643, June 2002.

[26] G. B. Giannakis, Z. Wang, A. Scaglione, and S. Barbarossa, “AMOUR–generalized multicarrier transceivers for blind CDMA regardless of multipath,” *IEEE Trans. commun.*, vol. 48, no. 12, pp. 2064–2076, Dec. 2000.

[27] X. Gui and T. S. Ng, “A novel chip-interleaving DS SS system,” IEEE Trans. Veh. Technol., vol. 49, no. 1, pp. 21–27, Jan. 2000.

[28] D. Guo, L. K. Rasmussen, S. Sun, and T. J. Lim, "A matrix-algebraic approach to linear parallel interference cancellation in CDMA," *IEEE Trans. Commun.*, vol. 48, pp. 152–161, Jan. 2000.

[29] J. M. Holtzman, "A simple accurate method to calculate spread-spectrum multiple-access error probabilities," *IEEE Trans. Commun.*, vol. 40, no. 3, pp. 461–464, Mar. 1992.

[30] J. F. Huber, D. Weiler, and H. Brand "UMTS, the mobile multimedia vision for IMT2000: a focus on standardization," *IEEE Commun. Magz.*, vol. 38, no. 9, pp. 129–136, Step. 1998.

[31] A. L. C. Hui and K. B. Letaief, "Successive interference cancellation for multiuser asynchronous DS/CDMA detectors in multipath fading channel," *IEEE Trans. Commun.*, vol. 46, pp. 384–391, Mar. 1998.

[32] H. Iwai and Y. Karasawa, "Wideband propagation model for the analysis of the effect of the multipath fading on the near-far problem in CDMA mobile radio system," *IEICE Trans. Commun.*, vol. e76-b, no. 2, pp. 103–112, Feb. 1993.

[33] K. H. A. Karkkainen and P. A. Leppanen, "Comparison of the performance of some linear spreading code families for asynchronous DS/SSMA systems," in *Conf. Rec., IEEE Military Commun. Conf.*, pp. 784–790, Nov. 1991.

[34] G. N. Karystinos and D. A. Pados, "New bounds on the total squared correlation and optimum design of DS-CDMA binary signature sets," *IEEE Tans. Commun.*, vol. 50, no. 1, pp. 48–51, Jan. 2003.

[35] A. Klein, G. K. Kaleh, and P. W. Baier, "Zero forcing and minimum mean-square-error for multiuser detection in code-division multiple-access channels," *IEEE Trans. Veh. Technol.*, vol. 45, no. 2, pp. 276–287, May 1996.

[36] C. Laot, A. Glavieux, and J. Labat, “Turbo equalization: Adaptive equalization and channel decoding optimized,” *IEEE J. Select. Areas Commun.*, vol. 19, no. 9, pp. 1744–1752, Sep. 2001.

[37] P. Laspougeas, P. Pajusco, J.-C. Bic, “Radio propagation in urban sma;; cells environment at 2 GHz: experimental spatial-temporal characterization and spatial wideband channel model,” in *Proc. IEEE Veh. Technol. Conf.*, vol. 2, pp. 885–892, Step. 1999.

[38] J. S. Lehnert and M. B. Pursley, “Error probabilities for binary direct-sequence spread-spectrum communications with random signature sequence,” *IEEE Trans. Commun.*, vol. 35, no. 1, pp. 87–98, Jan. 1987.

[39] G. Leus and M. Moonen, “MUI-free receiver for a synchronous DS-CDMA system based on block spreading in the presence of frequency-selective fading,” *IEEE Trans. Signal Processing*, vol. 48, no. 11, pp. 3175–3188, Nov. 2000.

[40] Y. X. Li and X. Huang, “The generation of independent Rayleigh faders,” in *Proc. IEEE Int. Conf. Commun. (ICC’00)*, pp. 41-45, 2000.

[41] D. Li, “The perspectives of large area synchronous CDMA technology for the fourth-generation mobile radio,” *IEEE Commun. Mag.*, pp. 114–118, Mar. 2003.

[42] Y.-N. Lin and D. W. Lin, “Chip interleaving for performance improvement of coded DS-CDMA systems in Rayleigh fading channels,” in *IEEE 58th Veh. Technol. Conf.*, Oct. 2003.

[43] F. Lin and L. B. Milstein, “Sucessive interference cancellation in multicarrier DS/CDMA,” *IEEE Trans. Commun.*, vol. 48, no. 9, pp. 1530–1540, Step. 2000.

[44] R. Lupas and S. Verdu, “Near-far resistance of multi-user detectors in asynchronous channels,” *IEEE Trans. Commun.*, vol. 38, pp. 496–508, Apr. 1990.

[45] U. Madhow and M. L. Honig, “MMSE interference suppression for direct-sequence spread spectrunm CDMA,” *IEEE Trnas. Commun.*, vol. COM=42, pp. 3178–3188, Dec. 1994.

[46] R. K. Morrow, “Bit-to-bit error dependence in slotted DS/CDMA packet systems with random signature sequences,” *IEEE Trans. Commun.*, vol. 37, pp. 1052–1061, Oct. 1989.

[47] R. K. Morrow, “Accurate CDMA BER calculations with low computational complexity,” *IEEE Trans. Commun.*, vol. 46, no. 11, pp. 1413–1417, Nov. 1998.

[48] S. Moshavi, “Multi-user detecion for DS-CDMA communications,” *IEEE Commun. Mag.*, pp. 124–136, Oct. 1996.

[49] A. Nahler, R. Irmer, and G. Fettweis, “Reduced and differential parallel interference cancellation for CDMA systems,” *IEEE J. Select. Areas Commun.*, vol. 20, no. 2, pp. 237–247, Feb. 2002.

[50] S. Parkvall, “Variability of user performance in cellular DS-CDMA–long versus short spreading sequences,” *IEEE Trans. Commun.*, vol. 48, no. 7, pp. 1178–1187, July 2000.

[51] P. Patel and J. M. Holtzman, “Analysis of a simple sucessive interference cancellation scheme in a DS/CDMA system,” *IEEE J. Select. Areas Commun.*, vol. 12, pp. 796–807, June 1994.

[52] M. Patzold, U. Killat, F. Laue, and T. Li, “On the statistical properties of deterministic simulation models for mobile fading channel,” *IEEE Trans. Veh. Technol.*, vol. 47, pp. 254-269, feb. 1998.

[53] A. Picart, P. Didier, and A. Glavieux, “Turbo-detection: a new approach to combat channel frequency selectivity,” in *Conf. Rec., IEEE Int. Conf. Commun.*, June 1997, pp. 1498–1502.

[54] M. F. Pop and N. C. Beaulieu, “Limitations of the sum-of-sinusoids fading channel simulators,” *IEEE Trans. commun.*, vol. 49, pp. 699–708, Apr. 2001.

[55] R. Price and P. E. Green, “A communication technique for multipath channel,” in *Proc. of the IRE*, pp. 555-570, Mar. 1958.

[56] J. G. Proakis, *Digital Communications, 3rd ed.* New York: McGraw-Hill, 1995.

[57] M. B. Pursley, “Performance evaluation for phase-coded spread-spectrum multiple-access communication—part I: System analysis,” *IEEE Trans. Commun.*, vol. 25, no. 8, pp. 795–799, Aug. 1977.

[58] M. B. Pursley, “Performance evaluation for phase-coded spread-spectrum multiple-access communication—part I: system analysis,” *IEEE Trans. Commun.*, vol. 25, no. 8, pp. 795–799, Aug. 1977.

[59] T. S. Rappaport, *Wireless Communications Principles and Practice.* Upper Saddle River, New Jersey: Prentice Hall, 1996.

[60] D. V. Sarwate and M. B. Pursley, “Crosscorrelation properties of pseudorandom and reltated sequences,” *Proc. IEEE*, vol. 68, no. 5, pp. 593–619, May 1980.

[61] M.-K. Simon and D. Divsalar, “Some new twists to problem involving the Gaussian probability integration,” *IEEE Trans. Commun.*, vol. 46, pp. 200–210, Feb. 1999.

[62] S. Stańczack, H. Boche, and M. Haardt, “Are LAS-codes a miracle?” in *IEEE Global Telecommun. Conf.*, Nov. 2001, pp. 589–593.

[63] S. Tachikawa, K. Toda, T. Ishikawa, and G. Marubayashi, “Direct sequence/spread spectrum communication systems using chip interleaving and its applications for high-speed data transmission on power line,” IEICE, vol. 74-B-1, no. 4, pp. 343–351, Apr. 1991.

[64] S. Tachikawa and G. Marubayashi, “Interference noise of the spread spectrum multiple access communication systens using delay trasnsmittion method,” IEICE, vol. 97-B, no. 1, pp. 32–38, Jan. 1984.

[65] *Technical Specification Group Radio Access Network*, 3GPP, “Spreading and Modulation (FDD).” Doc. 3G TS 25.213 ver. 4.1.0, June 2001.

[66] *Technical Specification Group Radio Access Network*, 3GPP, “User Equipment radio transmission and reception (FDD).” Doc. 3G TS 25.101 ver. 4.11.0, Mar. 2004.

[67] *Technical Specification Group Radio Access Network*, 3GPP, “Deployment aspects,” Tech. Rep. 3G TR 25.943 v5.1.0, June 2002.

[68] B. Ünal and Y. Tanik, “Code-hopping as a new strategy to improve performance of S-CDMA cellular systems,” in *Conf. Rec., IEEE Global Telecommun. Conf.*, Nov. 1996, pp. 1316–1319.

[69] S. Unawong, S. Miyamoto and N. Morinaga, “A novel receiver design for DS-CDMA systems under impulsive radio noise environments,” IEICE Trans. Commun., vol. E82-B, no. 6, pp.936-943, Jun. 1999.

[70] S. Unawong, S. Miyamoto and N. Morinaga, “Application of chip-interleaving and blanker for DS-SS system under microwave oven interference environment,” Electron. Lett., vol. 35, no. 9, pp. 695–696, 1999.

[71] M. K. Varanasi and B. Aazhang, “Multistage detection in asynchronous code-division multiple-access communications,” *IEEE Trans. Commun.*, vol. 38, pp. 509–519, Apr. 1990.

[72] S. Vembu and A. J. Viterbi, “Two different philosophies in CDMA—a comparison,” in *IEEE 46th Veh. Technol. Conf.*, Apr. 1996, pp. 869–873.

[73] A. J. Viterbi, *CDMA: principles of spread spectrum communication.* Addison-Wesley, 1995.

[74] G. Woodward, and B. S. Vucetic, "Adaptive detection for DS-CDMA," *Proc. IEEE*, vol. 86, no. 7, pp. 1413–1434, July 1998.

[75] F. Xiong, "Sequential decoding of convolutional codes in channels with intersymbol interference," *IEEE Trans. Commun.*, vol. 43, no. 2/3/4, pp. 828–836, Feb./Mar./Apr. 1995.

[76] Y. C. Yoon, R. Kohno, and H. Imai, "A spread-spectrum multiaccess system with cochannel interference cancellation for multipath fading channels," *IEEE J. Select. Areas Commun.*, vol. 11, pp. 1067–1075, Sep. 1993.

[77] X. Zhao, J. Kivinen, P. Vainikainen, and K. Skog, "Propagation characteristics for wideband outdoor mobile communications at 5.3 GHz," *IEEE J. on Select. Areas Commun.*, vol. 20, no. 3, pp. 507–514, Apr. 2002.

[78] X. Zhao, J. Kivinen, P. Vainikainen and K. Skog, "Characterization of Doppler spectra for mobile communications at 5.3 GHz," *IEEE Trans. Veh. Technol.*, vol. 52, no. 1, pp. 14–23, Jan. 2003.

[79] Y.R. Zheng and C. Xiao, "Simulation models with correct statistical propesties for Rayleigh fading channels", *IEEE Trans. Commun.*, vol. 51, no. 6, pp. 920–928, June 2003.

[80] S. Zhou, G. B. Giannakis, and C. Le Martret, "Chip-interleaved block-spread code division multiple access," *IEEE Trans. Commun.*, vol. 50, no. 2, pp. 235–248, Feb. 2002.

[81] S. Zhou, P. Xia, G. Leus, and G. B. Giannakis, "Chip-interleaved block-spread CDMA versus DS-DMA for cellular downlink: a comparative study," *IEEE Trans. Wireless Commun.*, vol. 3, no. 1, pp. 176–190, Jan. 2004.